Development of a user-friendly heterologous expression system and its applications for natural product biosynthesis

Dissertation

To Fulfill the

Requirements for the Degree of

„doctor rerum naturalium“(Dr. rer. nat.)

Submitted to the Council of the Faculty
of Biological Sciences
of the Friedrich Schiller University Jena

by Jun Lin (MPhil Pharmacy)

born on 29.02.1992 in Fuzhou, China

Diese Arbeit wurde am Leibniz-Institut für Naturstoff-Forschung und Infektionsbiologie e.V., Hans-Knöll-Institut Jena, in der Nachwuchsgruppe „Biobricks mikrobieller Naturstoffsynthesen“ – Lehrstuhl für Mikrobiologie und Molekulare Biologie, Friedrich-Schiller-Universität Jena, unter Leitung von Prof. Dr. Axel A. Brakhage angefertigt.

Gutachter 1: Prof. Dr. Axel A. Brakhage (Jena)

Gutachter 2: Prof. Dr. Miriam Agler-Rosenbaum (Jena)

Gutachter 3: Prof. Dr. Oskar Zelder (Ludwigshafen am Rhein)

Datum der öffentlichen Verteidigung: 15.12.2020

Table of Contents

Summary

Heterologous expression of natural product biosynthetic pathways is of rising interest to fungal bioactive compound discovery and engineering. However, most eukaryotic genes are regulated by individual regulatory elements and transcribed as monocistronic mRNA. Therefore, regardless of plasmid transformation or chromosomal integration of DNA, reconstruction and expression of biosynthetic gene clusters in the eukaryotic recipient require improved assembling pipeline of vectors and coordinated control of expression of multiple genes. Moreover, valuable medicine biosynthesis based on heterologous expression remains an ongoing challenge owing to the strict metabolic regulation in the chosen host.

To circumvent these obstacles, a specialized vector was designed, for flexible but modularized construction of multiple genes as the starting point. In the scheme, TEV protease and its recognition site combined with a previously documented P2A-mediated expression system, allow expression of eukaryotic genes in a “polycistronic” mRNA by co-translational and post-translational cleavages. As another highlight, the split fluorescent protein was introduced for visualizing and rapid screening of fungal transformants. I further applied the system for the heterologous production of complex meroterpenoid austinoids and the simple indole alkaloid psilocybin in the filamentous fungus *Aspergillus nidulans*. Significantly, the latter one identified from the "magic mushroom" *Psilocybe cubensis* received great attention for its psychotropic characteristics, which is considered a breakthrough therapy in depressive disorder and late-stage cancer-induced depression. The production of this valuable pro-drug demands a controllable and scalable manner. Thus, the budding yeast *Saccharomyces cerevisiae* was chosen as the chassis for the biosynthesis of this tryptophan-derived compound in the additional study. To enrich the intracellular tryptophan (Trp), Trp degradative pathways have been suppressed through gene deletion. In this recombinant yeast, I tried to facilitate the function of cytochrome P450 (PsiH) in the psilocybin biosynthetic pathway by co-expression of a newly identified P450 reductase from the same species, as a supplementary investigation. In a more specific application, the intracellular Trp biosynthesis was abolished for the production of isotope labeled psilocybin.

The result is an improved heterologous expression system for multiple genes promising fast assembly, synchronous transcription regulated by a sole promoter, and the quick yet reliable selection of correct mutants. On the basis of this new tool, the austinoid biosynthetic pathway has been rewired successfully in *A. nidulans*. Also, it represents the

first-time producing psilocybin heterologously using fermenting condition, from which the high titer 15.4 mg/g (110 mg/L) was achieved. Subsequently, the de-branching strategy was beneficial for the yield of psilocybin, which even lifted to 57 mg/g in the yeast cell-based factory. Meanwhile, the Trp auxotrophic strain has been endowed with the capability to synthesize isotope-labeled psilocybin in an atom-economic manner.

In conclusion, this practicable platform for multiple gene construction and heterologous expression paves the way in synthetic biology, as both filamentous fungi and yeast can be adapted for the natural product biosynthesis in a user-friendly way. Moreover, exemplified by the promoted amount of psilocybin produced in yeast, where the Trp flux has been redirected, I expect that this cell factory can act as an amenable workhorse to produce other indole alkaloids that are of pharmaceutical and economic interest in future applications.

Zusammenfassung

Die heterologe Expression von Biosynthesewegen von Naturstoffen ist von zunehmendem Interesse für die Identifizierung und Weiterentwicklung von bioaktiven Molekülen aus Pilzen. Allerdings wird der Großteil eukaryotischer Gene durch individuelle regulatorische Elemente gesteuert und als monocistronische mRNA transkribiert. Deshalb werden zur Rekonstruktion und Expression von biosynthetischen Genclustern im eukaryotischen Empfänger, unabhängig ob dies über Plasmid-Transformation oder chromosomaler Integration erfolgt, eine verbesserte Assemblierungspipeline der Vektoren und eine synchronisierte Transkription multipler Gene benötigt. Darüber hinaus bleibt die Biosynthese von wertvollen Medikamenten mittels heterologer Expression aufgrund der strengen Regulation des Stoffwechsels im ausgewählten Wirt eine ständige Herausforderung.

Um diese Hindernisse zu überwinden, wurde ein spezieller Vektor entworfen, der für die flexible, aber modulare Kombination mehrerer Gene als Ausgangspunkt diente. Dabei wird die 'polycistronische' Expression eukaryotischer Gene durch co-translationale und post-translationale Spaltungen der Polypeptidkette durch die TEV-Protease an ihrer Erkennungssequenz in Kombination mit dem zuvor beschriebenen P2A-vermittelten Expressionssystem ermöglicht. Als ein weiterer Höhepunkt wurde für das visuelle und schnelle Screening von Transformanten ein geteiltes fluoreszierendes Protein eingeführt. Ich habe dieses System für die heterologe Produktion von komplexen Monoterpenoid-Austinoiden sowie von Psilocybin, einem einfachen Indol-Alkaloid, im filamentösen Pilz *Aspergillus nidulans* angewendet. Bemerkenswerterweise erhielt letzteres, identifiziert aus dem 'magic mushroom' *Psilocybe cubensis,* in letzter Zeit große Aufmerksamkeit für seine psychotropen Eigenschaften, die sowohl zu einem Durchbruch in der Therapie depressiver Störungen als auch zur Behandlung von Depressionen im Spätstadium von Krebserkrankungen führten. Die Herstellung dieses wertvollen Medikamentes erfordert eine kontrollierbare und skalierbare Methode. Daher wurde die Hefe *Saccharomyces cerevisiae* als Grundlage für die Biosynthese dieser von Tryptophan abgeleiteten Verbindungen in der hier präsentierten Studie ausgewählt. Um das intrazelluläre Tryptophan (Trp) anzureichern, wurden Trp-Abbauwege durch Deletion von Genen unterdrückt. Bei einer zusätzlichen Untersuchung habe ich versucht, in dieser rekombinanten Hefe die Funktion von einem Cytochrom P450 (PsiH) im Psilocybin Biosyntheseweg durch die Co-Expression einer neu identifizierten P450 Reduktase aus derselben Spezies zu ermöglichen. In einer spezifischeren Anwendung wurde die

intrazelluläre Biosynthese von Trp ausgeschaltet, um Isotop-markiertes Psilocybin zu bilden.

Das Ergebnis ist ein verbessertes heterologes Expressionssystem für multiple Gene, welches eine schnelle Erzeugung des Expressionsvektors erlaubt, sowie eine synchronisierte Regulation durch einen einzelnen Promoter, und die schnelle und zuverlässige Auswahl korrekter Transformanten verspricht. Basierend auf diesem neuen System wurde die Austinoid-Biosynthese erfolgreich in *Aspergillus nidulans* ermöglicht. Dies war auch das erste Mal, dass Psilocybin heterolog und unter Fermentationsbedingungen hergestellt wurde, wobei ein hoher Titer von 15.4 mg/g (110 mg/L) erreicht werden konnte. Anschließend konnte durch die angewendete *de-branching* Strategie die Ausbeute an Psilocybin in der Hefe-basierten Produktion sogar auf 57 mg/g gesteigert werden. Parallel wurde der auxotrophe Tryptophan-Stamm mit der Fähigkeit ausgestattet, isotopen-markiertes Psilocybin auf ökonomischem Wege zu synthetisieren.

Zusammenfassend kann gesagt werden, dass diese praktikable Plattform für die Konstruktion and heterologe Expression multipler Gene den Weg in der synthetischen Biologie ebnet, da sowohl filamentöse Pilze als auch Hefen für diese benutzerfreundliche Methode der Naturstoffsynthese angepasst werden können. Zusätzlich ist zu erwarten, dass der in dieser Studie hergestellte Hefe-Produktionsstamm, dessen Tryptophan-Produktionsweg umgeleitet und damit die Psilocybin-Produktion erhöht werden konnte, zukünftig auch für die heterologe Herstellung anderer Indolalkaloide mit hohem pharmazeutischen und wirtschaftlichen Interesse, verwendet werden kann.

Chapter 1

Introduction

1.1 Fungal secondary metabolites

Secondary metabolite (SM), or natural product, so far is a term to describe a compound with low molecular weight yet exhibiting a bioactive function. Even though SMs derive from primary metabolism, instead of conferring essential roles for survival and growth, they contribute as info-chemicals against environmental stresses, predation, competition, or assist self-fitness and communications among symbionts (Jensen, 2016; Keller, 2019). Although the detailed functions of SMs are still undercover, their hitherto explored mainly brought them into usage as a pharmaceutical resource.

Fungi, as one of the major kingdoms, developed an abundance of SMs, many beneficial compounds among which were taken as antibiotics, antiparasitics, antitumoral agents, and so forth (Keller, 2019). The best-known case is penicillin which is widely applied as treatment of bacterial infections as far back as World War II (Quinn, 2013).

Fungal SMs are commonly classified as polyketides, non-ribosomal peptides, terpenes, and indole alkaloids (Keller et al., 2005). This definition mainly takes into accord which type of core biosynthetic enzyme and which kind of initial building block are responsible for the biosynthesis. Polyketides are synthesized by non-iterative or iterative polyketide synthases (PKS), which are mainly iterative type I in fungi, such as lovastatin synthase (Hendrickson et al., 1999; Hertweck, 2009). With CoA-esters (e.g., acyl-CoA and malonyl-CoA) as building blocks, the structure elongation is carried out by repetitive Claisen thioester condensations and is similar to fatty acid biosynthesis. However, in contrast to the saturated and immutable fatty acid chain, the chemical structure of polyketides is more diversiform due to the optional reduction in each elongation, and the varying length of the chain. Distinct from polyketides, both non-ribosomal peptide and indole alkaloids are derived from amino acids (Keller et al., 2005). For example, the L-tryptophan (Trp) that derives from the shikimate pathway is required for the biosynthesis of terriquinone A and psilocybin (**Scheme 1**, *ii* and *iii*) (Fricke et al., 2019; Schneider et al., 2008). Dimethylallyl pyrophosphate (DMAPP) is the building block of terpenes (or isoprenes), and this 5-C isoprene unit originates from acyl-CoA through the mevalonate (**Scheme 1B**). The diversity of terpenes depends on the number of DMAPP in their construction. For example,

the farnesyl diphosphate (farnesyl-PP) that is involved in the austinol biosynthesis is composed of three isoprene units (**Scheme 1A**) (Lo et al., 2012).

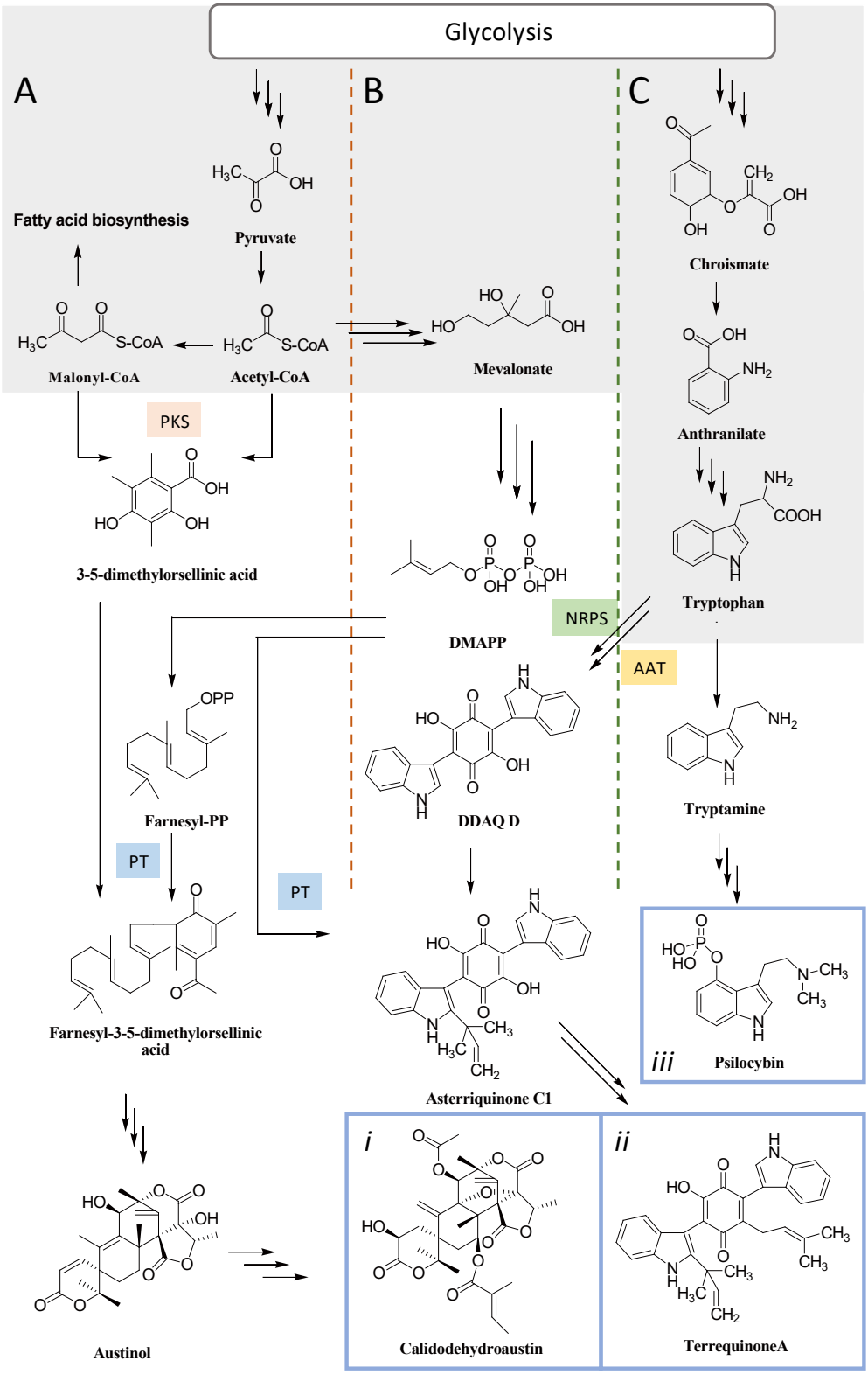

Scheme 1. Examples of SM biosynthesis in fungi starting with the CoA-esters or shikimate pathway. Fungal SMs biosynthetic pathways employ cross-talk. (A) Farnesyl-PP not only serves the biosynthesis of terpenes/terpenoids, but joins the CoA-esters derived PKS biosynthesis of 3-5-dimethylorsellinic acid towards austinol and its derivatives production (*i*). (B) The essential intermediate didemethyl-asterriquinone D (DDAQ D), which is produced from Trp by an NRPS and an aminotransferase (AAT), is prenylated by a prenyltransferase with DMAPP to gain the

bisindole alkaloid terrequinone A. (*ii*). Besides, (C) Trp can contribute to the formation of the simple indole alkaloid psilocybin (*iii*). The gray area indicates the primary metabolism. The dotted lines distinguish the pyruvate pathway, mevalonate pathway, and shikimate pathway. PKS: polyketide synthase; NRPS: non-ribosomal peptide synthetase; PT: prenyltransferase; AAT: amino acid transferase.

According to the fungal SMs that were studied in my project, the biosyntheses of austinoids and psilocybin are described in more detail in the following sub-sections.

1.1.1 Meroterpenoids and austinoid biosynthetic gene clusters

Albeit fungal SMs being mainly grouped into four classes, there are SMs originating from mixed biosynthetic roots. One such is the hybridized polyketide-non-ribosomal peptide (PK-NRP) compound (e.g., equisetin from *Fusarium* spp.), an indole terpenoid generated from both the shikimate and mevalonate pathways (e.g., okaramine S from *Aspergillus* spp), as well as a particularly important group known as meroterpenoids (e.g., pyripyropene A from *Aspergillus* and *Penicillium* spp.) (Burmeister et al., 1974; Hu et al., 2014; Petersen et al., 2014).

Meroterpenoids derive from the terpenoid pathway and comprise a non-terpenoid starter unit that is mainly produced from PKS. The varying length and cyclization patterns of terpenoids and the prenylation followed by the epoxidation with different stereo-forms all contribute to the likewise abundant chemical structures of meroterpenoids, which lead to extensive bioactivities: anti-insect, anti-inflammation, immunosuppression, anti-angiogenesis, among others (Matsuda & Abe, 2016). The biosynthesis of austinoids can demonstrate this structural complexity.

Austinoids are a group of 3,5-demethylorsellinic acid derived meroterpenoids, where both austinol and its spontaneous-oxidized form dehydroaustinol are produced by *Aspergillus nidulans* (Lo et al., 2012), *Aspergillus calidoustus* (Valiante et al., 2017), and *Penicillium brasilianum* (Kataoka et al., 2011). The discovered biosynthetic gene cluster related to austinol production in *A. nidulans* revealed a proposed biosynthetic pathway towards the end-product austinol by heterologous expressions (Lo et al., 2012; Matsuda et al., 2013), in which AusE, as a multifunctional dioxygenase, catalyzes iterative oxidation steps and a spiro-lactone ring formation. Later, a gene cluster (scaffold 10, **Fig. 1A**) was identified in the *P. brasilianum* strain MG11, in which a gene encodes a dioxygenase, namely AusE' (Matsuda et al., 2016). The functional study proved that AusE' shares the same enzymatic activity as the AusE from *A. nidulans*. Interestingly, the additional *aus* genes from the scaffold 6 (**Fig. 1A**) has been identified in this *P. brasilianum* strain. The encoded enzymes AusP, AusR, and AusQ were presumed to tailor dehydroaustin and yield acetoxydehydroaustin as the final product, which does not exist in *A. nidulans* (Mattern et

al., 2017). Compared with the separated clusters discovered from *A. nidulans* and *P. brasilianum*, the recent study by Valiante et al. (2017) uncovered a more integrated biosynthetic gene cluster of austinoid that harbors 25 genes in total in the *A. calidoustus* strain SF006504 (**Fig. 1A**). A gene deletions study shows an extended austinoids production derived from austinol (**Fig. 1B**).

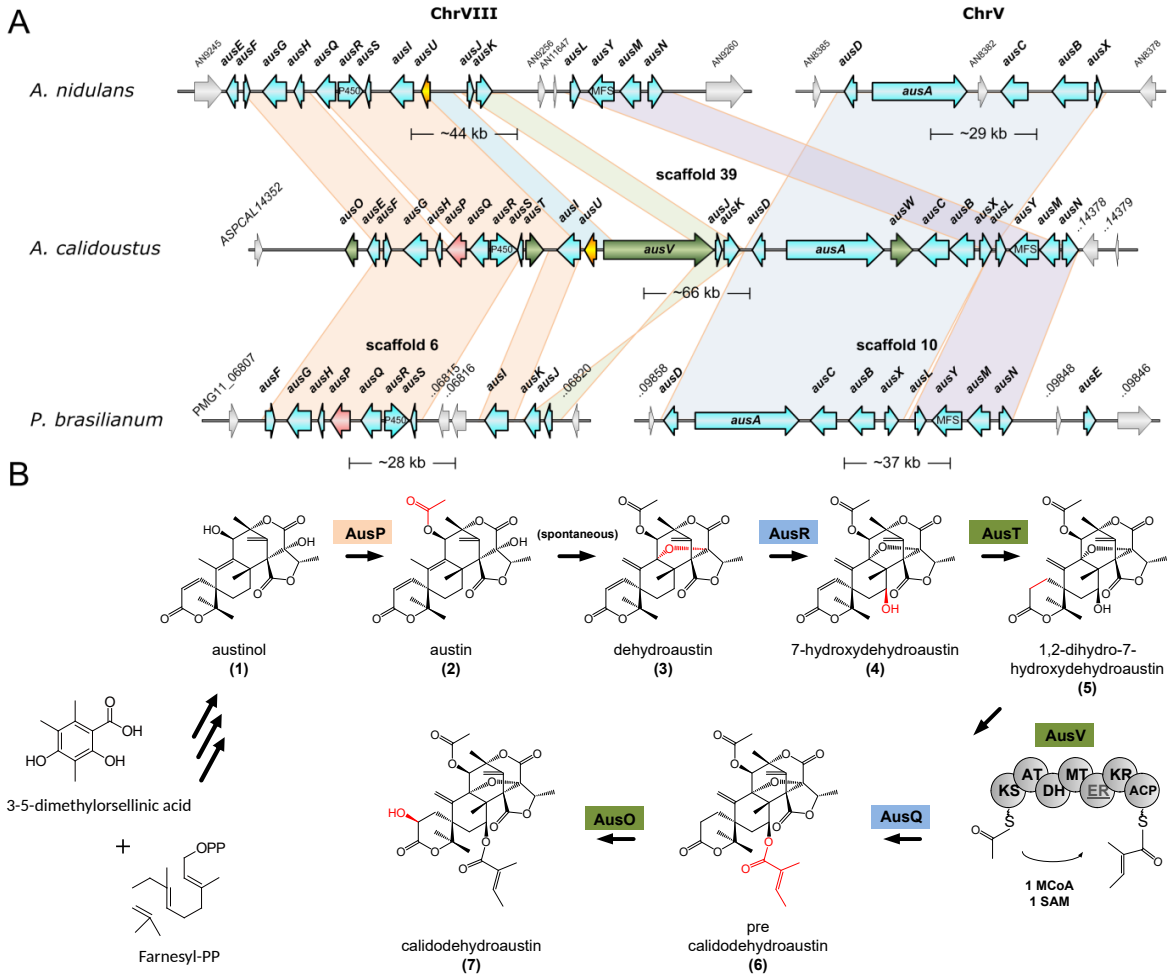

Fig. 1. The austinoid biosynthetic gene clusters and its extended biosynthetic pathway in *A. calidoustus*. (A) The gene cluster responsible for producing austinoids is broken and separated in both *A. nidulans* and *P. brasilianum*, while it is unabridged in *A. calidoustus*. The genes highlighted in sky blue are commonly shared in all three species, the yellow-colored *ausU* gene is found in *A. nidulans* and *A. calidoustus*, the pink-painted *ausP* gene only exists in *A. calidoustus* and *P. brasilianum*. Moreover, the green-marked genes are uniquely presented in *A. calidoustus*. Both *A. nidulans* and *P. brasilianum* have a remaining pseudogene similar to the missing PKS gene *AusV*. (B) Extended biosynthetic pathway in *A. calidoustus* from austinol (1). The color forms are inherited from the upper diagram. The PKS AusA-generated 3-5-dimethylorsellinic acid couples with mevalonate-derived farnesyl-phosphate to initiate the austinoid biosynthetic pathway. *ausV* gene encoding a non-iterative PKS bears the following domains: acyl carrier protein, keto-reductase, enoyl-reductase, methyltransferase, dehydratase, (malonyl)acyltransferase, and β-ketoacylsynthase. AusV-produced polyketide modifies the side chain of 1,2-dihydro-7-dydroxydehydroaustin (5). By the heterologous expression of the genes *ausP*, *ausO*, *ausT* and *ausV* in *A. nidulans*, the products (compounds 2-7) in the elongated pathway were detected, which demonstrated that the genes *ausR* and *ausQ* are still functional in this species. The figure and the figure-legend were adapted from Mattern et al., 2017 and Valiante et al., 2017.

Notably, the genes encoding the enzymes involved in the biosynthesis of SMs are commonly colocalized in the genome as a group, which are called biosynthetic gene clusters (BGCs). At the same time, a recent review (Rokas et al., 2018) pointed out that the biosynthetic pathway is also unclustered/partially clustered, such as the genes involved in the dothistromin biosynthesis in *Dothistroma septosporum* are distributed over six different loci; besides, the same biosynthetic pathway can vary in the structure and gene content between species, which is exemplified by the biosynthesis of trichothecenes among the *Fusarium* spp. The comparison of *aus* gene clusters from *A. nidulans* and *A. calidoustus* indicated that the lack of extended production of austinoids in the former one is due to the lack of four key enzymes, namely O-acetyltransferase (AusP), progesterone 5-β-reductase like protein (AusT), dioxygenase (AusO), and a non-iterative PKS (AusV), although it includes genes encoding an O-acetyltransferase (AusQ) and a cytochrome P450 monooxygenase (AusR) that are also essentially required in the pathway elongation.

1.1.2 Trp-derived indole alkaloids and the psilocybin biosynthetic pathway

Indole alkaloids have been well observed in plants, while fungi, typically Ascomycota and Basidiomycota, are also conferred as great resources of this class of bioactive compounds (Homer & Sperry, 2017; Xu et al., 2014). Using Trp or Trp derivatives, for example L-tryptamine, indole-3-pyruvate (IPA), indole-3-glycerol-phosphate (IGP), or 4-dimethylallyl tryptophan (4-DMAT), as a resource to donate an indole structure in alkaloids is a non-surprising strategy observed in fungal secondary metabolism (**Scheme 2**). The indole ring of Trp can undergo electrophilic addition, such as prenylation (e.g., 4-DMAT, **Scheme 2**) and methylation (e.g., physostigmine), as well as epoxidation (e.g., notoamide E) (Li et al., 2012; Liu et al., 2014; Metzger et al., 2009). These reactions modify the Trp into a more complicated structure within the biosynthetic pathway. Besides Trp, other amino acids, like L-proline, L-histidine, L-phenylalanine (Phe), and L-alanine, can be loaded to NRPS or hybridized PKS-NRPS to form dipeptide/tripeptide and hybrid indole alkaloids (Xu et al., 2014).

With the structural diversity come various bioactivities. Emindoles derived from IGP as the representatives of indole diterpene alkaloids have an inhibitory effect on cancer cell lines (Xu et al., 2014). Ergot alkaloids, as a group of bioactive compounds that share an identical precursor 4-DMAT, have a broad range of pharmaceutical activities, including uterotonic activity, blood pressure modulation, and anti-migraine (Metzger et al., 2009). A prenylated indole-containing class called asterriquinone, presents special anti-retroviral, anti-tumor, and anti-diabetic activities (Schneider et al., 2008). Terrequinone A is shown as

an example in **Scheme 1B**. This group of compounds is synthesized from IPA. Last but not least, by using tryptamine as the starter unit, simple indole alkaloids are developed and considered as important neurotransmitters (Hamid et al., 2017), such as psilocybin, which is famous on account of its potential therapeutic value towards treatment-resistant depression, especially for patients with advanced-stage cancer.

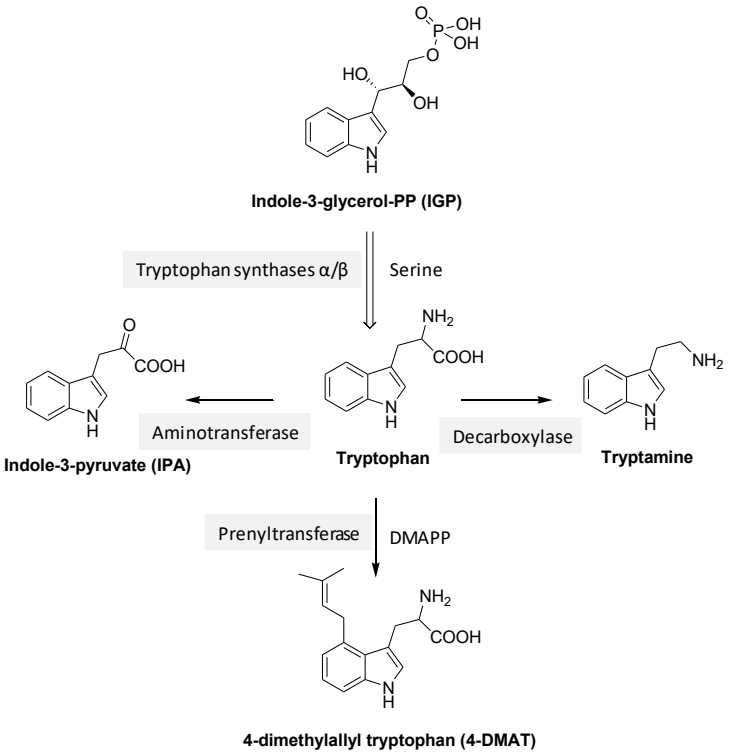

Scheme 2. Indole moieties from Trp catabolism and metabolism. With essential enzymes and substrate, the Trp precursor and its downstream derivatives are produced and used as the indole donors for indole alkaloids biosynthesis. PP: phosphate; DMAPP: dimethylallyl pyrophosphate.

Psilocybin is widely found in the genus *Psilocybe* ("magic" mushrooms) (**Fig. 2**, left). It is easily dephosphorylated in the hepatic metabolism to form the psychotropic compound psilocin, which acts as an agonist of the neurotransmitter serotonin (5-HT), with high affinity to the human 5-HT_{2A} and 5-HT_{2C} receptors in the brain (Fricke et al., 2019; Lenz et al., 2020). Additionally, psilocybin was granted a status as a "breakthrough therapy" by the U.S. Food and Drug Administration and will soon enter phase III clinical trials. Currently, the company COMPASS Pathway is responsible for providing psilocybin for clinical trials; with the cost at 5 USD/mg. Therefore, there is a high demand for a suitable synthetic methodology that can reduce production costs for the pharmaceutical market.

Although several reported chemical synthesis protocols of psilocin were established in the past to overcome the low natural production rate in the mushroom fruiting body, none of them can yet achieve more than 73% overall yield in an atom and step economic way (Bartolucci et al., 2016; Sherwood et al., 2020; Shirota et al., 2003), not to mention the

requirement of an additional chemical synthesis step to produce psilocybin after the formation of psilocin. Recently, the corresponding biosynthetic gene cluster of psilocybin has been identified from *Psilocybe cubensis* and *Psilocybe cyanescens* (**Fig. 2**, right), and a biosynthetic strategy is considered to be an anticipated substitution to overcome this "bottle-neck".

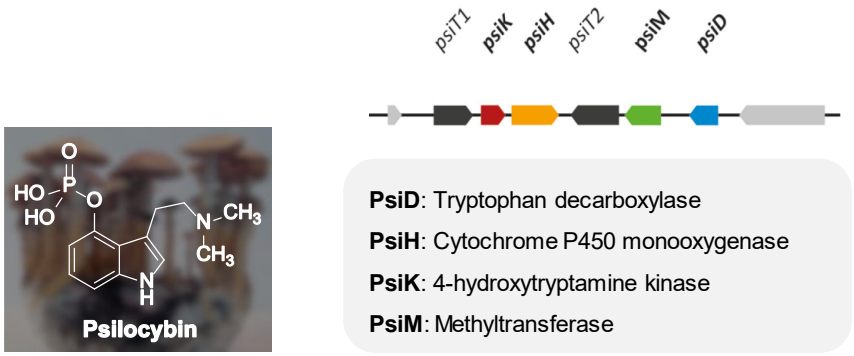

Fig. 2. Psilocybin chemical structure and its biosynthetic gene cluster. The gene cluster scheme is modified from Frick et al., 2017, and the *P. cubensis* image is adjusted from a photograph made by Felix Blei (PM, HKI, Germany).

In this genetic locus, three genes encoding the core enzymes, i.e., PsiD, PsiK, and PsiM, are essentially involved in psilocybin production. PsiD is a tryptophan decarboxylase, which connects the primary and secondary metabolism. An *in vitro* enzymatic study revealed that the necessary intermediate 4-hydroxytryptamine in psilocybin biosynthesis is either derived from Trp by decarboxylation and hydroxylation that is catalyzed by PsiD and cytochrome P450 monooxygenase (PsiH), or simply originates from 4-hydroxytryptophan, which only needs PsiD in the reaction (Fricke et al., 2017). Moreover, PsiK catalyzes the phosphotransfer reaction at the C-4 position, yielding norbaeocystin, from which PsiM additionally catalyzes the N-methyl transfer step for the production of intermediate baeocystin, the shunt product norpsilocin, and the final product psilocybin.

1.2 Genetic tools in heterologous expression

In the post-genomic era, the number of available fungal genome sequences is steadily increasing. The functional annotation of this data provides much information about biosynthetic pathways towards known or unknown SMs. As mentioned in the beginning, SM formation is peculiar towards different species, and the triggers of gene transcription for SM production are varying, depending on their ecological systems (Brakhage, 2013; Keller, 2019). Therefore, the undiscovered BGCs require a suitable strategy, since many of them are silent under standard laboratory culture conditions. Likewise, for the discovered and valuable SMs, like psilocybin, a controllable system is demanded to break the domestic host's production limitations. The better unknown BGCs are elucidated, the

deeper our biochemical understanding of the enzymatic steps involved is and the more efficiently it can be applied. Heterologous expression, as one of the synthetic biology approaches, can help fulfill both needs (Mattern et al., 2015). The suitable choices of host as well as the genetic manipulation and transformation of the biosynthetic pathway in the chosen host are fundamental points that need to be considered.

Previous reviews summarized the commonly used hosts for heterologous expression, including bacteria (e.g., *Escherichia coli*, *Bacillus subtilis*, and *Streptomyces* spp.), baker's yeast (*S. cerevisiae*), and filamentous fungi (e.g., *Aspergillus* spp.) (Anyaogu & Mortensen, 2015; He et al., 2018). The fast life cycle, possibility of genetic manipulation, as well as the capacity of vector harboring, lead *E. coli* and *S. cerevisiae* to the preferred hosts. Nevertheless, they are not the ideal chassis for the synthesis of complex PKS-derived SMs due to the insufficient conversion of essential secondary metabolite precursors and the difficulty in expressing certain plant enzymes, e.g., cytochrome P450, functionally (Kotopka et al., 2018). To circumvent this obstacle, besides additional chemical feeding or genetic modification in these simple microorganisms, filamentous fungi are the optimal alternative platforms for heterologous expression of large BGCs.

Various genetic tools could be employed to introduce the required heterologous gene(s) in an amenable host. To assemble the required gene into a vector, methods associated with polymerase chain reaction (PCR) (e.g., Fusion PCR and seamless cloning techniques) combining yeast homologous recombination is a promising strategy that is widely applied. For the site-specific integration of DNA fragments based on homologous recombination, other toolboxes are used to minimize non-homologous end-joining (NHEJ), e.g., CRISPR-Cas 9 activated double-strand DNA break and *ku70/80* homologous gene knockout (Deng et al., 2017; Nayak et al., 2006). Although the gene randomly integrating into the genome might trigger the disruption of adjoining genes, ectopic construct integration of PKS genes *via* this NHEJ machinery in filamentous fungi benefited SMs biosynthesis, as reported in another review withal (Anyaogu & Mortensen, 2015). Depending on the host characteristics, the heterologous gene(s) can either be assembled in the specified (single or multiple copies) shuttle vector, or transferred into the chromosome, or both. In order to attain a satisfactory gene expression level, the promoter selection should be taken into account: an inducible promoter is controllable for the transcription induced at a suitable growth stage, and a constitutive promoter is active in the cell under any circumstances.

The host species is also influencing the choice of the selective marker gene in the genetic transformation. The β-lactamase gene (*bla*) and the gene coding the aminoglycoside 3'-phosphotransferase (*aph*), are widely used in commercial vectors as bacterial selection

maker genes for *E. coli*. The latter has a hybridized analog, namely *KanMX* (Wach et al., 1994), that is utilized as a geneticin (G418) resistance gene in *S. cerevisiae* colony selection. Besides, yeast acquires a group of loci, such as *URA3*, *HIS3*, *LEU2*, *TRP1*, providing not only auxotrophic markers but also genomic integration positions (Kotopka et al., 2018). Similarly, the orotidine-5'-decarboxylase gene *PyrG* from *Aspergillus* spp. has an equal function to *URA3*. Thus, it is a prevalent auxotrophic marker for heterologous expression in filamentous fungi (Dohn et al., 2018; Richter et al., 2014; Zhu et al., 2013). Besides, L-arginine (Arg) auxotrophic marker *ArgB* cassettes, pyrithiamine resistance gene *ptrA,* and hygromycin resistance genes *hph*, have been reported as efficient selective makers that are frequently used in the model fungus *Aspergillus nidulans* (He et al., 2019; Upshall, 1986). Although the auxotrophic marker gene might interrupt the host metabolism when it is overexpressed, yet, for the industrial-preferred strains, the auxotrophic/nutritional selective marker is more acceptable in the food-grade application (Mignon et al., 2015).

1.2.1 Connecting well-known SMs to unknown gene clusters

The biosynthetic pathway of some SMs discovered in the past remains unclear and could be clarified by combining the use of bioinformatics tools with heterologous expression. Genome mining tools can analyze the open reading frames (ORFs) from the draft genome sequence once the genome information of a fungal species is available. The alignment with other similar genes and catalytic domains can result from BLAST (Basic Local Alignment Search Tool from NCBI), and the putative BGCs that are generated by other gene cluster predictors (e.g., antiSMASH 5.0 and MIBiG 2.0) will provide the possible gene cluster candidates for the target SM (Blin et al., 2019; Kautsar et al., 2019). After chemical structure analysis of this known compound, the possible enzymatic reactions involved in biosynthesis could be assumed, especially for NRPs which have a clear composition of amino acids and corresponding adenylation domains. Upon the prediction, the individual gene in the cluster candidates could be focused on, and the target genes can be reconstructed and expressed in a heterologous host for further compound determination. This is one of the strategies to link the well-studied bioactive product with its original gene cluster.

The identification of the psilocybin gene cluster is one of the examples following this approach. The compound structure requires an aromatic amino acid decarboxylase, hydroxylase, methyltransferase, kinase, and omits any PKS or NRPS in the gene cluster. In both *P. cubensis* and *P. cyanescens*, each has one locus that carries genes that fit this

requirement and there is a high similarity between them. Therefore, four genes encoding enzymes were heterologously expressed in *E. coli* separately and purified for enzymatic reactivity, by which the proposed biosynthetic pathway of psilocybin was successfully verified (Fricke et al., 2017).

Another approach is to heterologously express the entire PKS gene cluster in a filamentous fungus. To prepare a suitable host with low secondary metabolic background, the researchers in the Wang lab deleted seven well-known gene clusters from *A. nidulans* using homologous recombination based on the loop-out strategy. They created the strain LO30080 as an ideal platform for heterologous expression (Chiang et al., 2013). Upon this unique strain, they clarified the new gene cluster of the earlier-discovered SM citreoviridin (Lin et al., 2016). Earlier C13 labelling studies revealed the possible precursor of citreoviridin and the required CoA-esters building blocks. In parallel, a structurally similar compound aurovertin was reported, that was synthesized by a highly reducing PKS (HR-PKS) (Mao et al., 2015). Hence, an HR-PKS cluster was isolated from the citreoviridin-producing *Aspergillus aureoterreus*, in which genes encoding methyltransferase, hydroxylase, and monooxygenase are promising for the methyl groups in the structure and required bisepoxidation. Based on the strain LO30080, several *A. nidulans* mutants were constructed by introducing *ctvA*, *ctvB*, *ctvC*, and *ctvD* into the genome, through which the citreoviridin biosynthetic pathway was elucidated.

1.2.2 Identification of novel SMs

To discover a novel SM from a cryptic gene cluster, which is different from the above mentioned concept, requires a combination of tools and approaches. On the one hand, we have to consider the size of target genes and the possible alternative splicing within the pre-mRNA transcription during the reconstruction of the gene cluster. On the other hand, as with the silent gene cluster, whether the gene is mutated is another point merits special attention. Like in the austinoids biosynthesis study, only a pseudogene residue was identified in the austinol gene cluster from *A. nidulans* that has a certain similarity with the PKS gene *ausV* in *A. calidoustus* (Mattern et al., 2017). As with the example of citreoviridin shown above, there is another *Aspergillus terreus* strain NIH2624, which harbors an analogous gene cluster sharing about 90~95% similarity with the *ctv* gene cluster in *A. aureoterreus* CBS503.65. However, by heterologous expression of the putative PKS gene (ATEG_09617) that was isolated from this NIH2624 strain, the expected compound has not been detected (Lin et al., 2016), likely due to genetic mutation in the PKS gene.

Although with relatively high difficulty, there are cases achieving to activate the silent gene clusters using artificial chromosomes and metabolic scoring systems based on heterologous expression (Bok et al., 2015; Clevenger et al., 2017; Harvey et al., 2018). This strategy constructs a large library of artificial shuttle vectors and transforms them into a suitable host for heterologous expression. The extracted samples are measured using high-resolution mass spectrometry. The dereplication of known SMs allows high-throughput screening of unknown gene clusters and filtering of novel SMs. The highlights of the work from Harvey *et al.* (2018) are: 1) the yeast shuttle vectors carrying gene clusters were introduced to the *S. cerevisiae* host, through which both growth and protein expression have been improved. This strain optimization included expression of fungal cytochrome P450 and phosphopantetheinyl transferase encoded by *npgA*; 2) the selected gene clusters from both ascomycetes and basidiomycetes offer more possibilities to address unknown SMs. Except using an yeast platform, the other example is harnessing non-modified *A. nidulans* (Bok et al., 2015). In this study, a fungal-*E. coli* shuttle vector features the fungal replicating element *AMA1* (Gems et al., 1991) and a commercial bias-free linear vector allowed the *E. coli*-based vector construction and large size BGCs heterologous expression in fungi. Both methods discovered more than ten unknown SMs from the BGCs library. Although the remaining one-fourth of cryptic gene clusters are still not elucidated in both types of methodologies, they offer a quick selection of unknown gene clusters containing still fully functional enzymes in their sequences.

1.3 Multigene expression systems for SM biosynthesis

In synthetic biology, multiple gene expression strategies are in high demand for both, heterologous production and homologous expression, as there are generally multiple genes in any given BGC. In several reported approaches for protein co-expression (Mansouri & Berger, 2014; Szymczak & Vignali, 2005), the multigene carrier could be a shuttle vector/artificial chromosome or the genomic DNA, depending on the host type. An ePathBrick expression vector (Xu et al., 2012) contains restriction sites of isocaudamers (*Avr*II, *Xba*I, *Spe*I, and *Nhe*I) located before the T7 promoter, and before/after the T7 terminator in the vector. This design allows multiple genes to iteratively assemble in one shuttle vector in a monocistronic operon or pseudo-operon configuration. Moreover, this expression vector was adopted by Adams *et al*. for psilocybin heterologous production in *E. coli* (Adams et al., 2019).

As an eukaryotic host, the yeast *S. cerevisiae* and filamentous fungi *Aspergillus* spp. can use the locus-directed genomic integration method that is promoted by homologous

recombination, as a group of selective marker loci in these species has been well-characterized (Chiang et al., 2013; Kotopka et al., 2018). Nevertheless, this method consumes marker genes that are limited in filamentous fungi during genetic transformation; hence, the marker recycling design can enable the repeated usage of one or two selective markers. Zhang *et al*. reported a recycled system in *Aspergillus oryzae*, namely Cre-*loxP* mediated self-excision (Zhang et al., 2017). It features two mutated *loxP* sites (34 bp of each) that are spaced by an *A. nidulans* selective marker *adeA* gene fused with the *cre* gene encoding Cre recombinase in the shuttle plasmid. This plasmid also harbors the gene intended to be expressed in the genome. In theory, after genomic integration, the expressed Cre can recognize the *loxP* sites with the same sequence direction and delete the DNA fragment between the sites. Therefore, the same selective marker can be used again for several genetic manipulations.

Apart from "one ORF with one promoter", the "polycistronic" manner known from prokaryotes can be acquired for multigene expression in the eukaryotic host by inserting cleavage sites between the genes. As both were discovered from the picornavirus family, the internal ribosomal entry site and the 2A peptide have been adopted from multiprotein expression, and the latter is more attractive as it has a shorter sequence (18~22 bp) and has non-protease dependent cleavage (Koh et al., 2013; Szymczak & Vignali, 2005). This ribosomal recoding is due to the conserved C-terminal end of 2A peptides (D-X-E-X-N-P-G-P). During translation, the ribosome skips the peptide bond formation between glycine and proline and start the translation with proline as first residue continually (Sharma et al., 2012), which guarantees the simultaneous co-expression of multiple proteins. To evaluate the best version of 2A sequences, preview comparison among several 2A peptides demonstrated that P2A has the highest cleavage efficiency in eukaryotic models (Daniels et al., 2014; Kim et al., 2011). Intriguingly, an advanced study showed that exchanging the last amino acid from proline to alanine did not prevent the ribosomal recoding process in *Aspergillus niger* using P2A (Schuetze & Meyer, 2017), yet this result stands out in contrast to the other study using F2A (Sharma et al., 2012). This might also suggest the high efficiency of P2A. Additionally, the efficiency screening of twenty-two 2A peptides in the yeast *S. cerevisiae* has been done by analyzing the intensity of expressed protein in a western blot after the 2A-mediated 'cleavage' (Souza-Moreira et al., 2018), where P2A had 85% 'cleavage' efficiency. The above assessments affirm the capacity of P2A in both budding yeast and *Aspergillus* spp. Importantly, the co-expressed multiple proteins, including one large PKS and four tailoring enzymes, after P2A-mediated cleavage still hold relatively high abundances in the heterologous host *A. nidulans* (Stroe et al., 2020).

This quantification on the protein level indicates the considerable productivity of multiple proteins by P2A-involved co-translation.

The elegant application of P2A is heterologously expressing the entire gene cluster of the classical fungal-derived antibiotic penicillin under one inducible promoter in *A. nidulans* (Unkles et al., 2014). Although the 2A sequence length is shorter than other splicing sites for protein co-expression, the attached 2A tag at the C-terminal end might influence the folding of some enzymes, even abrogate their activity. This negative effect was observed in P2A tag fused acetyltransferase AusP for austinoids heterologous production in *A. nidulans* (Mattern et al., 2017). Hence, *ausP* had to be assembled in an additional plasmid for fungal transformation.

More and more strategies are available in this research field and are beneficial for strain engineering and optimization. Hybridizing these ideas can improve the host capacity to bear even more genes for valuable compound production.

1.4 Yeast cell factories for valuable SMs production

Unlike total chemical synthesis, cell-based biosynthesis can omit expensive or complicated feedstocks, toxic wastes, and inflexible synthetic routines. Various kinds of high-value products, including biopharmaceuticals, biofuels, biochemicals, and SMs, are provided commercially by microorganisms that serve as cell factories (Souza-Moreira et al., 2018). However, in contrast to petrochemical companies, biotech companies using fermenters for their production only occupied little of the global economic market based on statistical data (Davy et al., 2017). We can imagine that, once this new type of green manufacturing holds a reliable, renewable, and controllable production system, it has considerable market space to expand into.

Long historical development, the most well-studied eukaryotic genome, available genetic editing, and being generally recognized as safe (GRAS) status, have paved the way for the yeast *S. cerevisiae* to become the most widely used cell factory by far (Baghban et al., 2018; Souza-Moreira et al., 2018). Companies like Evolva and Amyris Inc. focus on deliverable plant SMs using *S. cerevisiae* yeast cell factories, e.g., health care bioactive resveratrol and anti-malarial/anti-cancer prodrug artemisinic acid (Wong et al., 2017; Xia et al., 2017). As a unicellular model ascomycete fungus, baker's yeast combines the easy cultivation and rapid growth of bacteria with the capacity of featuring the necessary post-translational modifications of eukaryotes. Although budding yeast indeed has a few weaknesses, such as codon preference, incomplete phosphopantetheinyl transferase

collection, and different intron splicing (He et al., 2018); metabolic engineering can optimize strains to meet those requirements.

1.4.1 Metabolic engineering

In early 1998, people started to create recombinant yeast *S. cerevisiae* strains for the improvement of vinification (Puig et al., 1998). Designing and engineering the metabolic pathway is a crucial part of the construction of a robust yeast cell factory. The first critical step is to equip the heterologous biosynthetic pathway with the endogenous primary metabolism in yeast. Depending on the type of end-product, arranging the enzymes active in between as the bridge to tune the primary metabolic flux(es) towards particular synthetic pathways and reach the desired SMs is possible, if sometimes complex.

An outstanding example is the complete biosynthesis of pain-releasing medicine opioids in engineered *S. cerevisiae* as whole-cell biocatalyst (Galanie et al., 2015). Without additional chemical supplements, the pathway starts from simple sugars and involves numerous enzymes (>20 in total) derived from plants, mammals, bacteria, and yeast. Although this study only obtained a trace amount much lower than the commercial requirement, it still provides several metabolic engineering strategies that could benefit other yeast cell factories.

1.4.1.1 Substrate/precursor enrichment in the biosynthetic pathway

As mentioned, CoA-esters and aromatic amino acids, i.e., L-tyrosine (Tyr), Phe, and Trp, are the key materials in the formation of PKs, NRPs, phenolic compounds and alkaloids (Lian et al., 2014; Nielsen, 2015). However, the carbon metabolic flux towards these units is highly regulated on the gene and protein level. Besides engineering the upstream pathway to enhance the intracellular substrate pool, another feasible approach is to de-branch the side-pathways that constitutively consume the needed precursor. Circumventing the other superfluous side paths can be achieved by either introducing a heterologous enzyme(s) shortening the passageway or prohibiting the enzyme(s) catalyzing precursor degradation.

Some studies introduced an engineered bypass to convert pyruvate to acetyl-CoA in the cytosol with high efficiency, redirecting the carbon flux towards the acetyl-CoA accumulation in the yeast for terpenoids or flavonoids bioconversion. (Lian et al., 2014; Liu et al., 2017a). By excluding the mitochondrial targeting sequences from the protein, Lian *et al*. constructed a cytosolically localized pyruvate dehydrogenase, since this one-step reaction only occurs in the mitochondria, and the synthesized acetyl-CoA cannot be exported to the cytosol in yeast. Liu *et al*. engineered the cytosolic acetyl-CoA conversion

by overexpressing a protein complex comprising of an endogenous acetaldehyde dehydrogenase and a heterologous acetyl-CoA synthetase mutant with increased enzyme activity, which catalyzed a two steps conversion from pyruvate-derived acetaldehyde to acetate, and then formed the acetyl-CoA. In both cases, the desired products increased significantly, indicating that the reconstructed bypass circumvents the limit of cellular compartmentalization.

Similarly, this strategy works for a Tyr-derived substrate. For example, a point-mutated cytochrome P450 was made by DeLoache *et al*. which has only hydroxylase activity without oxidase function. This engineered enzyme repressed the Tyr-formed substrate, namely L-3,4-dihydroxyphenylalanine, toward the side pathway, therefore enhancing the further synthesis of (*S*)-reticuline, a benzylisoquinoline alkaloid from plants (DeLoache et al., 2015). For the Phe supplement, the degradation of Phe can be blocked by the deletion of *ARO10*, which encodes a phenylpyruvate decarboxylase. Hence, with such a strategy, through p-coumaric acid, the downstream production of resveratrol has been upregulated by about 23% in the yeast *S. cerevisiae* (Li et al., 2016).

Besides the Tyr-Phe branch in shikimate-derived pathways, the Trp intracellular pool in yeast is benefited by Trp biosynthesis and uptake of extraneous supplement. Nevertheless, the Trp level in yeast is not sufficient to produce the desired compound in a high level. Because the intracellular Trp is kept in a dynamic balance strictly regulated by its biosynthetic enzymes, typically the anthranilate synthase, which has a feedback inhibition response (Miozzari et al., 1978). Thus, repressing Trp catabolism might fuel the intercellular Trp pool and enrich the Trp-derived SM biosynthesis in yeast.

In conclusion, to develop an overproducing strain that can overcome the tight regulation of intracellular levels, the possible optimizations cover gene/protein engineering, reconstruction of the biosynthetic pathway, and redirection or regulation of metabolic fluxes that include the substrate, precursor, product and byproduct (Davy et al., 2017). A fine-tuned system in a yeast-based factory can balance the healthy growth of cells and the considerable yield of the desired product. This could be achieved further by considering carbon source selection, CO_2 concentration, and ethanol effects, in large-scale fermentation.

1.5 Aim of the thesis

Fungal SMs are formed in a limited amount in their original species. Thus, taking advantage of synthetic biology and metabolic engineering of the host is a powerful strategy to produce bioactive compounds in a controllable, scalable, and environmentally

considerate manner. On the one hand, the premise of this idea is that a feasible system for reconstruction and heterologous expression of the target gene cluster is necessary. Nevertheless, the modularized assembling, the "polycistronic" expression of multiple genes, and the fast screening of correct mutants are hard to achieve simultaneously for the eukaryotic host using the vector-based methods reported previously. On the other hand, the microbial host requires genetic modifications to serve as the amenable chassis for the desired product. The idea of baker's yeast as the workhorse for the biosynthesis of heterologous SMs is being vigorously developed. Past lessons have taught us that the successful metabolic engineering of yeast requires a platform strain, which can be used for the same class of SMs (Nielsen, 2015). Upon this theory, a tryptophan-enriched "platform" strain is needed for indole alkaloid production. Therefore, based on the demands, there were three aims for this work.

The first aim was to update a previously documented 2A-system (Unkles et al., 2014) for polycistronic expression of multiple genes. A standardized assembly pipeline and reliable but rapid selection method needed to be equipped to this system, which should be evaluated by heterologous expression of a large-sized gene cluster.

The second scope was to exploit this improved system for the heterologous production of the valuable pro-drug psilocybin in filamentous fungi. This compound remains at trace amount levels in the native 'magic' mushrooms producing it and holds high demand in the pharmaceutical market.

The last goal was to metabolically engineer the anabolic pathways of Trp in the budding yeast for the enrichment of the intracellular Trp pool. By combining the biosynthetic pathway with the recombinant yeast, the titer of psilocybin will be quantified, which acts as an indicator for the changing of intracellular Trp after genetic modifications.

Results

2.1 Development of a heterologous expression platform for multigene expression

Multiple genes assembly for heterologous expression was feasibly achieved by our smart cloning strategy based on the designed plasmid, namely, pV2A-T (please see Methods and Materials Section 4.2.1.2). It was built for four primary purposes: 1) a flexible assembly of requested genes; 2) co-expression of multi-genes with only one promoter/terminator and one selective marker; 3) reliable fluorescence-based screening of completed ectopic integration and expression of genes; 4) and separation of the residual tag from expressed protein.

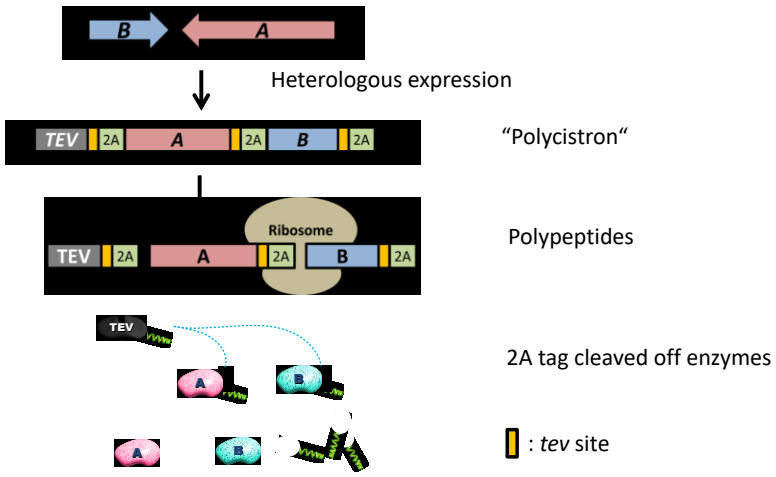

Fig. 3. The machinery of the 2A C-terminal tags that need to be removed from enzymes after translation. In the 2A system, each essential gene is assembled with the *tev* site and the sequence coding 2A peptide. The artificial polycistron is transcribed in the heterologous host, and 'cleavage' of polypeptides is done by the ribosome "stop-carry on" manner, which is triggered by the 2A peptide. Subsequently, the attached 2A tag is cleaved from each key enzyme after translation.

The twice-repeated sequences encoding 2A peptides were spaced by one restriction site *Eco*RV, which allows the insertion of the target gene in this backbone vector. Two rarely used restriction sites *Pme*I and *Swa*I that were introduced directly near the 2A sequences and inside the antibiotic-resistant marker Kan^R, are supposed to assemble the bicistronic or the polycistronic construct in a repeatable manner (shown in Methods and Materials Section 4.2.1.2). This method was utilized successfully for multiple genes overexpression cases mentioned in this study. In the heterologous host, during translation, the ribosome processes the "stop-carry on" machinery, by which polypeptides are formed (**Fig. 3**). Afterwards, the linear epitope, termed *tev* cleavage site (ENLYFQG), can be recognized by

the *tobacco etch virus* (TEV) peptidase (TEVp), which was co-produced with other key enzymes during translation. The cleavage occurs between Q and G (Kapust et al., 2001), in order to remove the attached 2A peptide.

2.1.1 Function of TEVp elucidated by immunoblot assay

The TEVp-mediated cleavage of 2A tag *in vivo* was primarily assessed in the model yeast *S. cerevisiae* by the use of immunoblot. In the host, *mRuby* and the TEVp coding sequence flanked by split-YFP fragments were co-expressed in the strain tSH18, which was compared with strains tSH16 and tSH17 that omit the gene coding TEVp (**Fig. 4A**). The tSH00 strain contains the empty vector pYES2 as an uracil prototrophic control strain. The anti-2A antibody was used to detect the remaining 2A peptide in total protein extracts of strains tSH00, tSH16, tSH17, and tSH18. Since it is unnecessary to introduce the *tev* site after *VenusN* in the design of the pV2A-T vector, the Venus-N is always fused with 2A tag *in vivo* after translation. Indeed, the band of Venus-N (~31 kDa) was detected from protein extracts of strains tSH16, tSH17, and tSH18 in the immunoblot (**Fig. 4B**), although the Venus-N band is relatively weak in the sample of tSH16. The sample of tSH17 shows a second significant band with a size of about 27 kDa equivalent to the mRUBY, which was not detected in the tSH18 protein extract sample as the 2A tags were removed from mRUBY proteins. This result proves the high efficiency of cleavage by TEVp *in vivo*.

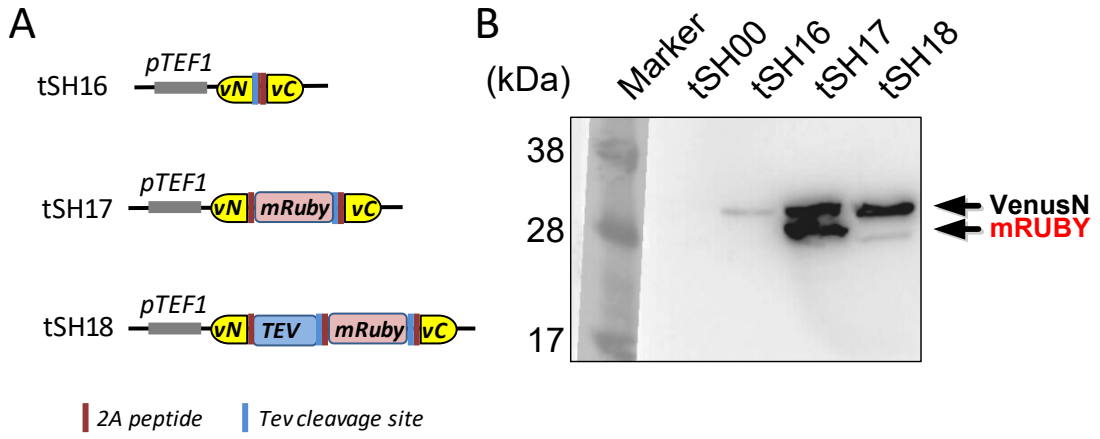

Fig. 4. 2A tag is cleaved off *in vivo* as known by western blot using anti-2A antibody. Figure modified from Hoefgen et al., 2018. (A) Shows the construction of each plasmid that was transferred into yeast BY4741 forming strains tSH16, tSH17, and tSH18. (B) Heterologously produced TEVp was not detected in tSH18 by western blot (theoretical molecular mass: ~27 kDa) reveals the 2A tag attached to itself can be obliterated, and the same is true for mRUBY. At the same time, the tSH17 failed to clean the C-terminal 2A peptide when the gene coding for TEV peptidase (*TEV*) is omitted in the polycistronic construct.

2.1.2 Joined Venus-N and Venus-C observed in the nucleus *via* fluorescence microscopy

One of the highlights in our heterologous expression platform is the YFP-based fluorescence screening system, in which the split-YFP, i.e., Venus-N and Venus-C subunits, can join when all the introduced genes are ultimately expressed from the beginning to the end without a break/stop in between and are translated (**Fig. 5**). A 34 residue leucine zipper motif (Magliery et al., 2005) was introduced to each subunit of split-YFP but in an antiparallel orientation: one leucine zipper domain (LZD) LzA is added at the C-terminus of VenusN, and the N-terminus of VenusC is modified by another leucine zipper helix B (LzB). Besides, the SV40 constitutive nuclear localization signal (NLS) (Kalderon et al., 1984) was additionally affiliated to the N-terminal part of VenusN and before LzB in the VenusC, separately.

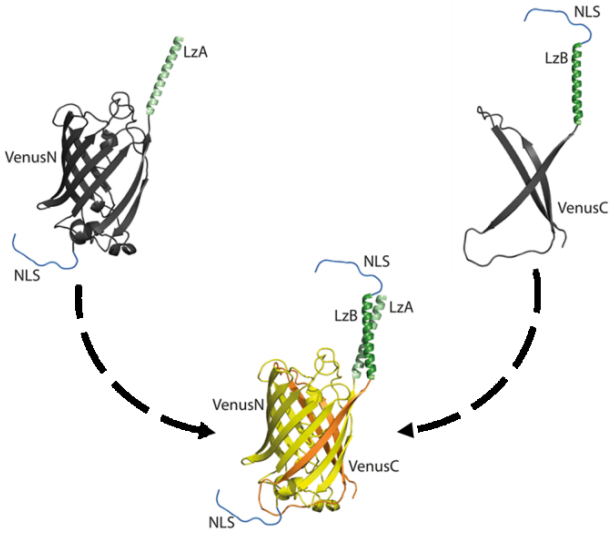

Fig. 5. Co-localization and dimerization model of split-YFP in the nucleus. Figure modified from Hoefgen et al., 2018. YFP was split between the eighth and the ninth beta-sheets to generate the N-terminus (VenusN) and C-terminus (VenusC). Both subunits co-locate in the nucleus, and this pair of Venus fragments can form the complete and functional YFP through two alpha-helices of leucine zippers, which have a dimer structure. Protein data bank (PDB) ID of YFP, LZD and NLS are listed respectively: 1yfp, 4dmd, and 4wv6.

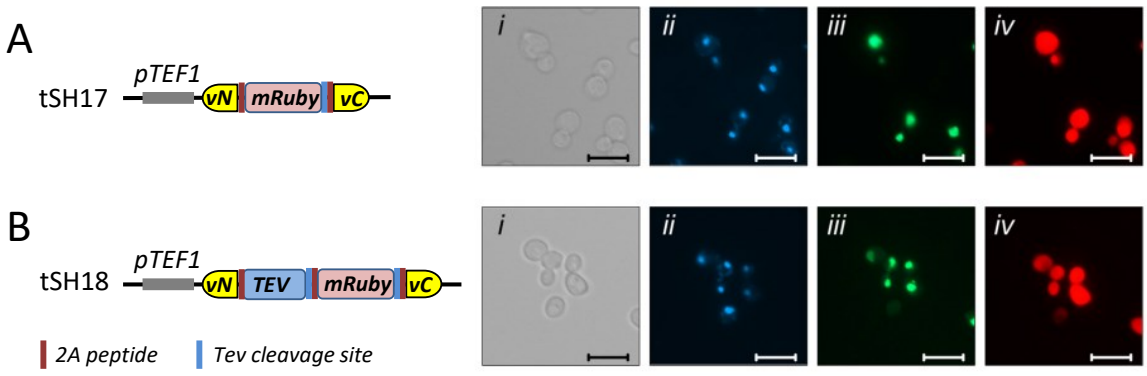

Fig. 6. Fluorescence scan for strain tSH17(A) and tSH18(B). Figure modified from Hoefgen et al., 2018. Comparing with the bright field (*i*), the Hoechst stain (presented in false blue color) indicates the position of nuclei in the yeast cells (*ii*). Using our developed heterologous expression method, the mRUBY and split-YFP proteins were produced completely and correctly in both strains, indicated by the accumulated YFP signal (*iii*; emission wavelengths of λ = 527 nm) in the nuclei (presented in false green color) and the red fluorescence (presented in false red color) suffuses in the cytoplasm (*iv*; emission wavelengths of λ = 605 nm). Scale bars: 10 µm.

Indeed, besides the immunoblot results, the Hoechst stained nuclei (**Fig. 6A** *ii* and **6B** *ii*) acted as the references for the YFP-fluorescent pictures of strains tSH17 and tSH18 (**Fig. 6A** *iii* and **6B** *iii*). This indicates the YFP-signals were observed only in the nuclei of yeast cells and the red fluorescence was pervaded the whole cells (**Fig. 6A** *iv* and **6B** *iv*). Compared with these two strains, a much weaker YFP signal was detected in the cells of strain tSH16 (result is not shown), which corresponds to the slight band of Venus-N shown in the line of strain tSH16 in the western blot. And the reason of this result is not clear.

2.2 Developed expression system tested by completing austinoids production in *A. nidulans*

The utility of this developed pV2A-T system in the eukaryotic host was verified by completing the austinoids production in *A. nidulans via* expressing four *aus* genes isolated from *A. calidoustus*, including *AusP*, *AusO*, *AusT*, and a large gene *AusV* (Mattern et al., 2017).

The *TEV* and *aus* gene cluster were constructed based on the pV2A-T assembling manner, as previously described, and formed a ~14.4 kb polycistronic construct including the genes of split-YFP subunits. The multigene expression in the strain NidtJL02 was controlled by the D-xylose-inducing promoter *xylP* (Zadra, 2000) in the host *A. nidulans*; *TEV* and genes for split-YFP in strain NidtJL01 were heterologously co-expressed under the control of a tetracycline-inducible promoter in the *Tet*^{on} system (Meyer et al., 2011) (**Fig. 7**). Since the *ArgB* was used as Arg auxotrophic marker for transformation-based ectopic integrations, strain NidtJL01 serves as the blank control, having an Arg prototrophic background.

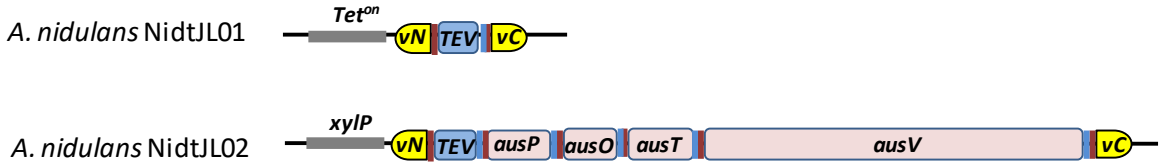

Fig. 7. Ectopic integration of polycistronic genes in *A. nidulans*. Strain NidtJL01, as the blank control, only has a *TEV* sequence and genes for the split-YFP subunits, which were constructed in the pV2A-T backbone and expressed under the control of the *Tet*^{on} promoter. NidtJL02 carries the *aus* gene cluster with *TEV* flanked by split-YFP genes, and the expression of these multiple genes is driven by the *xylP* promoter.

2.2.1 Fluorescence-based screening of NidtJL01 and NidtJL02 *A. nidulans* transformants

After the transformation of *aus* genes in the gDNA of *A. nidulans*, the obtained transformants of NidtJL01 (~30 colonies) and NidtJL02 (~20 colonies) were inspected by fluorescence microscope-based screening. Strain NidtJL02 showed only two positive

transformants (NidtJL02-V2 and V15), while strain NidtJL01 has more than twenty transformants exhibiting a yellow fluorescent signal. This phenomenon is reasonable, as we always observe that the longer polycistronic construct is more likely to be damaged than the shorter one during ectopic integration. Since the screening time using fluorescence microscopy was held to about one hour, this type of methodology is convenient regarding timesaving.

The positive transformants can easily be confirmed using fluorescence imaging, on account of the co-localization of Venus-N and Venus-C in the nuclei of fungi (**Fig. 8A**). The dot-like fluorescence only showed in the positive mutants (**Fig. 8A**, panels *v* and *vi*), while for the negative control strain RMS011, no fluorescence was detected. Additionally, this unique feature of fluorescence is distinguishable from the auto-fluorescence background in fungal mycelium.

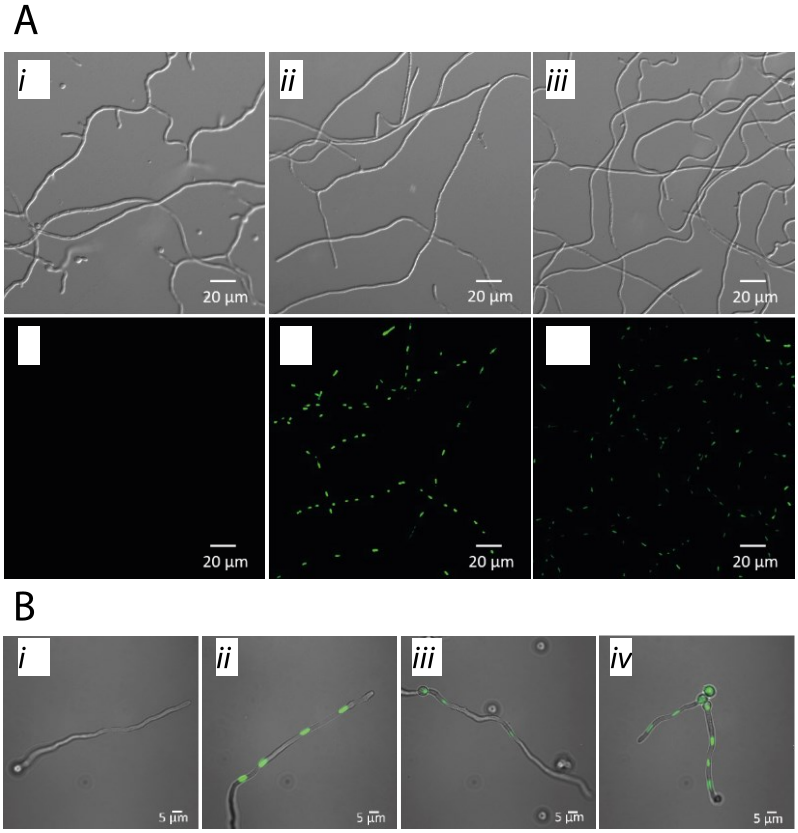

Fig. 8. Fluorescence microscopy imaging of strains RMS011, NidtJL01, and NidtJL02. The YFP fluorescent screening for mycelia grown on agar plates (A): The wild type (wt) strain RMS011 shows no fluorescence (panel *iv*) while the genetically modified *A. nidulans* strains with the correct integration of multiple genes exhibit particular fluorescence that only accumulates in the nuclei (panels *v* and *vi*). Panels *i*, *ii*, and *iii* are mycelia observed under bright field. Additionally, the merged images of the white light channel and light emissions at λ = 527 nm show mycelia grown in AMM broth (B): *i*) *A. nidulans* RMS011, *ii*) Positive control strain NidtJL01; different transformants V2 *iii*) and V15 *iv*) of strain NidtJL02, which harbors the *aus* gene cluster. The fluorescence is represented in false green color.

Fluorescence intensity varies among the positive transformants. The transformants of strain

NidtJL01 (**Fig. 8A**, panel *v*) with positive YFP signal showed a stronger fluorescence compared to the signal-positive transformants of NidtJL02 (**Fig. 8A**, panel *vi*). In NidtJL02, only two mutants showed significant nucleic localization visible as fluorescent dots (**Fig. 8B**, panels *iii* and *iv*), in which V15 has higher fluorescence intensity than V2. This variability of fluorescence intensity might be due to the different inducible promoters (*xylP* and *Tet*^{on}) that were used in the two strains, as well as the size of polycistronic genes that were inserted in the fungal genome.

2.2.2 Confirming the integration of the *aus* gene cluster in genomic DNA using southern blot

To assess the efficiency of YFP-based fluorescence screening, a southern blot experiment was performed, as confirmation for the *A. nidulans* RMS011 transformation with plasmid pJL009. Four probes were prepared to examine the correct integration of the long polycistronic construct carrying the *aus* gene cluster. The southern blot indicated that each V2, V3, or V15 transformant individually obtains a single copy of pJL009 in its genome (**Fig. 9B**). Note, too, that only V2 and V15 exhibit YFP fluorescence, while the V3 mutant did not show any signal. This result confirmed the fluorescence-positive mutants.

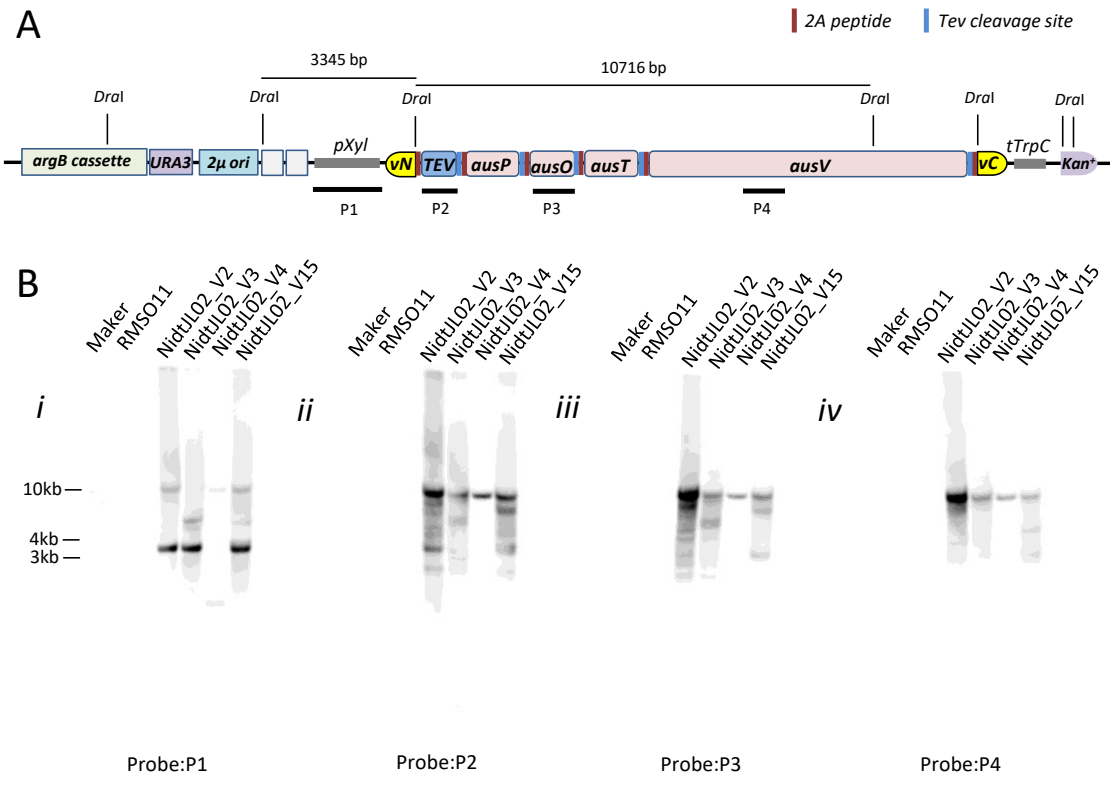

Fig. 9. Southern blot analysis of *A. nidulans* mutants of strain NidtJL02. (A) Schematic map of linearized pJL009 plasmid, in which multiple *Dra*I restriction sites are marked. In the graph, the probes are indicated with a black bar, *Venus N* (*vN*), and *Venus C* (*vC*) are showing in yellow. The other genetic features, like *argB* cassette, *URA3*, *Kan*^{R}, and yeast *2μ* origin of replication (*ori*) sequence, are also presented. The expected size of DNA fragments detected by the probe P1 is

3345 bp, and for the DNA sequence, which can hybridize with probes P2, P3, and P4 is about 10 kb. Two fluorescence-negative transformants V3 and V4 were picked together with the signal-positive mutants V2 and V15 for the test. The extracted gDNA of these four mutants was digested with *Dra*I, and blotting, was hybridized with four probes (B) which detect *i*) the *xylP* promoter, *ii*) TEVp coding gene, *iii*) *ausO* , and *iv*) a part of *ausV*. The left lane of (B) is the 1kb marker (Bioline, Germany).

2.2.3 Production of austinoids detected by HRMS

As described in the introduction part (Section 1.1.1), compared to *A. calidoustus*, the fungus *A. nidulans* carries a similar austinoid metabolic pathway, yet the latter one is missing *ausP, ausO*, *ausT*, and *AusV* (Valiante et al., 2017). Based on the machinery of split-YFP screening, the transformed mutant with a positive fluorescent feature is expected to produce the enzymes AusP, AusO, AusT, and the PKS AusV, and these enzymes can complete the biosynthetic pathway of austinoid in the host *A. nidulans* (**Fig. 10A**). The YFP-fluorescence positive mutants V2 and V15 of strain NidtJL02 were cultured in the complex medium supplied with inducer D-xylose (Mattern et al., 2017). Compared with the negative control strain NidtJL01, these two mutants produced the extended compounds 1-6 (**Fig. 10B**). However, the last compound calidodehydroaustin (7) was not detected, probably because the precursor compound precalidodehydroaustin (6) was significantly lower compared to the amount it was detected in the previous report (Mattern et al., 2017), in which the final product was detected.

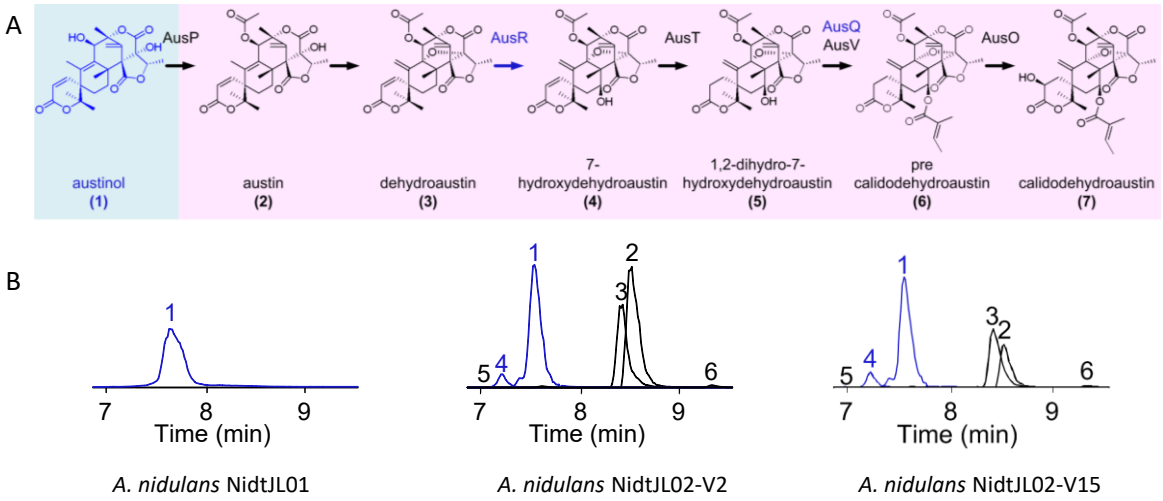

Fig. 10. Extended austinoid metabolic pathway through heterologous expression of *ausP*, *ausO*, *ausT*, and *ausV*. Figure modified from Hoefgen et al., 2018. (A) Austinoid metabolic pathway ends with austinol (1) in *A. nidulans*; while the heterologous expression of additional *aus* genes can reconstitute the further steps that exist in the fungus *A. calidoustus* and produce the other meroterpenoids (compounds 2-7). Domestic enzymes in *A. nidulans* are marked with blue color, and the introduced enzymes are indicated in black color. (B) Merged extracted ion chromatograms (EICs) of strains NidtJL02 (V2 and V15) and NidtJL01 are shown. Observed *m/z* $[M + H]^+$ of compounds 1-6 (list in **Table 1**) correspond to the peaks 1-6 in the EICs.

What is noteworthy is that the emerging intermediates 2 to 6 indicate the AusP activity was

maintained after removing the 2A tag at the C-terminal site by TEVp *in vivo*. Moreover, the transformant NidtJL02-V3 showing a positive result in the southern blot assay cannot produce the compound 6 overall (data not shown), likely because the PKS gene *ausV* was not expressed correctly.

Table 1. The exact masses of austinoids detected in the strain NidtJL02

Compound	Chemical Formula	Expected *m/z*	Observed *m/z*
Austinol **1**	$C_{25}H_{31}O_8$	459.2018	459.2011
Austin **2**	$C_{27}H_{33}O_9$	501.2124	501.2110
Dehydroaustin **3**	$C_{27}H_{31}O_9$	499.1968	499.1955
7-Hydroxydehydroaustin **4**	$C_{27}H_{31}O_{10}$	515.1917	515.1906
1,2-Dihydro-7-hydroxydehydroaustin **5**	$C_{27}H_{33}O_{10}$	517.2073	517.2056
Precalidodehydroaustin **6**	$C_{32}H_{39}O_{11}$	599.2486	599.2479
Calidodehydroaustin **7**	$C_{32}H_{39}O_{12}$	615.2436	Not detected

This rewired biosynthetic pathway of austinoid in the heterologous host *A. nidulans* demonstrates the practicability of this developed platform, by which the correct assembly and expression of the polycistronic construct, even with the long size of gene like *ausV* (~8.1 kb), can be achieved. The TEVp-associated cleavage was proven to restore the activity of the expressed enzymes in *A. nidulans*, and the split-YFP technique minimizes the false positive results shown in the southern blot assay.

2.3 Heterologous production of psilocybin in filamentous fungi

In nature, the psilocybin quantity in the fruiting body varies between 0.5~2% dry weight among twenty-three mushroom species (Mahmood, 2013). To obtain this valuable prodrug in a more straightforward manner, several methodologies have been previously established, including total synthesis and enzymatic catalysis *in vitro* (Fricke et al., 2019). Nevertheless, a more suitable, controllable, and scalable method is always needed for such a useful bioactive compound. Especially a strategy like pharmaceutical fermentation is more adaptable to fit the good manufacturing practice (GMP) guidelines, which is preferable for the industry.

For a broader application of this developed pV2A-T system, we transferred the psilocybin biosynthetic pathway from the higher fungus *P. cubensis* entirely into the mold *A. nidulans*. In this case, the psilocybin can be simply produced heterologously, using convenient shaking cultures. The cDNA of four essential genes encoding PsiH, PsiD, PsiK, and PsiM (Fricke et al., 2017) were assembled into the pV2A-T expression system as a polycistronic construct, namely pJF36. The expression of this *psi* gene cluster was regulated by the tetracycline-induced Tet^{on} promoter (Meyer et al., 2011). After the genetic transformation of *A. nidulans* with pJF36, the expression of the polycistron can be turned

on by adding doxycycline (Dox), which is the analogue of tetracycline.

2.3.1 Positive mutants indicated by YFP fluorescence signal

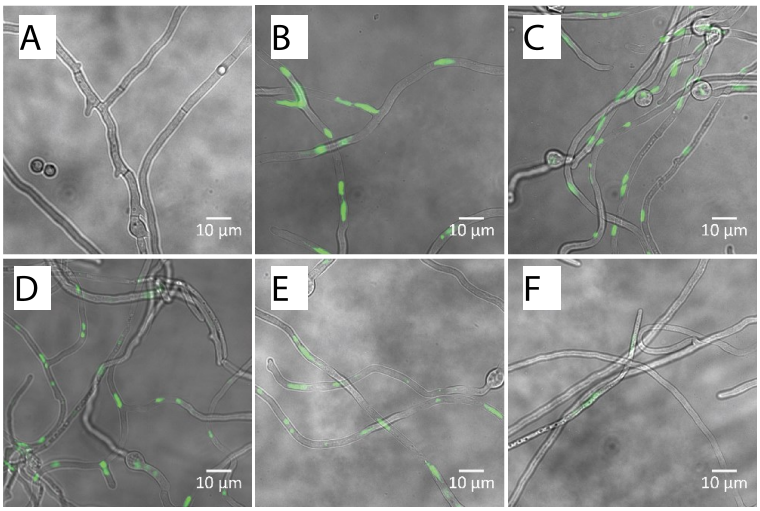

Fig. 11. Fluorescence screening of the psilocybin-producing strain NidtJF03. *A. nidulans* host strain RMS011 (A) is the negative reference for the positive mutants 1-5 (B-F) of NidtJF03. The overlapping images show the merged channels of bright light and light emissions at λ = 527 nm. The fluorescence is presented in a false green color.

Since previous experiments have confirmed the efficiency of split-YFP subunits, the only further screening required for the obtained *A. nidulans* recombinants of NidtJF03 was YFP-based fluorescence microscopy. Because the size of the psilocybin gene cluster construct is smaller (~7.4 kb) compared with the austinoid gene cluster, the number of positive mutants was more - five out of twenty-four showed fluorescence (**Fig. 11**, **B-F**). Although all of these five transformants had the positive signal, the signal intensity varied. The first mutant exhibited the highest intensity (**Fig. 11B**), while the fourth and the fifth presented weaker patterns (**Fig. 11E** and **11F**).

2.3.2 Quantification of psilocybin based on standard curves

All five fluorescence-positive mutants of NidtJF03 were first grown in a medium with Dox supplied as an inducer for psilocybin heterologous production. Each methanol-extracted sample was injected in ultra-high-performance liquid chromatography (UHPLC) for chromatographic analysis. The observed curves can be seen in **Fig. 12A**. Mutants NidtJF03_1, NidtJF03_3, and NidtJF03_5 had a higher yield of psilocybin compared to the other transformants, stating that fluorescence intensity is not directly related to the amount of product generated. This phenomenon was also shown before in the austinoids production strain NidtJL02, in which the mutant V2 performed better compared to V15 (**Fig. 10B**), yet the latter presented the stronger fluorescence signal (**Fig. 8B**).

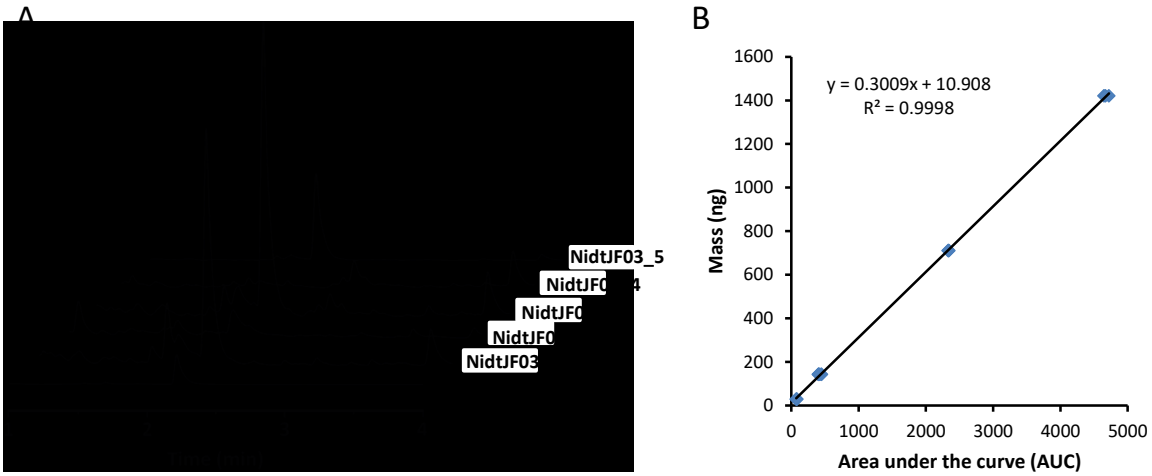

Fig. 12. Psilocybin quantification method. (A) Chromatographic analyses of five positive mutants (1-5) of *A. nidulans* NidtJF03 (Figure is modified from Hoefgen et al., 2018). After cultivation in AMM medium under shaking conditions, the five fluorescence-positive transformants were chosen for the psilocybin extraction, which was analyzed using UHPLC. The chromatograms were extracted at λ = 280 nm, showing the peaks corresponding to psilocybin, which is marked with a dashed line at 2.2 min retention time, referring to the authentic standard. The area under the curve (AUC) of the psilocybin standard corresponds to 70ng. (B) Established standard curve of psilocybin for quantification.

To quantify the titer of psilocybin heterologously produced in *A. nidulans*, a standard curve was generated using authentic psilocybin (**Fig. 12B**). Among all the mutants we obtained, in this measurement, the best producing strain NidtJF03_3 yielded psilocybin at a level up to 110 mg/L, equivalent to 1.5% of dry mycelial mass weight (15.4 mg/g) (**Fig. 13D**). Baeocystin, the precursor of psilocybin, was also measured, and the titer is marginally lower than the amount of psilocybin (data not shown). The *m/z* values of psilocybin and baeocystin were checked by high-resolution mass spectrometry (HRMS), and only a trace amount of psilocybin was detected in the culture of strain NidtJF03 in the absence of Dox (**Fig. 13B**), verifying that the *Tet*^{on} system is turned off under non-inducing conditions.

This is the first report of psilocybin being heterologously produced in a filamentous fungus at such a high titer, at that time, without any optimization. As opposite to the chemical synthesis and enzymatic production, using microorganisms to process psilocybin under fermenting conditions from relatively simple biochemical precursors, e.g. Trp, provides an advantage for reproducible and scalable manufacturing, which can be controlled and optimized in the further steps.

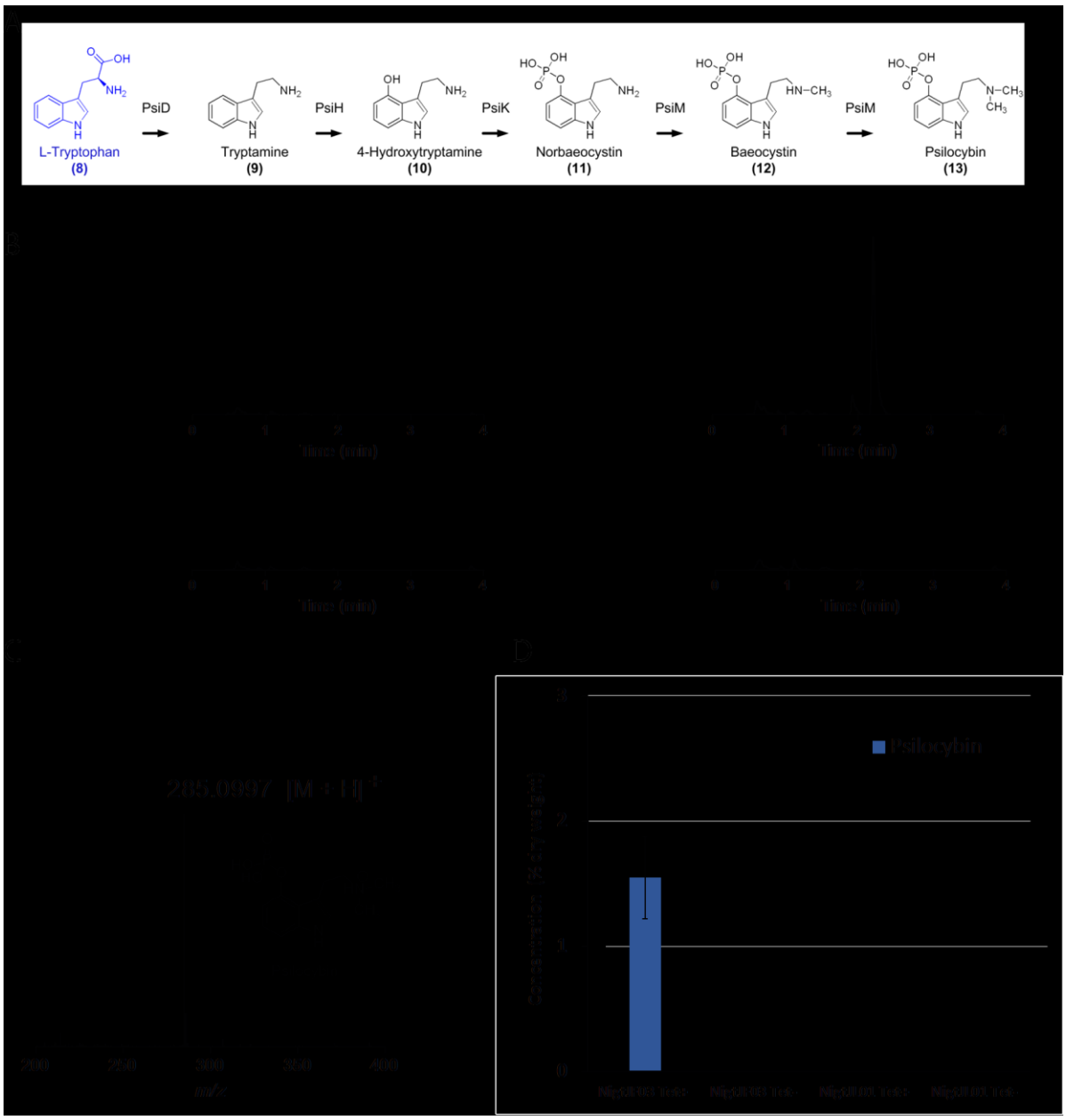

Fig. 13. Heterologous production of psilocybin in *A. nidulans*. (A) Identified biosynthetic pathway of psilocybin in *P. cubensis*. The precursor Trp is indicated in blue color. (B) The blank strain NidtJL01 and psilocybin-producing strain NidtJF03 were both cultured in AMM medium under *Tet*^{on}-inducing conditions (*i* and *iii*) and the non-inducing condition (Tet-; *ii* and *iv*). The DAD chromatograms were extracted at λ = 280 nm. The peaks reflect the compound baeocystin (12) and our target product psilocybin (13) with the exact mass *m/z* 285.0997 $[M + H]^+$ detected using HRMS shown in positive mode (C). (D) Produced psilocybin (13) calculated in relative concentrations (% dry mycelial mass weight) for the two strains NidtJL01 and NidtJF03 grown in Tet+ and Tet- conditions as described above. The error bar represents the standard deviation.

2.4 Budding yeast engineered as a cell factory for production of Trp-derived psilocybin

Utilizing our developed heterologous expression system, in the convenient shaking culture, filamentous fungus *A. nidulans* achieved a high yield of psilocybin. However, to develop a more simplified and environment-friendly, yet alternative strategy for *in vivo* biosynthesis

of this valuable pro-drug with a higher titer is very meaningful. In this advanced project on Trp-derived biosynthesis, we harness an even simpler model organism as a cell factory - the budding yeast *S. cerevisiae*. Not only is yeast a simple microorganism that has been used for fermentation throughout history and easy to clean after manipulation in the industry, but it is also a eukaryotic species capable of synthesizing SMs.

Psilocybin biosynthesis originates from Trp (**Fig. 14C**). Avoiding Trp degradation in order to enrich its intracellular pool in *S. cerevisiae* is our strategy. Besides for protein synthesis, Trp is effused through Ehrlich and kynurenine (KYN) bypasses in *S. cerevisiae* (**Fig. 15**) (Dickinson et al., 2003; Panozzo et al., 2002; Toyn et al., 2000). A century before, Ehrlich proposed the catabolism of amino acids through transamination, decarboxylation, and reduction/oxidation (Ehrlich, 1907). Indeed, one way of Trp degradation *via* indole-3-pyruvate perfectly fits this theory. Among the predicted aminotransferases (AATs) in yeast, namely Aro8, Aro9, Bna3, Bat1p, Bat2p, and Yer152Cp, Aro8 and Aro9 play the dominant roles in the first transamination using glucose as a carbon source, which was revealed by several studies in the evaluation of gene expression levels, catalytic activity and cell growth (Hazelwood et al., 2008; Rząd et al., 2017).

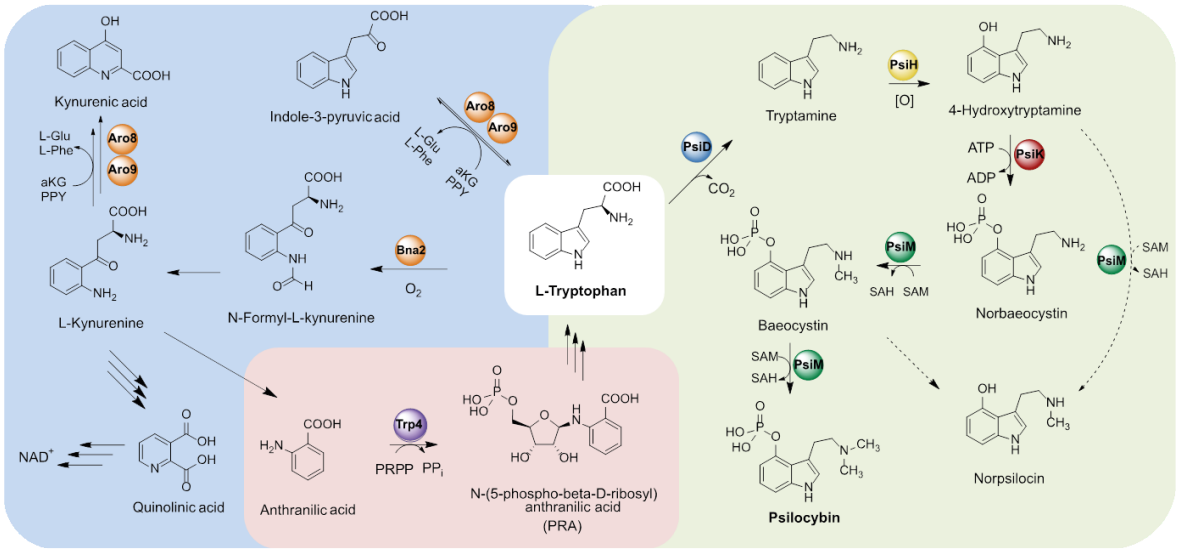

Fig. 14. Schematic and simplified overview of Trp catabolism and metabolism. (A) In yeast, two degradative pathways were relatively well-studied in Trp catabolism, among which the aminotransferases Aro8 and Aro9 catalyze the deamination of Trp to generate the indole-3-pyruvic acid, as well as involve in the KYN pathway to catalyze an irreversible deamination of KYN to KA (Ohashi et al., 2017). In this pathway, the indoleamine 2,3-dioxygenase Bna2 catalyzes the first step of this KYN pathway (Panozzo et al., 2002). (B) Besides, the KYN pathway also supplies the *de novo* NAD^+ synthesis through quinolinic acid, and this pathway contains a branching point towards anthranilate that is the precursor of the biosynthesis of Trp, in which Trp4 catalyzes the first essential step (Kurnasov et al., 2003; Toyn et al., 2000). (C) With four key enzymes PsiD, PsiK, PsiH, and PsiM, psilocybin is derived from Trp. The dashed lines indicate the minor production of norpsilocin, which is either spontaneously dephosphorylated from baeocystin or enzymatically formed from the 4-hydroxytryptamine in the shunt steps. L-Glu: glutamic acid; Phe: L-phenylalanine; αKG: α-ketoglutaric acid; PPY: Phenylpyruvate; NAD^+: oxidized form of

nicotinamide adenine dinucleotide; PRPP: 5-phospho-α-D-ribose-1-diphosphate; PPi: Diphosphate; SAH: *S*-adenosyl-L-homocysteine; SAM: *S*-adenosyl-L-methionine.

As opposite to the other AATs, Aro8 and Aro9 are classed as aromatic amino acid aminotransferase I and II with a broad-substrate specificity (Hazelwood et al., 2008). Especially Aro8 has shown activity towards L-lysine (Lys), L-histidine, and three aromatic amino acids in the yeast *Candida albicans* (Rząd et al., 2017). Interestingly, the same research also discovered a concentration-dependent catalyzing phenomenon - Aro8 and Aro9 (typically for Aro9) mainly function in the catabolism when corresponding amino acids as present in a high concentration.

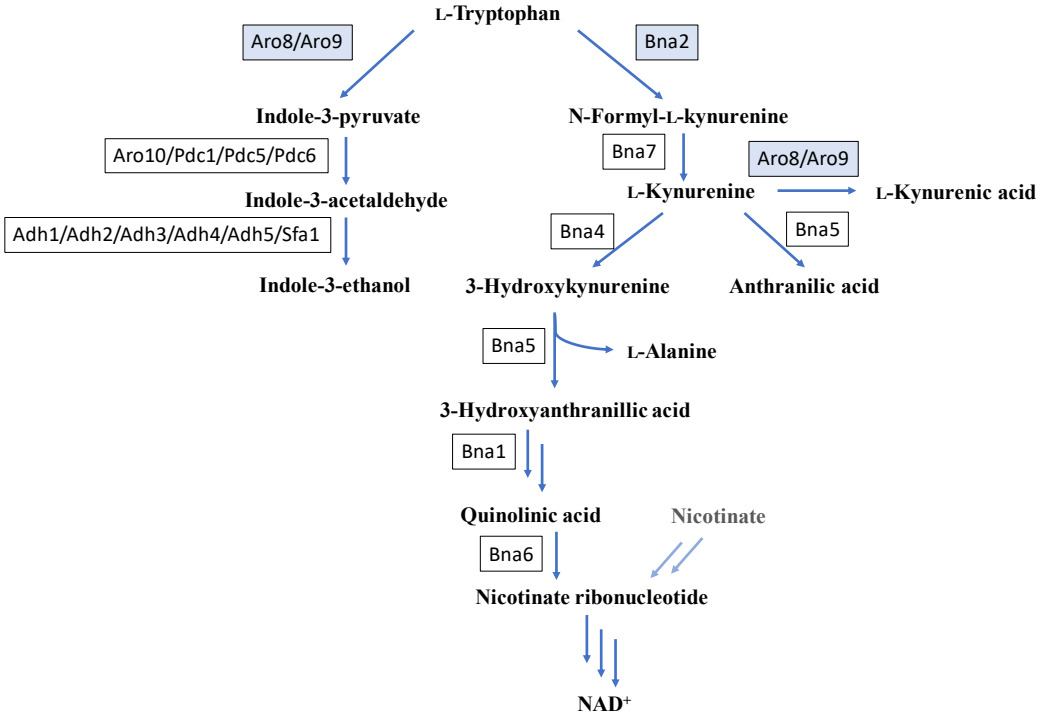

Fig. 15. Schematic view of the Ehrlich pathway and kynurenine bypass in *S. cerevisiae* for Trp degradation. The catabolism of the aromatic amino acid Trp leads to the formation of 'fusel alcohol' (the mixture of several alcohols) and the biosynthesis of NAD^+, the latter one is also incorporated by nicotinic acid (Dickinson et al., 2003; Ohashi et al., 2017; Panozzo et al., 2002). The correlated enzymes are marked by a black frame.

Additionally, the functions of these two AATs have been proven in the KYN degradation pathway for kynurenic acid (KA) construction (**Fig. 15**) (Ohashi et al., 2017). Panozzo *et al.* (2002) discovered a series of Bna enzymes in the KYN pathway, where Bna2 as an indoleamine 2,3-dioxygenase (IDO) catalyzes the first step.

Based on this knowledge, a debranching design for Trp accumulation in yeast targeted and destroyed the AATs and IDO, i.e., Aro8, Aro9, and Bna2, in the first step of both degrading processes (**Fig. 14A**).

2.4.1 Diagnostic PCR confirms the deletion of *ARO8* and *BNA2*

In our deletion strategy, based on homologous recombination, the genes required to be deleted were replaced by autotrophic marker genes (*LEU2* and *HIS3*), which have various sizes. Each deletion event was checked by diagnostic PCR using specific primer pairs, and the amplified DNA fragment band was contrasted to the band generated from the negative control strain (**Fig. 16**). Through amplification of specific DNA fragments, PCR can detect genetic mutation(s), e.g., deletion and insertion, and reveal their positions and sizes *via* electrophoresis (Karim, 2019).

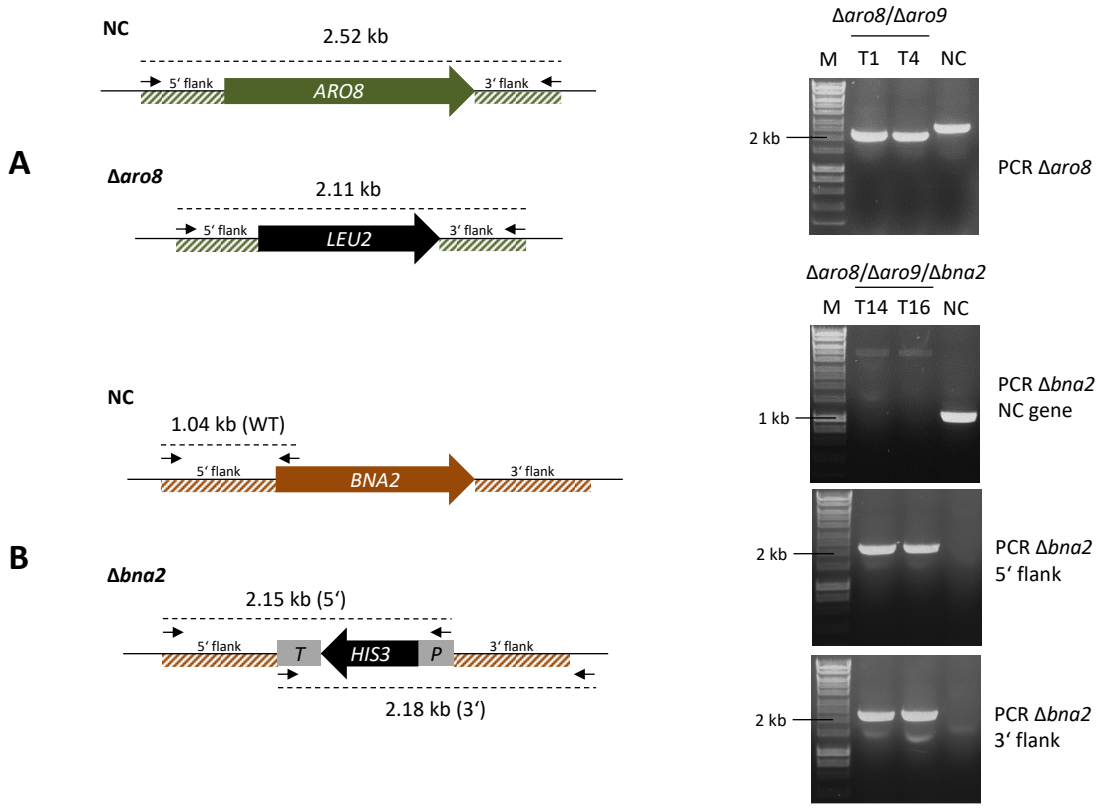

Fig. 16. Diagnostic PCR strategies and electrophoresis gel results to confirm the *ARO8* and *BNA2* deletions. (A) Δ*ARO8_LEU2* fragment (2.11 kb) was amplified from colonies of the Δ*aro8* strain in the colony PCR, which contrasted with the DNA fragment (2.52 kb) amplified from the negative control (NC) strain. The visible bands with different sizes were observed in the electrophoresis gel picture, indicating the *ARO8* gene was deleted in both colonies T1 and T4 of strain YtSJ01. (B) To check the Δ*bna2* feature in the Δ*aro8*/Δ*aro9* background, three pairs of primers were utilized. The reverse primer of the first pair specifically attaches to the sense strain of *BNA2*; hence, one band (~1 kb) shows up in the gel picture regarding the NC. The second or third pair of primers can only be used to obtain the *HIS3* with 5' flanking region or with 3' flanking region, correspondingly. Indeed, the bands generated from positive transformants T14 and T16, yet not shown in the NC, prove the successful construction of the triple deletion strain YtSJ02.

When the length of the introduced marker gene significant differs from the deleted gene, i.e., *ARO8* and *LEU2*, the site-directed deletion event was confirmed only using the outer primer pair (**Fig. 16A**) in the PCR setup. Alternately, after *HIS3* replaced *BNA2*, the sizes of the newly inserted DNA fragments were similar to the original genes. To detect the

transformants with correct deletion events in this situation, we designed primers which specifically bind to the target genes for the PCR diagnosis (**Fig. 16B**). The obtained gel electrophoresis pictures confirmed that the transformants T1 and T4 of strain YtSJ01 (Δ*aro8*/Δ*aro9)*, as well as the transformants T14 and T16 of strain YtSJ02 (Δ*aro8*/Δ*aro9*/Δ*bna2*) are carrying the proper deletion features.

2.4.2 Strain with Δ*aro8*, Δ*aro9*, and Δ*bna2* is sensitive towards Trp

Constructed strains YtSJ01 (Δ*aro8*/Δ*aro9*) and YtSJ02 (Δ*aro8*/Δ*aro9*/Δ*bna2*) together with the commercial yeast strains BY4741 (wt), Y01965 (Δ*aro9*), Y04569 (Δ*aro8*), and Y02556 (Δ*bna2*) were assessed using various concentrations of Trp. Since the Trp degradation capacity is deficient at different degrees among these strains, we investigated whether the YtSJ01 and the YtSJ02 were sensitive to a higher amount of Trp supplied in the medium based on the exhibited phenotype.

Consequently, a single *ARO9* deletion resulted in a mutant more sensitive to elevated Trp concentrations (>5 mM) when compared to other single deletions of *ARO8* or *BNA2*. The concomitant deletion of *ARO8* in the Δ*aro9* background even enhanced this sensitivity (**Fig. 17**). This observation confirmed a previous study (Ohashi et al., 2017) showing that Aro8 and Aro9 are the dominating enzymes acting to detoxify excessive Trp in the cell. Especially, compared to Aro8, the effect of Aro9 in the detoxification of excess Trp is stronger.

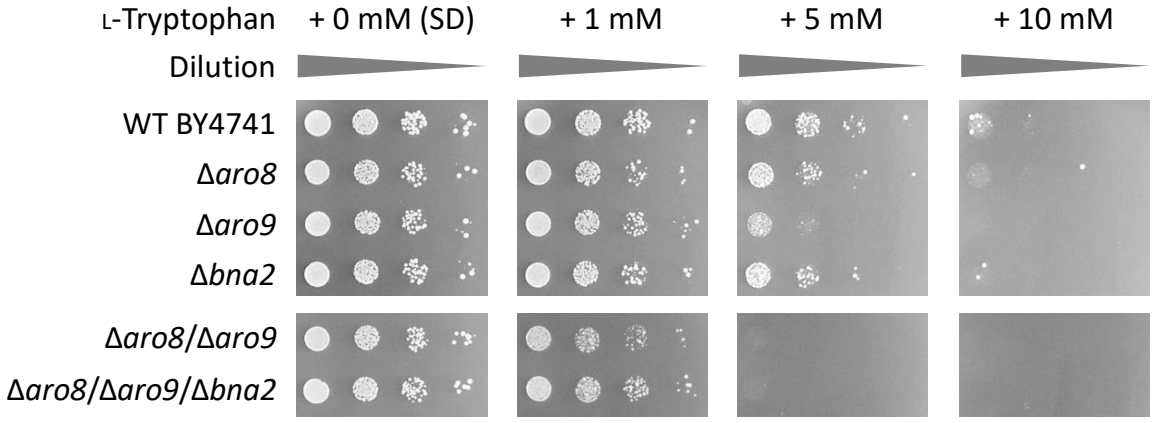

Fig. 17. Growth phenotype of Trp catabolism deficient mutants. The indicated cells were grown for 3 days in the absence or presence of Trp in a concentration gradient: 1 mM, 5 mM, and 10 mM. The commercial yeast nitrogen base that was used for synthetic defined (SD) agar preparation contains nicotinic acid; therefore, the Δ*bna2* strain is viable in the assay plates. Two independent colonies of Δ*aro8*/Δ*aro9* mutant and Δ*aro8*/Δ*aro9*/Δ*bna2* mutant were both tested, but due to the identical phenotype they show, only one colony of each strain is presented in the figure.

Yet, the previous study did not construct and test the triple mutant Δ*aro8*/Δ*aro9*/Δ*bna2*. In this assay, there is only a slight distinction of phenotype between double deletion strain

and triple deletion strain. From the result, the abolished Bna2 in the triple deletion mutant allowed for slightly better growth than the double mutant Δ*aro8*/Δ*aro9*. The Trp breakdown through the KYN pathway is initiated by the heme-dependent indoleamine 2,3-dioxygenase Bna2 (Panozzo et al., 2002). Bna2 converts the Trp to *N*-formyl-L-kynurenine, which is required for anthranilate production in intracellular Trp biosynthesis. Therefore, I assume that this additional *BNA2* deletion not only attenuated the Trp catabolism but also minimized the intracellular supplement of Trp. In other words, the Trp level in the triple deletion strain might be slightly lower than in the double mutant strain Δ*aro8*/Δ*aro9* at a certain growth stage, i.e., in or after the stationary phase.

2.4.3 YFP-based fluorescence screening and PCR diagnosis of yeast transformants

The wt strain BY4741 and other genetically modified yeast strains that were transformed with the expression vector pJF34 or pJF77 need essential screening to obtain positive transformants. *Transcription elongation factor1* promoter (*TEF1p*) assembled in the plasmids allows the constitutive expression of the following genes without the need of an inducer.

The obtained transformants of each strain were screened first based on YFP-signal; only the colonies with the correct transcribed and translated polycistron showing the nucleic fluorescence (**Fig. 18A**) were picked for the further confirmation. Although we claimed that the YFP-based fluorescence screening is a feasible method to select positive transformants (Hoefgen et al., 2018), afterwards, we also observed that genes were removed from the polycistronic construct during transformation.

This problem is most likely due to the repeated 2A peptide sequences in the polycistronic construct, which could induce homologous recombination in the yeast. Hence, to avoid this case, all the fluorescence-positive colonies containing pJF34 or pJF77 were further analyzed *via* colony PCR. The plasmids pJF34 (**Fig. 18C**, *i*) and pJF77 (**Fig. 18C**, *ii*) were both constructed in the pV2A-T system for psilocybin heterologous production. pJF77 was constructed for the co-expression of gene *pcCPR* with the *psi* gene cluster, which is described in detail in Section 2.4.6. In the electrophoresis gel results, the colonies carrying the expected band were defined as the correct mutants (**Fig. 18C**), while a few of the others presented bands lower than the reference band indicated the negative mutants (data not shown). Two correct transformants of each yeast strain were selected for the psilocybin heterologous production.

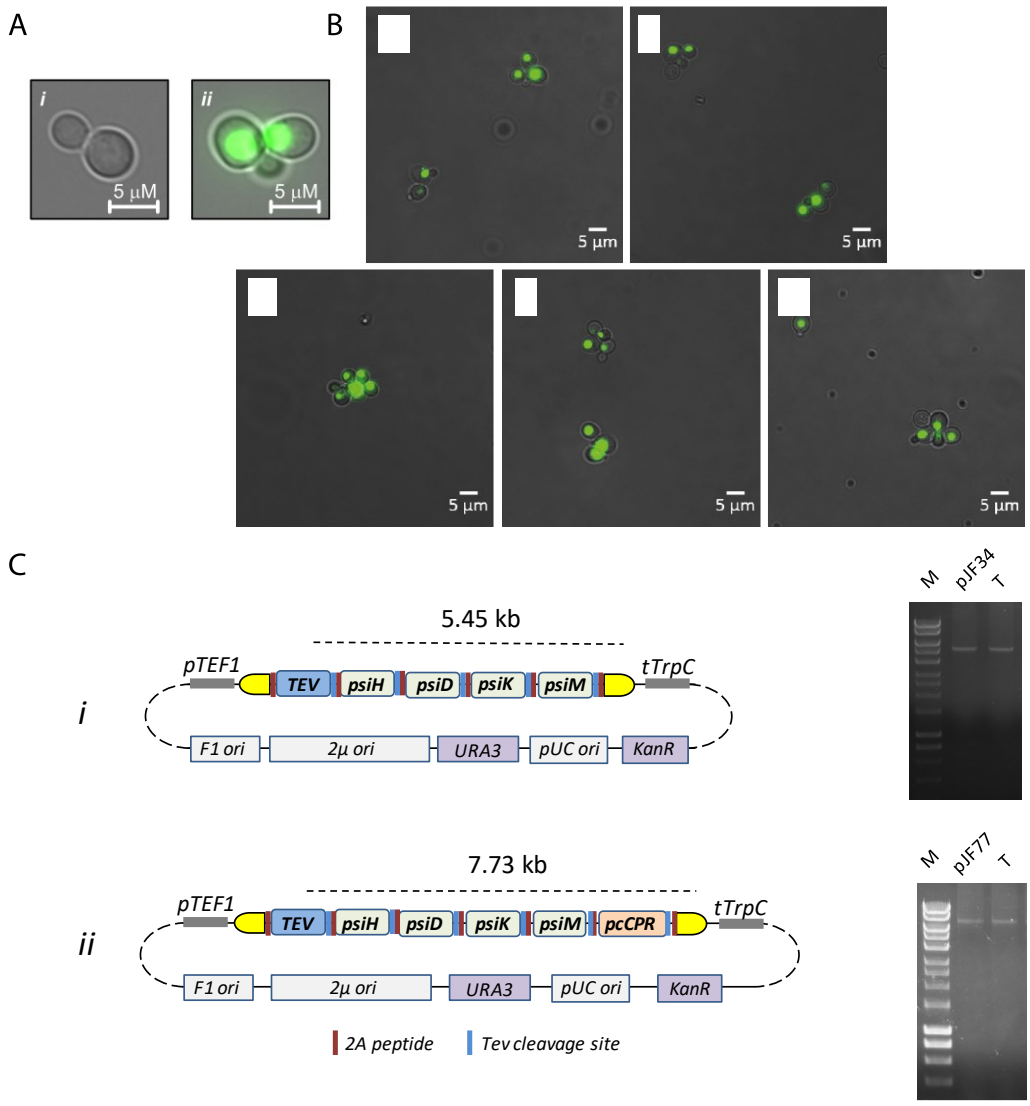

Fig. 18. YFP-based fluorescence screening and colony PCR applied to confirm the complete expression of polycistronic genes in the yeast strains. The fluorescence is represented in green false color. (A) The negative control strain is tSH00 (*i*) and does not show fluorescence, while fluorescent nuclei (*ii*) indicate positive transformants when transformed with pFJ34. (B) As examples, the five fluorescence screening fields showed the merged channels of bright light and light emissions at λ = 527 nm for the fluorescence-positive yeast cells of strains YtSJ07 (*i*), YtJL04 (*ii*), YtJL06 (*iii*), YtJL08 (*iv*), and YtJL10 (*v*). (C) Colony PCR was adopted to check the integrity of the transformed plasmid. The expected band amplified from plasmid pJF34 (*i*) is about 5.4 kb, and the band generated from plasmid pJF77 is about 7.7 kb. The amplified band from each transformant was referred to the band shown in the plasmid lane (positive control). The gene drawn on the schematic diagram does not represent in the actual size scale. M: 1 kb marker (Bioline, Germany), T: lane of represented positive transformant.

2.4.4 Production of psilocybin in the triple deletion strain bearing Δ*aro8*/Δ*aro9*/Δ*bna2*

Before we quantified the yield of psilocybin in the yeast mutants, the authentic psilocybin, baeocystin, norpsilocin, and Trp had been measured using UHPLC-MS as a reference in order to standardize the related retention times (**Fig. 19**) and exact masses *m/z* $[M+H]^+$.

To learn more about the intracellular metabolic fluxes, we not only intended to quantify the titer of psilocybin but also to measure the psilocybin precursor, namely, baeocystin, the

shunt metabolite norpsilocin, the branch-point KYN and its derivative product KA in the Trp catabolism. So, besides the previously achieved standard curve of psilocybin (**Fig. 12B**), the other standard curves of baeocystin, norpsilocin, KYN, and KA, were generated (**Fig. 20**).

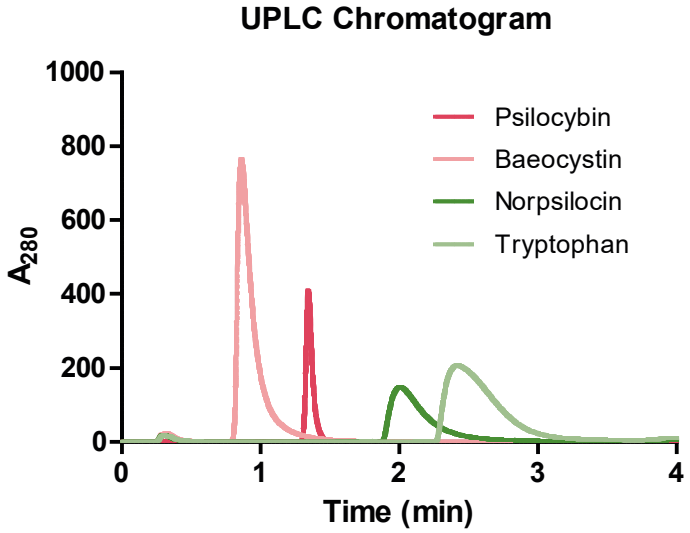

Fig. 19. Overlapped UHPLC chromatograms of psilocybin, baeocystin, norpsilocin, and Trp. 1 mM of each sample was injected and measured. The chromatograms were extracted at λ = 280.

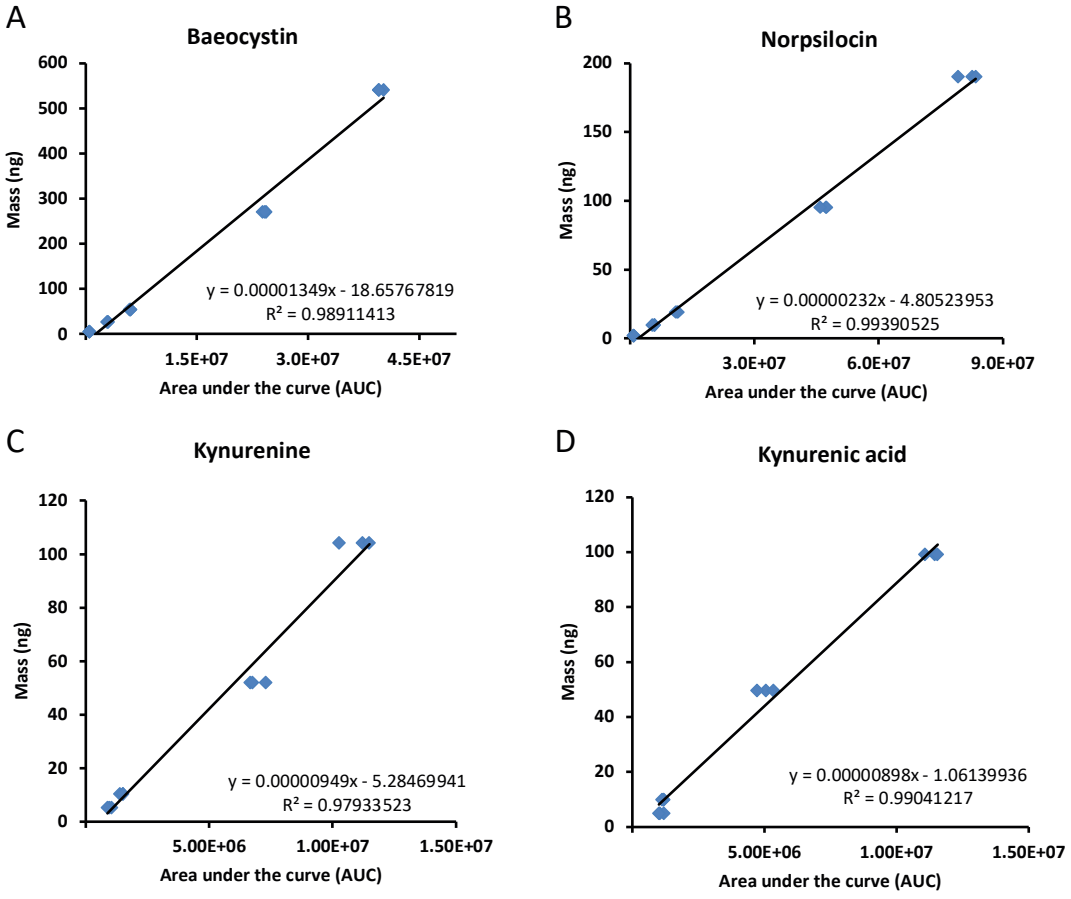

Fig. 20. Standard calibration curves of baeocystin, norpsilocin, KYN, and KA. The serially diluted solutions of the authentic compounds were injected in the UHPLC, and the related AUC in the chromatograms was measured to match the corresponding mass (ng) in the graph.

The yeast cell concentration in liquid culture can be monitored based on the optical density (OD) at λ = 600nm. In order to investigate whether the growth status of transgenic yeast strains (*S. cerevisiae* × pJF34) with Δ*aro8*/Δ*aro9* and Δ*aro8*/Δ*aro9*/Δ*bna2* genotype backgrounds are influenced when the intracellular Trp degradation is inefficient, the OD_{600} of the BY4741 strain, double mutant Δ*aro8*/Δ*aro9*, and the triple mutant Δ*aro8*/Δ*aro9*/Δ*bna2* were measured at different time points, i.e., 6 h, 24 h, and 48 h, during shaking cultivation.

The drawn graph roughly represents the growth curves of these strains (**Fig. 21**). The growth of Δ*aro8*/Δ*aro9* and Δ*aro8*/Δ*aro9*/Δ*bna2* mutants were more attenuated than the growth of wt BY4741, which indicates that the abolition of the Trp catabolic pathways might retard biomass accumulation.

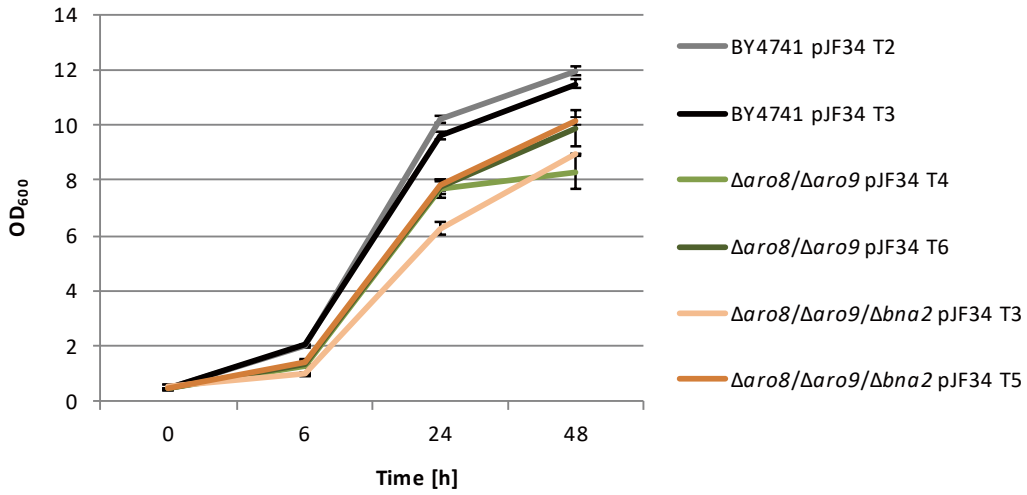

Fig. 21. The growth of yeast cultures in a minimal medium. Every two independent transformants of the BY4741 × pJF34 (YtSJ08), double mutant Δ*aro8*/Δ*aro9* × pJF34 (YtSJ06), and the triple mutant Δ*aro8*/Δ*aro9*/Δ*bna2* × pJF34 (YtSJ07), were grown in the uracil/uridine omitted SD medium (SD-Ura) with 1 mM Trp supplementation for 48 h under shaking conditions (180 rpm). The initial OD_{600} was 0.5. Three biological replicates were performed for each transformant, and the error bars represent the standard deviation.

In our pre-experiment for the incubation time of main cultivation, the wt BY4741 strain harboring the expression vector pJF34 were cultured for 24 h, 48 h, and 72 h, individually, and the titer of psilocybin was the highest in the extracted sample from the 48 h cultivation (data not shown). Therefore, we fixed the time of the main cultivation at 2 days for the psilocybin production in yeast.

The yeast cultivation is shown in Methods and Materials Section 4.5.2. The quantified psilocybin, baeocystin and norpsilocin were calculated in mg/g dry biomass and are shown in **Fig. 22**. In the analyzed result, the psilocybin titer in the Δ*aro8*, Δ*aro9*, and Δ*bna2* single deletion strains was virtually identical to that in the wt control. Contrary to this, the

yield of psilocybin increased to 46 mg/g biomass in the strain which has parallel deficiency for both *ARO8* and *ARO9*. The psilocybin production even prominently accelerated about five-fold more in the strain with additional repression of the Bna2-mediated catabolic pathway, and it reached a yield of 57±3 mg/g biomass (**Fig. 22**). Moreover, baeocystin production performed with a similar tendency among these strains. The accumulation of this psilocybin precursor was significantly enhanced in the double mutant Δ*aro8*/Δ*aro9* and the triple mutant Δ*aro8*/Δ*aro9*/Δ*bna2*. This phenomenon conforms to the expected consequence of disabled competition of Trp usage *via* *ARO8*, *ARO9*, and *BNA2* deletion. Curiously, as the shunt product, norpsilocin formation dropped down in all the gene-mutated strains compared to the wt BY4741, and it was lower than 0.2 mg/g biomass in the triple deletion strain. It suggests that, when the intracellular Trp is redundant, the trend of metabolic flux in the psilocybin biosynthetic pathway is more toward the production of the final compound, which has a relatively stable structure.

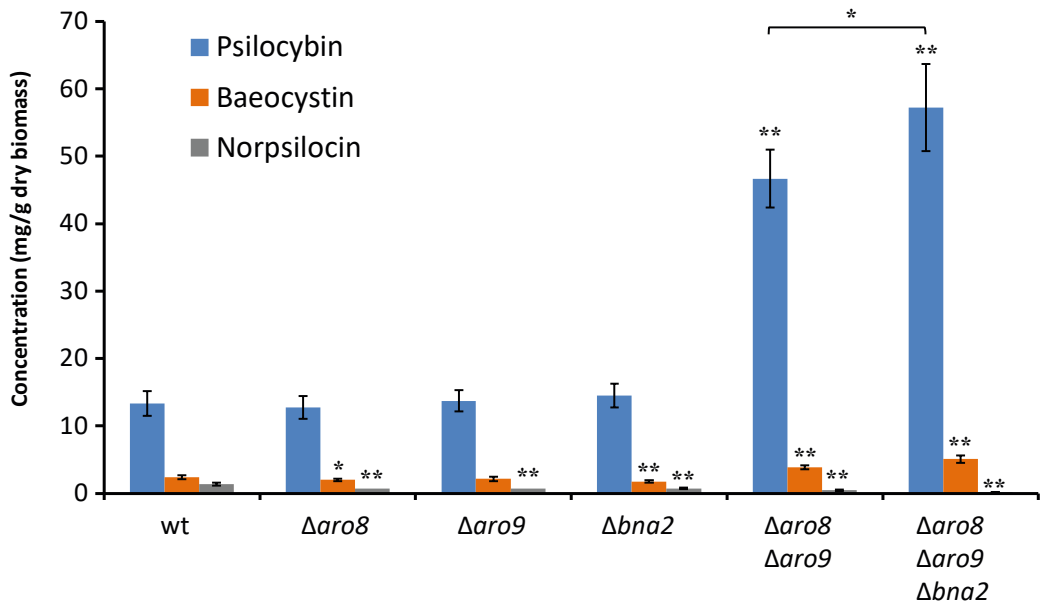

Fig. 22. Production of psilocybin, baeocystin, and norpsilocin in engineered yeast strains with repressed catabolism of Trp. The strains were grown in SD -Ura +1 mM Trp for 48 h, and error bars represent the standard deviation. The student's *t*-test (* = $p<0.05$, ** = $p<0.01$) was performed using two independent mutants and three biological replicates for each strain.

Additionally, the successful deletion of *ARO8*, *ARO9* or/and *BNA2* was proven by the quantified KYN and KA. The significantly decreased KA in the Δ*aro8* or Δ*aro9* single deletion mutant, as well as the undetectable KA in the strain Δ*aro8*/Δ*aro9*, verified that the formation of KA derived from KYN is catalyzed by both Aro8 and Aro9 that complement each other as AAT (**Fig. 23**). This obtained data of KA production is coincident to the result reported before (Ohashi et al., 2017). However, in this report, the production of

KYN in the strain Δ*aro8*/Δ*aro9* was about nine-fold higher than it was detected in the wt strain, which was not observed in our experiment (**Fig. 23**). The statistical analysis suggested that there is no significant difference between the wt strain and the strain with double deletion of *ARO8* and *ARO9* for the KYN amount. From my perspective, this observation might be due to the introduced psilocybin biosynthetic pathway in the yeast strain. We could presume that the more stringently Trp catabolism is blocked, the better the heterologous psilocybin pathway would function as the sole sink for this amino acid.

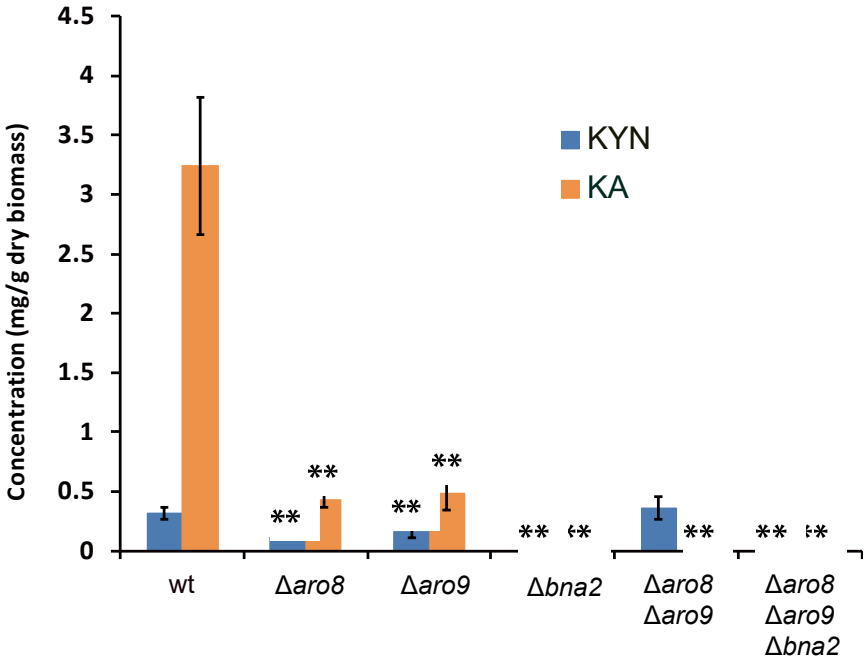

Fig. 23. Production of KYN and KA in engineered yeast strains with repressed catabolism of Trp. The strains were grown in SD-Ura + 1 mM Trp for 48 h, and error bars represent the standard deviation. The student's *t*-test (* = $p<0.05$, ** = $p<0.01$) was performed using two independent mutants and three biological replicates for each strain.

2.4.5 Biosynthesis of isotope-labeled psilocybin

As a valuable drug candidate, intensive pharmacological and physiological research of psilocybin has been ongoing recently, leading to an increased demand for a traceable version of this compound. Thus, it is worth to apply our yeast expression system to produce stable isotope-labeled psilocybin. Additionally, this specific application can provide a repeatable strategy for the labelling of other bioactive Trp-derived indole alkaloids with the highest chemical conversion efficiency. To construct the demanded strain that is only viable relies on the extracellular Trp supplement, we deleted the gene coding Trp4 (TrpD) enzyme, which catalyzes the phosphoribosylation of anthranilate *en route* to Trp (Miozzari et al., 1978; Toyn et al., 2000) (**Fig. 14B**). Therefore, the elimination of *TRP4* results in an auxotrophic strain and allows the yeast strain to take Trp

up only extracellularly.

In the beginning, we presumed that the Trp catabolism impaired strain Δ*aro8*/Δ*aro9*/Δ*bna2* with the fourth deletion of *TRP4* may produce the comparable titer of psilocybin as the amount shown in the previous test. However, in this quadruple deletion strain, both catabolism and metabolism of Trp are depleted, it is hard to conclude the consequence. Hence, we investigated the psilocybin production in both the quadruple deletion strain and *TRP4* single deletion strain compared to the yield from the Δ*aro8*/Δ*aro9*/Δ*bna2* triple mutant, which served as the positive control.

2.4.5.1 Diagnostic PCR confirms the deletion of *TRP4*

Applying the same strategy described in Section 2.4.1, the *TRP4* was replaced by the autotrophic marker gene *MET15*. The deletion event was checked by diagnostic PCR using specific primer pairs, followed by the treatment of restriction enzyme *Xba*I. The fragment bands were contrasted to the bands generated from the negative control strain (**Fig. 24**). The obtained gel electrophoresis pictures confirmed that the transformants T3 and T4 of strain YtJL07 (Δ*aro8*/Δ*aro9*/Δ*bna2*/Δ*trp4*) are carrying the proper deletion features.

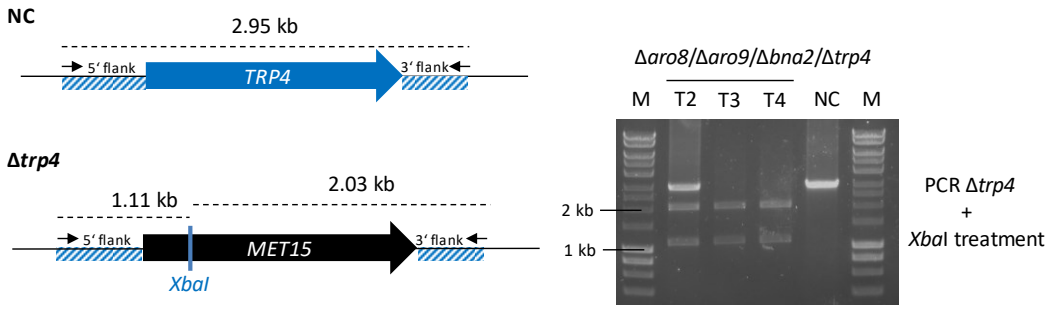

Fig. 24. Diagnostic PCR strategy and electrophoresis gel result to confirm the *TRP4* deletion. As an alternative method, restriction enzyme digestion of PCR-amplified DNA fragments was applied to control the deletion of *TRP4*, since the solo restriction site of *Xba*I exists in the auxotrophic marker *MET15* that was used to replace the *TRP4*. After restriction digestion of the PCR products, samples were loaded and run through an agarose gel, and bands were generated in the lanes of transformants T3 and T4, indicating the successful deletion of *TRP4*, while T2 has an additional upper band which is identical to the band shown in the NC.

2.4.5.2 Production of psilocybin in the Δ*trp4* strains

Not surprisingly, the amount of psilocybin in the Δ*aro8*/Δ*aro9*/Δ*bna2*/Δ*trp4* quadruple strain vastly dropped down, contrasted with it in the triple deletion mutant, yet it was still slightly higher than in the Δ*trp4* single mutant (**Fig. 25**). Likely, the repression of the Trp anabolic and catabolic pathways deplete the intracellular pool of Trp, thus lowering the Trp-derived product, psilocybin, although the supplied Trp in the culture medium was overloaded. Under these circumstances, we chose the Δ*trp4* single mutant for the further production of isotope-labeled psilocybin.

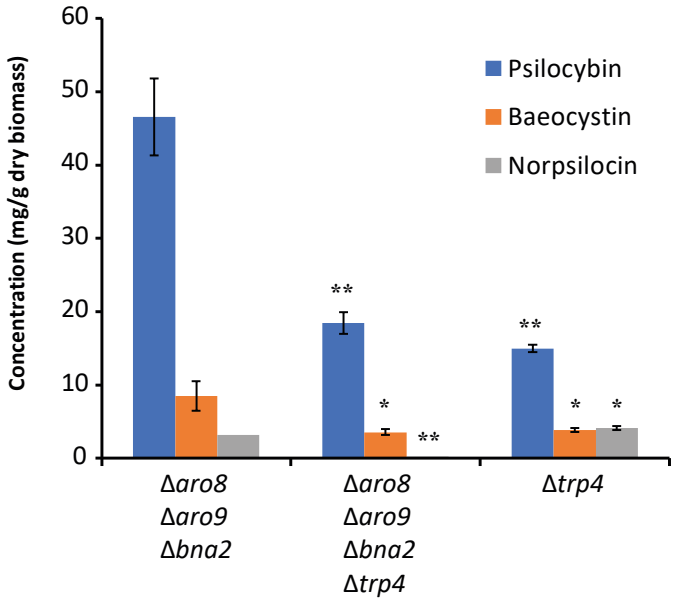

Fig. 25. Production of psilocybin, baeocystin, and norpsilocin in the mutants with abolished Trp catabolism and metabolism. The strains were grown in SD-Ura + 1 mM Trp for 48 h, and error bars represent the standard deviation. Statistical analysis was performed by student's *t*-test (* = $p<0.05$, ** = $p<0.01$) using three biological replicates for each strain.

2.4.5.3 UHPLC-MS measurement of [$^{13}C_{10}$]psilocybin, [$^{13}C_{10}$]baeocystin and [$^{13}C_{10}$]norpsilocin in the Δ*trp4* strain

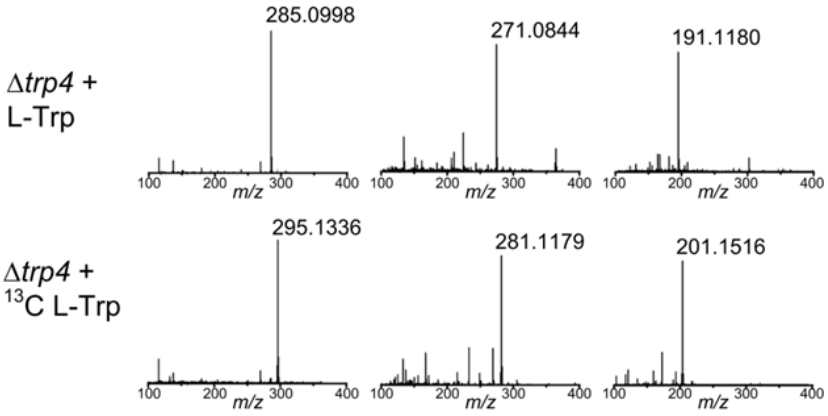

Fig. 26. Production of psilocybin in the Δ*trp4* single mutant incubated with non-isotope labeled Trp (upper panels) and with L-[$^{13}C_{11}$]tryptophan (lower panels). The strains were grown in SD-Ura + 1 mM Trp or 1 mM L-[$^{13}C_{11}$]Trp for 48 h. Peaks correspond to the following masses: psilocybin *m/z* 285.0998 $[M+H]^+$, baeocystin, *m/z* 271.0844 $[M+H]^+$, norpsilocin, *m/z* 191.1180 $[M+H]^+$, [$^{13}C_{10}$]psilocybin *m/z* 295.1336 $[M+H]^+$, [$^{13}C_{10}$]baeocystin, *m/z* 281.1179 $[M+H]^+$, and [$^{13}C_{10}$]norpsilocin, *m/z* 201.1516 $[M+H]^+$.

The Δ*trp4* single mutant transformed with pJF34 (strain YtJL10) was cultivated for 48 h in SD medium-Ura under addition of either 1 mM of Trp or L-[$^{13}C_{11}$]tryptophan, exclusively. High-resolution MS-based chemical analyses of both extracted samples undoubtedly showed that only [$^{13}C_{10}$]psilocybin had been produced and identified in the culture that was

only supplied fully labeled Trp. [$^{13}C_{10}$]psilocybin presented exact mass *m/z* 295.1336 $[M+H]^+$ compared with unlabeled psilocybin, i.e., by 10 mass units (**Fig. 26**). The akin phenomenon existed in the detection of [$^{13}C_{10}$]baeocystin (*m/z* 281.1179 $[M+H]^+$) and [$^{13}C_{10}$]norpsilocin (*m/z* 201.1516 $[M+H]^+$). In conclusion, the yeast strain with a Δ*trp4* genotype allows an atom-economic production of stable-isotope labeled [$^{13}C_{10}$]psilocybin.

2.4.6 *pcCPR* co-expression with *psi* gene cluster in the triple deletion strain

The last point for strain improvement was focusing on cytochrome P450 (CYP) catalyzed hydroxylation, which is a rate-limiting step in the psilocybin biosynthetic pathway. CYP has versatile capabilities for diverse oxidative reactions, where the monooxygenation is the most common one (Hrycay & Bandiera, 2015). The catalytic reaction strongly depends on the available cofactor NADPH and the efficient redox partner, namely NADPH-cytochrome P450 reductase (CPR). Both CYP and CPR are anchored in the endoplasmic reticulum (ER) membrane by its membrane-binding domain and form the complex; therefore, two electrons are shuttled from NADPH to the heme active site in the P450 enzyme *via* flavin adenine dinucleotide (FAD) and flavin mononucleotide (FMN) in CPR (Cederbaum, 2015; Xia et al., 2019). To provide valid CPR additionally is one way to enhance the electron transfer for heterologously expressed CYP in this rate-limiting catalyzation (Li et al., 2018; Lundemo & Woodley, 2015). Indeed, co-expression of CPR with CYP has been applied for the biosynthesis of alkaloids, terpenoid, and flavonoid at a high titer in the yeast cell (Ignea et al., 2016; Leonard et al., 2005; Li & Smolke, 2016; Trenchard & Smolke, 2015).

In the psilocybin biosynthetic pathway, *psiH* encodes the CYP monooxygenase (**Fig. 14C**) that catalyzes hydroxylation selectively at 4-position of tryptamine to build 4-hydroxytryptamine (Fricke et al., 2017). Transferring the above idea to our application, accordingly, we identified the unique putative gene encoding CPR in the same species *P. cubensis* (*pcCPR*). We hypothesized that the co-expression of *pcCPR* cDNA with the *psi* gene cluster in the yeast host might upregulate the yield of the final product psilocybin. To investigate this hypothesis, two yeast strains YtJL04 and YtJL06 were obtained as shown in **Fig. 27**. Thus, the expression of *pcPCR* either was regulated by the native *MET15p* promoter in the genomic DNA or was expressed in the vector under the control of the constitutive *TEF1p* promoter. The diagnostic PCR confirmed the genetic integration of *pcCPR* in the strain YtJL04, and the result is shown in the below Section 2.4.6.1. The integrity of the transformed expression vector in strain YtJL04 or YtJL06 was confirmed by the diagnostic PCR and YFP-based fluorescence screening (shown in the previous

Section 2.4.3, **Fig. 18**).

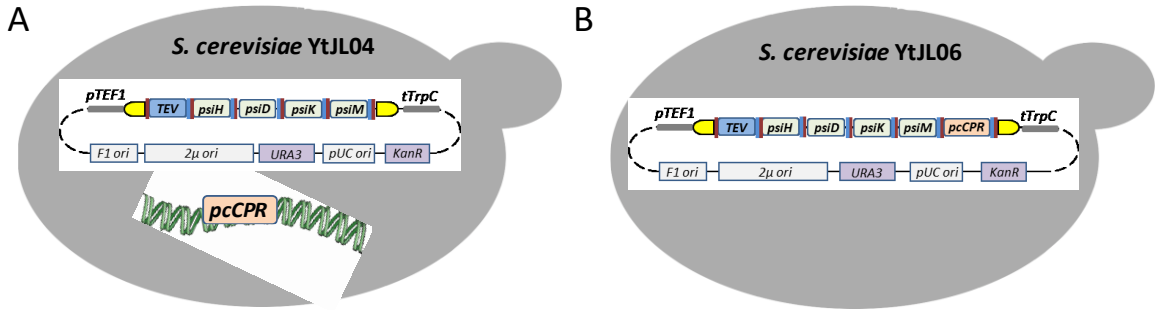

Fig. 27. Co-expression of *pcCPR* with *psiH* for psilocybin production. (A) In the triple deletion mutant with the pJF34 plasmid, *pcCPR* was integrated into the genomic DNA and expressed under the control of the *MET15* native promoter *MET15p*. (B) pcCPR co-expressed with PsiH (CYP) controlled by the strong constitutive promoter *TEF1p* in the high copy number vector pJF77. The gene drawn on the schematic diagram does not represent in the actual size scale.

2.4.6.1 Diagnostic PCR confirms the genomic integration of the *pcCPR* gene at the *MET15* locus

To integrate the *pcCPR* into the yeast genomic DNA, the last unused auxotrophic marker gene *MET15* was utilized, which was connected to *pcCPR* with the 2A peptide sequence and *tev* cleavage site (shown in Methods and Materials Section 4.2.2) for a "bicistronic" transcription.

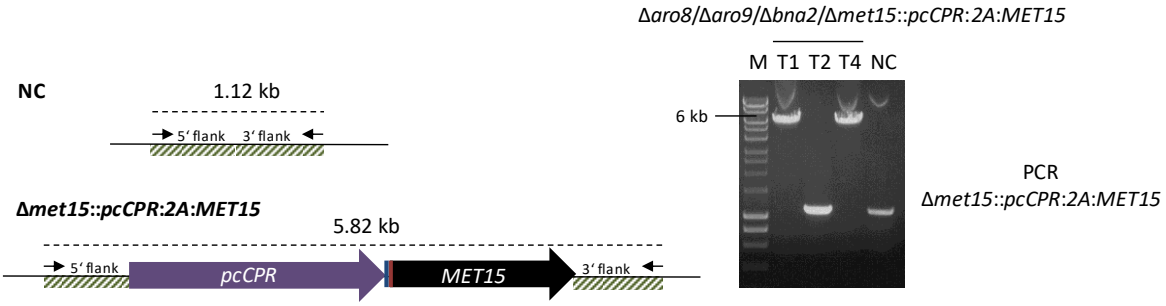

Fig. 28. *pcCPR_2A_MET15* genetic integration verified by diagnostic PCR. In the diagram, *pcCPR* and *MET15* were fused by *tev* cleavage site (blue) and *2A* sequence (red). The expected size of the PCR-amplified fragment from the correct transformants is 5.82 kb, and there is no additional band with 1.12 kb length as in the NC. Hence, T1 and T4 are positive colonies of strain YtJL02.

The constructed *pcCPR_2A_MET15* DNA fragment includes two flanking regions, which are homologous to the upstream and downstream sequences of the *MET15* gene and was inserted into the *MET15* locus under the control of the *MET15p* promoter. To verify the successful genetic integration of *pcCPR*, the outer pair of primers was used for the PCR diagnosis of yeast colonies. The result shown in the agarose gel indicated that the correct transformants (T1 and T4) with the expected band (~6 kb) contrast to the band in the NC lane (~1 kb) (**Fig. 28**).

2.4.6.2 Production of psilocybin in the strains YtJL04 and YtJL06

Psilocybin production was evaluated in both strains and compared with the performance of the Δ*aro8*/Δ*aro9*/Δ*bna2* triple mutant that was set as the positive control. Against our expectations, in both strains, the titer of psilocybin declined, and the amount was lower than 10 mg/g biomass (**Fig. 29**), which is the average yield of it in the wild-type background strain YtSJ08. Theoretically, as the redox partner, CPR oxidizes the NADPH to $NADP^+$ and provides the electrons to CYP (Li et al., 2018). Therefore, the co-expression of cognate pcCPR with PsiH is supposed to strengthen the oxidation of tryptamine and form more available 4-hydroxytryptamine in the pathway of psilocybin formation (**Fig. 30**).

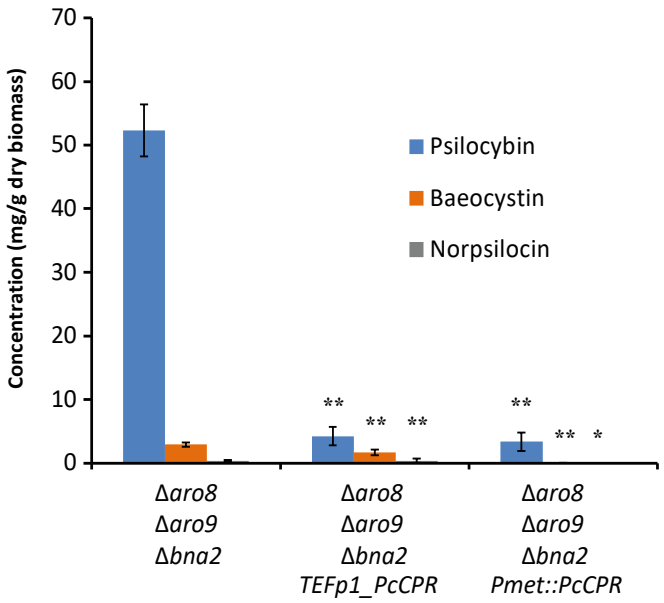

Fig. 29. Production of psilocybin, baeocystin, and norpsilocin in the yeast strains YtSJ06, YtJL04, and YtJL06. The strains were grown in SD-Ura + 1 mM Trp for 48 h, and error bars represent the standard deviation. Statistical analysis was performed by student's *t*-test (* = $p<0.05$, ** = $p<0.01$) using three biological replicates for each strain.

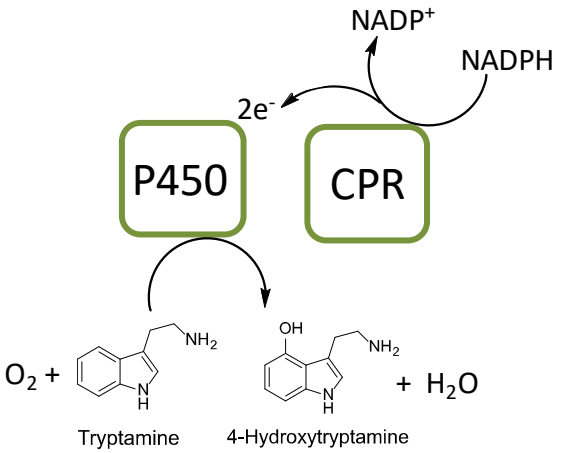

Fig. 30. Efficient electron transfer from NADPH to heme iron in CYP requires NADPH-dependent CPR.

This negative regulation of co-expression of the *psiH* and *pcCPR* might occur due to various reasons. As a common strategy to enhance the activity of CYP, the harmful sides of overexpressed CPR were studied and reported. The large excess of CPR present might result in uncoupled redox activity, and the release of reactive oxygen species (ROS) that are toxic to the cell and reduce the yield of the desired compound (Bassard et al., 2012; Paddon et al., 2013). This could be one of the reasons explaining the low production of psilocybin since the *pcCPR* is expressed from the strong promoter *TEF1p* on the high-copy plasmid (*2μ* plasmid) in one of the constructed strains, YtJL06. However, the alike result from another strain YtJL04 might suggest a different reason. *pcCPR* in this mutant is integrated as a single copy in the genome and regulated under the regulable *MET15p* promoter, which could be repressed by high exogenous methionine (Met) as feedback inhibition (Cherest et al., 1969). In our SD culture medium, 0.2 mM of Met is supplied, and this concentration is enough to partially decrease the expression of the *MET15p*-downstream gene (Mumberg et al., 1994). This may lead to an unbalanced coupling of pcCPR and PsiH.

Chapter 3

Discussion

Synthetic biology is a discipline that focuses on engineering a microbe as amenable chassis to host a value-added product (Keasling, 2008). The construction of a cell-based producer requires powerful genetic tools that can handle multiple genes coding key enzymes to complete the biosynthetic pathway in a cellular environment. In parallel, metabolic engineering is needed to direct metabolic flux, such as chemical building blocks or start materials towards the desired compound *via* a central metabolic pathway. In this work, the biosynthetic applications upon a heterologous expression platform contributed to both aspects. However, questions that occurred during the study need to be addressed (**Fig. 31**). The capability of a multigene assembly system, the combination of TEVp and 2A in polycistronic expression, and the reliability of fluorescence-based screening are discussed from the perspective of producer construction in Section 3.1. Plus, in the experiments involving yeast metabolic engineering, the probable causes of unexpected results, particularly in co-expression of CYP/CPR and redirection of Trp metabolic flux, as well as the further optimizations are considered in Section 3.2.

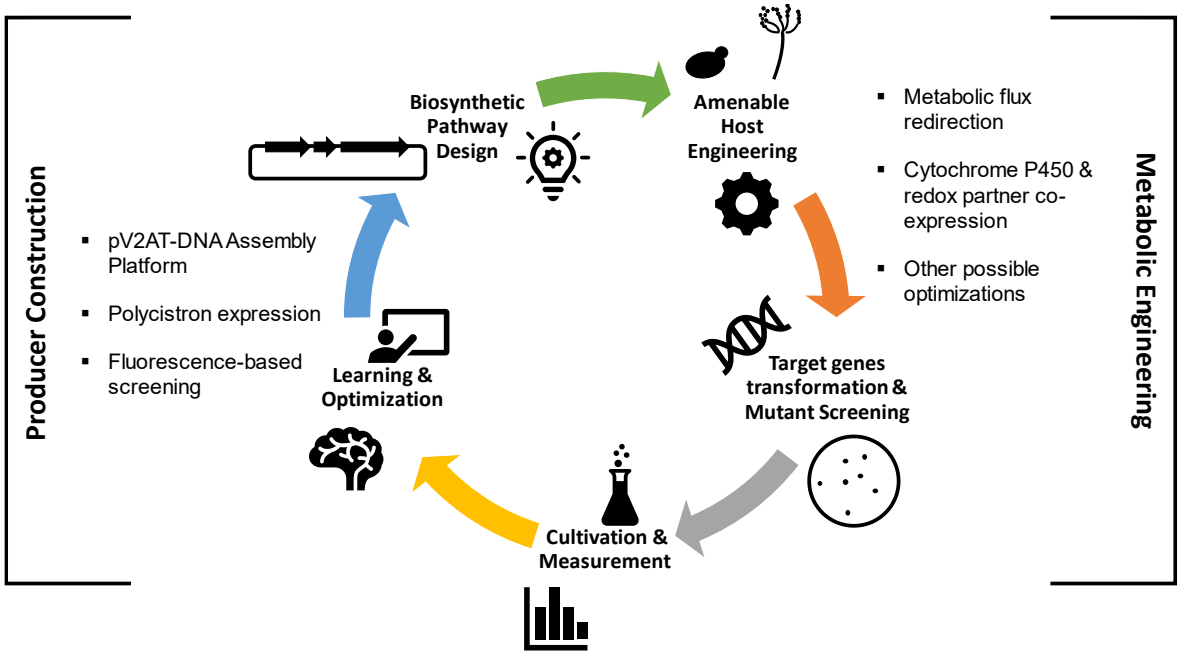

Fig. 31. The workflow for biosynthesis of a SM.

3.1 A user-friendly platform for multigene expression

3.1.1 Modularization of DNA assembly and pV2A-T based construction

DNA assembly methodology is necessary for cloning and constructing a gene cluster, typically when the PKS gene has a long and highly repetitive DNA sequence, which is not ideal for gene synthesis. As the vitally important toolkit in the field of molecular biology nowadays, the vector is constitutively developed and adapted for its expanding applications in biosynthesis. In the past, there were many assembling systems designed for vector-based multiple gene expression, which can mainly be grouped into two directions: a Cre*/loxP* mediated recombination and endonuclease-mediated cloning approach. For example, Kriz *et al.* reported a Multi-Label system using a *loxP* sequence to combine two plasmids into one *in vitro* (Kriz et al., 2010); yet each round requires a new selective marker gene that limits the number of genes for expression. This kind of system usually requires a complicated assembly design, depending on the orientation of the *loxP* sites and the expression of Cre. Besides, each fusion of plasmids doubles the size of the next-stage plasmid, which demands a cut-ligation step to remove the redundant sequence (Lin et al., 2003). Therefore, a modular-type operation is the new trend for an assembling system, in which enzyme digestion plus ligation or seamless cloning is still the favored strategy.

Using two restriction sites alternately has been employed to minimize the number of enzymes in an assembly line, the *Bpi*I/*Bsa*I or *Sap*I/*Bsa*I-joined toolkit based on the idea of Golden Gate method have been applied, mostly (Binder et al., 2014; Engler et al., 2014; Taylor et al., 2019; Vecchione & Fritz, 2019). However, these toolkits always have two vectors to fit two different construction features. Otherwise, the pair of enzymes cannot be harnessed repeatedly on several levels' assemblage. In contrast, a most wildly applied method is the BioBrick system that has compatible cohesive ends resulting from *Xba*I and *Spe*I digestion. And it allows an iterative assembly (Knight, 2003; Shetty et al., 2008). This method was developed in many other versions, such as ePathBrick (Xu et al., 2012). It standardizes the use of four isocaudamer restriction enzymes in one vector and ends up with six different ligations that can meet the different expression demands, as mentioned in the introduction. However, the digestion and ligation of isocaudamers might result in asymmetrical sequences that may stop the enzyme cleavage for the next round. Additionally, the more isocaudamers are used, the higher the possibility of unwanted cuts, since it does not depend on homologous fragments for ligation, and the identical 6 bp restriction site can frequently be found in the gene that needs to be assembled.

Hence, in the pV2A-T backbone (see Methods and Materials Section 4.2.1.2), only the

*Pme*I and *Swa*I restriction sites are necessary for assembly, which is more user-friendly. The *Pme*I and *Swa*I were chosen because both isoschizomers have 8-bp recognition sites, which are present in a low frequency in the genes. However, the *Pme*I and *Swa*I restriction sites need to be removed from the gene that needs to be assembled, if the recognition sites are present in the DNA sequence. Once every gene of interest is isolated and assembled in pV2A-T, the obtained plasmid can act as the acceptor vector by being digested with *Swa*I, or serve as the donor by being treated with *Pme*I. Because of the vector design, the gene in the acceptor vector is always constructed in front of the donor vector's gene. Thus, the gene order can be arranged flexibly according to the chosen enzyme. After restriction digestion, the recombination is according to the homologous regions, i.e., the 2A peptide sequence and a part of the kanamycin-resistant gene sequence. After each ligation, these restriction sites reset again, which enables the next round of assembly. Repeating this digestion and ligation with *Pme*I and *Swa*I, the bicistronic or polycistronic construct can be built feasibly as from the assembling pipeline (shown in Methods and Materials Section 4.2.1.2). Plus, the pair of *Pme*I/*Swa*I synthesized in the Kan^R gene avoids some incorrect assembling events, as the proper reconstruction of this gene functions as the selective marker for the colony. Furthermore, this method saves not only time in the PCR but also the primers during cloning, since each target gene only needs a forward primer and reverse primer with homologous tails for the PCR amplification in the beginning step.

Moreover, the pV2A-T plasmid presents a single *Pac*I restriction site in front of the ATG start codon, which allows the additional insertion of a selective marker cassette, a suitable promoter, and other essential elements. This feature promises that the plasmid can be either adapted to an expression vector in the yeast cell factory or integrated into the genome of various hosts. The heterologous expressions of the austinoid gene cluster and psilocybin gene cluster were achieved using this pV2A-T plasmid, which reveals that the capability of this plasmid can reach ~25 kb, in which the size of the polycistron is up to 14.2 kb. This does not exploit the limits of this method, although we observed that the number of *E. coli* colonies was lower after seamless cloning when the size of multiple genes was larger than 26 kb.

3.1.2 Using the 2A peptide in multigene expression

As opposed to the *E. coli* expression platform taking the ribosomal binding site to connect multiple genes in a 'polycistron' expression (Xu et al., 2012), the 2A peptide sequence was introduced to mediate co-translational cleavage of an artificial polycistronic construct in eukaryotic species. As a well-known technique in the application of multigene expression,

it holds attention because of its short size, high efficiency for ribosome skipping, and need of a single promoter.

In this work, P2A-led expression has been used for bioactive compound production and strain engineering, indicating the versatile applications of this short peptide. Typically, the bicistronic expression system, where the selective marker gene is located after a target gene, can minimize the number of false-positive transformants growing on the selective plates, because some frameshift mutations can destroy the conserved motif GDVEXNPGP, which results in unsuccessful skipping of the ribosome and wrong translation of the downstream protein.

Despite the advantages of 2A peptides, the widespread application requires more systematic studies of position effects, gene number limitation, and transportation or targeting of co-expressed proteins. The position effects have been observed in some investigations in the past. In the bicistronic construct, the protein expression is significantly lower at the second position using fluorescent proteins as reporters (Liu et al., 2017b), yet the expression level highly depends on the protein itself, as it was observed in another study (Wang et al., 2015). For the tricistronic construct, the position influence was tested by luciferase expression using P2A, and the protein expression was negatively regulated at the first position (Schuetze & Meyer, 2017). Conversely, Liu *et al.* found that the first position had the best performance, and the second one was the worst when they co-expressed three different fluorescent proteins, in which P2A was used to space the first two genes and T2A was utilized to link the last. The same study also revealed that no matter whether mixed 2A peptides or the identical 2A peptide (P2A) were employed, the expression level was continuously dropping from the 5' side toward 3' end in the quadcistronic construct. Therefore, the activity of expressed multiprotein from the polycistronic construct can vary depending on the gene number, the sort order in the construct, and the type of protein.

In the heterologous expression of the austinoid gene cluster mediated by P2A, the last compound calidodehydroaustin (7) that is formed by AusO, has not been detected. Since the largest PKS gene *ausV* was assembled at the 3’ end of the construct, i.e., the fifth position, the expression of AusV could be the lowest compared to other co-expressed enzymes, according to this position effect. Although the AusV expression level was not quantified, the production of the AusV-associated compound precalidodehydroaustin (6) was dramatically lower than detected from another strain cultivation, in which AusV was located at the third position based on P2A-connected quadcistron (Mattern et al., 2017). Therefore, as the precursor of compound (7), low-yielded (6) might not be enough to fuel

the biosynthesis of the final product. It seems that the position effects are the limitation of the 2A system, while further research could take it as an advantage to mediate the strength of gene expression.

Besides, the limiting number of genes in the 2A system is still not determined. Up to eight discrete proteins have been expressed upon 2A-mediated 'self-cleavage' in yeast for the co-expression of the *psi* gene cluster with *pcCPR*. After genetic transformation, it was observed that when the P2A peptide DNA fragment links more genes, there is a higher possibility of gene deletion in the transformed cells. This phenomenon might be due to the homologous recombination machinery in the engineered fungal hosts. Fortunately, this gene-removed event can be easily checked using diagnostic PCR.

Last, whether the expressed SMs biosynthetic enzymes formed by 2A-mediated co-translation can still be transferred into the host's destined locations needs greater understanding. Typically, an enzyme that involves SMs synthesis is correctly compartmentalized in specific subcellular units that can promise pathway efficiency, e.g., a high penicillin production has been observed when the number of peroxisomes increased in the strains of *Penicillium chrysogenum* (Meijer et al., 2010). Therefore, this is a node worth considering in synthetic biology. Usually, the nascent peptide synthesis through the ribosome and then the precursor protein is either translocated in the lumen of the ER or incorporated into the ER membrane itself and transferred to vesicles in the Golgi mediated exocytosis at the hyphal tip and the septum (Kistler & Broz, 2015; Riquelme & Sánchez-León, 2014). A previous study noticed that when the protein upstream of 2A was led by the signal recognition particle (SRP)-dependent signal sequence and localized in the Golgi, even when the mitochondrial targeting signal or NLS was added before the next gene, the encoded second protein only localized within the ER (de Felipe & Ryan, 2004). The correct localization in mitochondria and nucleus happened to the second protein when the SRP-dependent signal was removed from the first gene in the bicistronic construct. From this report, the post-translational signal present in the first gene of the 2A-associated polycistron seems vital for the transfer of the remaining discrete proteins. In our applications, the polycistronic constructs always start with the *VenusN* subunit, in which the N-terminus was modified by an NLS. Although both synthesized austinoids and psilocybin in our applications can indicate the correctly expressed enzymes, whether the nascent proteins generate from the 2A-mediated ribosome skipping is due to co-translational or post-translational translocation needs further exploration.

3.1.3 Addition of TEVp to the 2A system

As the protease identified from the *tobacco etch virus*, TEVp is one of the most commonly used tools for peptide-bond cleavage in biotechnology, as it is cofactors-independent, highly sequence-specific, and can recognize a seven-amino-acid motif peptide substrate (Sanchez & Ting, 2020).

A combination of 2A and TEVp is an innovative idea in our application. Generally, after 2A-cleavage, except for the first-formed peptide, the other mature peptides have a proline at the N-terminus, and this feature can enhance protein half-life (Varshavsky, 2011). However, as a technical drawback in the later process, the remaining ~20 amino acids of the 2A peptide fused at the C-terminus of the protein interfere with the enzymatic function that has been documented (Mattern et al., 2017; Subramanian et al., 2017). In the assessment of this developed heterologous expression system, assisted by TEVp cleavage, 2A-free AusP kept its enzymatic activity, therefore, can assemble with other *aus* genes in one polycistron to save marker genes for fungal transformation. Besides, to reduce the autoproteolysis of TEVp *per se*, the gene encoding the TEVp mutant S291V (Kapust et al., 2001) was equipped in the pV2A-T, where this *TEV* gene was followed by 2A. In the immunoblot analysis, no additional band refers to 27 kb in the lane of strain YtSH18 (Fig. 4B), also proving that the 2A-tag was wholly cleaned from TEVp by its 'self-cleavage' efficiently.

Commonly, TEVp is applied in fusion protein cleavage and purification, as it is better characterized compared to other proteases, e.g., different TEVp variants with strengthened catalytic activity have been adopted for one-step on-resin cleavage and purification (Waugh, 2011; Zhu et al., 2017). In contrast to the application of TEVp for multiprotein cleavage, it is also applied in multiprotein expression in *E. coli* and in mammalian cells (Chen et al., 2010). One recent application using TEVp and its recognition site in polyproteins demonstrated that the thirteen nitrogen fixation genes have been grouped in four giant genes connected by the *TEV* site, and enabled the synthesis of active nitrogenase in non-diazotrophic *E. coli* (Yang et al., 2018).

Nevertheless, the reported applications of TEVp in synthetic biology were few, maybe due to some technical drawbacks when using TEVp alone in multigene expression. On the one hand, despite it has specific cleavage performance, the catalytic turnover of TEVp is significantly lower than other proteases (for example, trypsin and subtilisin) (Sanchez & Ting, 2020). This might not be promising for the several cleavage actions in a large polyprotein. Indeed, the unexpected protein fractions presented in the western blot analysis

represented uncut tri-chimeric and bi-chimeric proteins when using a TEV-based system for the heterologous expression of tri-cistronic constructs in yeast (Ghiaci et al., 2014). On the other hand, although all proteins can be expressed at an equimolar level, they are localized in the same subcellular compartment. Even though the additional targeting sequences would assist TEVp localization in the nucleus, mitochondria, peroxisome, or ER (Cesaratto et al., 2016), it is hard to fulfill all the requirements of SM synthetic enzymes having diverse localizations within the cell. Moreover, fusion protein cleavage *in vivo* might negatively influence the foldability and stability of the downstream proteins (Shih et al., 2005). Therefore, using TEVp exclusively in SM biosynthesis has inescapable limitations. In our heterologous expression platform, 2A-leaded co-translational 'cleavage' happens before the mature protein formation, and TEVp performs the later cut-off of the 2A-tag, which avoids this structural interference.

To be cautious, the remnant of the recognition site is attached at the C-terminus as the E-N-L-Y-F-Q tail after TEVp cleavage. The extra chain includes six amino acids, and though it is shorter than the 2A peptide tag, can still down-regulate enzyme activity, since the tailing tolerance varies with different proteins. For example, the activity of nitrogenase cofactor maturase NifB decreased by 30% with the ENLYFQ-tail, and the NifK as the beta subunit of molybdenum-iron protein cannot tolerate this C-terminal tail (Yang et al., 2018). Hence, before using the pV2A-T expression system for a known biosynthetic pathway, evaluating the tailing tolerance of key enzymes is an option.

3.1.4 Joined YFP indicates the complete expression of genes

In the past, southern blot hybridization was a widely used and reliable method to verify the genome's alteration after fungal transformation. Nonetheless, it is very laborious and time-consuming to handle a large number of transformants. As a highlight innovation in our developed platform, the fluorescence-based screening system based on the association of split-YFP subunits enormously shortens the workload and allows for high-throughput testing. This idea was adopted from bimolecular fluorescence complementation assays for protein-protein interaction (Kudla & Bock, 2016). The split position of "Venus" YFP was decided between the eighth and the ninth beta-sheets for Venus-N and Venus-C fragments because the split fragments with about a 2:1 size ratio can reduce the self-assembly (Romei & Boxer, 2019). The genes encoding these subunits are located separately at each end of the polycistronic construct, granting that the translational efficiency can be examined visually, which differs from the southern blot assay that only analyzes the modification at the genetic phase.

Two additional features modified the split-YFP further, to strengthen the application. For more efficient, specific, and essentially irreversible interaction of the two subunits, the antiparallel leucine zippers, as the ubiquitous domains benefiting the edge-edge interaction (Magliery et al., 2005), were introduced to drive the reassembly. Meanwhile, the post-translational signal sequence, namely NLS (Kalderon et al., 1984), added to both Venus-N and –C, orientates the YFP only targets in the cell nucleus. The rejoined subunits provide the dot-like fluorescence in the mycelia, which can easily be observed and distinguished from the fungal autofluorescence background to omit a false-positive result. For example, during the microscope screening, the strain with a dim view indicated negative transformants, while the mycelia filled with fluorescence diffusion has been revealed as incorrect mutant in the experiments.

The reliability of this design has been confirmed by southern blot assay of *A. nidulans* NidtJL02 mutants. Intriguingly, mutant NidtJL02-V3, that passed the southern blot analysis, has been proven as a false-positive transformant by fluorescence screening and HRMS measurement of chemical extracts. This indicates that the YFP-based approach is more dependable than the southern blot test. In the initial expectation, the fluorescence can be observed in the nuclei only when the whole polycistronic gene is entirely transformed and translated. Unexpectedly, we also experienced that the mutants harboring damaged polycistronic constructs showed fluorescent signal. I presumed that this was owing to either the broken gene not influencing the codon reading of the ORF or the entire gene loss not interfering with the ribosome skipping during translation. This observation adjusted the estimate of 'correct' transformant. Hence, the presence of a fluorescent signal can affirm the complete translation of transformed genes, and the PCR diagnosis can prove whether the entire polycistronic construct is transformed and expressed as expected. This updated strategy has been successfully used for the transformant screening of yeast strains harboring pJF34 or pJF77 giant expression vector.

Interestingly, from the observation, the intensity of the YFP signal is correlative to the size of the assembled genes. This phenomenon could be used to evaluate the maximum capacity of polycistronic expression in eukaryotes. However, the signal strength is not directly linked to the production amount of the expected compound in the biosynthesis.

3.2 Biosynthesis of Trp-derived psilocybin in the cell-based factory

The discovery of the psilocybin biosynthetic pathway triggered cell-free enzymatic biosynthesis and cell-based heterologous biosynthetic methods for psilocybin production. By supplementation of L-serine, pyridoxal phosphate (PLP), β-subunit in the tryptophan

synthase (TrpB), and three critical enzymes, i.e., PsiD, PsiK, and PsiM, psilocybin was successfully obtained in a one-pot enzymatic reaction *in vitro* (Blei et al., 2018). Because the TrpB can catalyze the PLP-dependent condensation of 4-hydroxytryptophan and L-serine to form 4-hydroxytryptamine. In the same year, using the pV2A-T based system, the filamentous fungus *A. nidulans* was harnessed for the first time to produce this valuable compound heterologously in a high titer without any optimization (Hoefgen et al., 2018). Later on, the idea of a one-pot enzymatic reaction was transferred by Adams et al. (2019) and applied on the *E. coli* cell factory. Differing from this, in the heterologous expression system, *psiD*, *psiK*, and *psiM* were placed separately in three expression vectors with middle, high, and low copy numbers in the *E. coli* strain, which has the overexpressed native tryptophan synthase TrpAB. After fermentation optimization, this bacterial strain achieved up to 1.16 g/L titer of psilocybin. However, due to the impossibility of functionally producing the cytochrome P450 monooxygenase involved in psilocybin biosynthesis, namely PsiH, *E. coli* production was achieved by using 4-hydroxyindole in the growth medium.

A strategy of supplying several starting substrates might be uncompetitive compared to the total chemical synthesis when considering the economic cost. Thus, the yeast *S. cerevisiae* was considered as an alternative type of cell-based factory. In parallel with our further study in the genetically modified *S. cerevisiae*, a research group from Denmark recently published their work, in which the psilocybin was likewise yielded in the baker's yeast and obtained 627 mg/L in a fed-batch fermentation (Milne et al., 2020). In yeast engineering, they enhanced the shikimate pathway and Trp biosynthetic pathway to accumulate intracellular Trp levels and to upregulate psilocybin titer from 130 mg/L to 200 mg/L. Our work targeted the degradation pathways of precursor in order to elevate the psilocybin yield in the recombinant yeast. As both biosynthetic strategies achieved large-scale yield, these ideas provide Trp-enriched yeast platforms. It is an additional advantage in metabolic engineering, because bioprocessing can be modified for the production of other Trp-derived analogs with clarified biosynthetic pathways.

For the better comprehension of the yeast strains constructed in our work, some unexpected results and the further possible optimization are discussed in the subsections below.

3.2.1 The consequences of redirected intracellular Trp flux

Although baker's yeast is the most well-studied microorganism, the gene deletions provoked a change of metabolic networking that requires a more comprehensive

understanding for the better engineering of a cell factory. In yeast, Trp levels are dynamic through different growth stages, as a bunch of enzymes regulate the metabolism and catabolism. In our study, the Δ*aro8*/Δ*aro9*/Δ*bna2* triple mutant gained increased psilocybin production, and a downregulated yield came from additional deprivation of the Trp biosynthesis.

In the Δ*aro8*/Δ*aro9*/Δ*bna2* triple mutant, the deficient Aro8 and Aro9 not only knockdown the Trp degradation, but also switch off the Tyr and Phe intracellular production, since both enzymes catalyze the last transamination step of biosynthesis of these amino acids (Iraqui et al., 1998). These changes all somehow redirect the bypasses and lead chorismic acid mainly towards the Trp pool.

Another phenomenon is that a low OD_{600} value of the Δ*aro8*/Δ*aro9* or Δ*aro8*/Δ*aro9*/Δ*bna2* mutants has been shown during yeast cultivation (**Fig. 21**). Mutants that have a lower biomass accumulation than the wild type might be subject to impaired biosynthesis of a number of amino acids and the NAD^+ production through the KYN pathway. Besides catalyzing the formation of Tyr and Phe with Aro9, Aro8 features a broad substrate specificity, and underlies the biosynthesis of Lys (Bulfer et al., 2013). The salvage biosynthesis pathway from nicotinic acid is more important than the *de novo* pathway from Trp catabolism for the NAD^+ synthesis; however, the latter one is initiated by Bna2 and also cannot be neglected. Typically, the high NAD^+/NADH ratio can stimulate respiration for biomass accumulation with adenosine triphosphate (ATP) (Sporty et al., 2009; Xu & Tsurugi, 2006). For this reason, the NAD^+/NADH ratio might be decreased in the aerobic culture of the Δ*aro8*/Δ*aro9*/Δ*bna2* mutant, thus slowing the growth. Although growth impairment is not measured in our work, the result might be equivalent to a recent test by Deed *et al.*, where a delayed log phase has been observed in the yeast commercial strain F15 with the Δ*aro8*/Δ*aro9* genotype. This strain needed twice the time compared to the wild type to reach the log phase (Deed et al., 2019). Thus, the biomass of the triple mutant could be 'restored' when the fermentation time is prolonged, which suggests a necessary optimization of fermentation for future tests.

As a thought-provoking point, how deeply the Ehrlich pathway is affected by Δ*aro8* is unclear, since the alcohol yield was not determined. In the Δ*aro8*/Δ*aro9* double mutant, two distinct AATs, i.e., mitochondrial Twt1p (Bat1p or Eca39p) and cytosolic Twt2p (Bat2p or Eca40p), might facilitate the transamination for the first step in the Ehrlich pathway, in a low level (Hazelwood et al., 2008). Aro10 is a dominant decarboxylase catalyzing the second step, which is the only irreversible process in the pathway. It has been noticed that *ARO10* is consistently upregulated in the Δ*aro8* yeast strain when

cultured in a medium with ammonium as a nitrogen source (Romagnoli et al., 2015). This might result in a higher yield of alcoholic products, although we defined the cultivation in the aerobic condition.

If this hypothesis is correct, it is reasonable that the additional deletion of *TRP4* negatively impacted the yeast strain with the Δ*aro8*/Δ*aro9*/Δ*bna2* background. Regardless of the equal significance of each enzyme implicated in Trp biosynthesis, only the deletion of *TRP1* or *TRP4* lowers the ethanol stress tolerance of yeast and leaves the cell sensitive to alcohols including ethanol, L-propanol and L-pentanol (Fujita et al., 2006). In this work, yeast cultures were performed in aerobic conditions, while the samples had an alcohol smell during harvest after 48 h fermentation, despite ethanol formation was not being measured in our study. The ethanol production is possible due to the short-term Crabtree effect with 1% glucose supplied as a carbon source (Hommes, 1966). 6% ethanol in the yeast culture can cause a decrease of the growth rate by half for BY4741 (Kubota et al., 2004). A similar phenomenon presented for the BY4742 strain with 5% ethanol and an additional single *TRP4* gene knockout showed an even delayed growth rate (Hirasawa et al., 2007). Besides, ethanol also alters intracellular metabolism (Hu et al., 2007). Upon the above information, the low production of psilocybin in the Δ*aro8*/Δ*aro9*/Δ*bna2*/Δ*trp4* quadruple mutant can be explained by the impact of self-produced ethanol, since this strain has a low ethanol tolerance.

The second possibility of this consequence might occur relative to the limitation of Trp uptake through the membrane-associated permease. Tat2p permease is a Trp-specific carrier found by Schmidt *et al.* in the Δ*trp1* cells, which depends on the uptake of Trp from the growth medium (Schmidt et al., 1994). However, the sorting of Tat2p depends on the Trp concentration in the medium. Umebayashi and Nakano discovered that the GFP-labeled Tat2p mainly targeted the vacuole and perivacuolar late endosomes rather than the plasma membrane when the cell presented in the medium containing 1 mM Trp (Umebayashi & Nakano, 2003). This phenomenon was observed in both Trp prototrophic and auxotrophic strains. Therefore, I can infer that in the main culture supplied with 1 mM Trp, the Trp biosynthetic pathway is the dominant route to support the Trp requirement for psilocybin production. Predictably, in the quadruple deletion mutant this route is defective, and the supplied Trp in the medium was utilized in a low rate *via* Tat2p. Thus, the intracellular Trp in the quadruple deletion mutant makes it hard to afford psilocybin production compared to the triple deletion strain Δ*aro8*/Δ*aro9*/Δ*bna2*. Yet, whether the intracellular Trp concentration affects the transcriptional level of *TAT2* is still not known.

Aiming to break the first limitation, the deletion of *TRP4* could be replaced by Δ*trp3*,

which does not alter the ethanol tolerance of yeast and blocks the formation of Trp *in vivo*, since Trp3 is a bifunctional synthase that catalyzes two steps reactions in the Trp biosynthetic pathway in the *S. cerevisiae* (Fujita et al., 2006; Miozzari et al., 1978). For the second bottleneck, if it is possible to overexpress the *TAT2* in the Δ*pep12* mutant background, the efficient Trp shuttle might be restored, and the cell can even grow in a high Trp environment. As from the syntaxins family, Pep12p is responsible for docking of Golgi-derived transport vesicles at the late endosome, and Δ*pep12* can inhibit sorting to the endosome and redirect the vacuolar proteins to the cell membrane (Becherer et al., 1996). The Tat2p is indeed localized in the cell membrane in the Δ*pep12* mutant, despite the high Trp concentration supplied in the medium (Umebayashi & Nakano, 2003).

The consequences of redirected metabolic flux in the recombinant yeast is hard to predict due to the dynamic amino acid pools in the living cell. The realistic regulation of genes implicated in amino acid anabolic processes are very complex. For example, yeast contains at least six aminotransferases, four decarboxylases, six alcohol dehydrogenases involved in the Ehrlich pathway (Hazelwood et al., 2008; Ohashi et al., 2017). Plus, the expression level of the genes encoding these enzymes vary depending on different growth status, other intracellular amino acids (nitrogen source), and carbon sources (Dickinson et al., 2003). The permeases responding to these amino acids' uptake are also impacted by the culture temperature, extracellular nutrition, the protein kinase TOR (target of rapamycin), ergosterol biosynthesis, as well as the Ssy1p-Ptr3p-Ssy5 membrane sensor (Daicho et al., 2009; Fernandes et al., 2015; Forsberg & Ljungdahl, 2001; Umebayashi & Nakano, 2003). Therefore, to engineer a biosynthetic pathway in the cell factory requires thorough thought.

3.2.2 Coupling CYP with a suitable redox partner

To investigate whether the endogenous pcCPR can facilitate the catalytic efficiency of monooxygenase PsiH in this rate-limited reaction, both strains YtJL04 and YtJL06 have been constructed to express pcCPR in a low and lofty level. However, the psilocybin production strikingly dropped in both mutants with a Δ*aro8*/Δ*aro9*/Δ*bna2* genotype background (**Fig. 29**). Intriguingly, after we documented this result, an opposite outcome has been published, in which the co-expression of *pcCPR* and *psiH* has achieved an increased yield of psilocybin in yeast (Milne et al., 2020). This result revealed the positive effect of pcCPR to its homologous CYP. Since the experiment designs between these two studies are different, I presume the contrasting phenomenon might be due to three alternative points in their study: 1) both *psiH* and *pcCPR* were codon-optimized; thus the encoded enzymes performed better; 2) Trp intracellular level was enhanced by "pushing"

the Trp biosynthetic pathway, which created a different metabolic background; 3) and both *psiH* and *pcCPR* had one-copy integrated into the yeast genome that was induced by the strong *TEF1p*.

Among these three points, the last one reveals that the function of PsiH can be assisted by the co-expression of *pcCPR* equivalently. This indicates that the ratio of formed CYP and its CPR is a critical point. In the strain YtJL04, *psiH* was constructed with other *psi* genes as a polycistron regulated by *TEF1p*, yet the expression of *pcCPR* was controlled by the promoter *MET15p,* which is not constitutive. In this situation, PsiH was expressed higher than the amount of pcCPR. For the strain YtJL06, both *psiH* and *pcCPR* were assembled in the 2A-mediated polycistronic construct. Owing to the position effects, the expressed PsiH and pcCPR also have difficulties matching the optimal ratio.

A previous *in vitro* study based on Nanodisc revealed that high CPR:CYP ratios positively influence the rate of CYP catalysis (Grinkova et al., 2010). However, we cannot directly transfer this idea to the *in vivo* study because of the different microenvironment of the cell. Zhao et al. (2016) observed that the pool coupling of CYP and CPR could overproduce reactive oxygen species, significantly affecting yeast cells. Moreover, both CYP and CPR are usually insoluble and ER anchored proteins, thus over-yield of these enzymes can induce a disordered ER. Traced by confocal microscopy, the overexpressed CPR led to the perturbation and swelling of the ER network (Bassard et al., 2012). Similarly, overexpressed CYP from a high-copy number plasmid caused an abnormal morphology of the ER, the loss of plasmid, and the low yield of the target product (Trenchard & Smolke, 2015). This may explain the downregulated production of psilocybin in YtJL04 and YtJL06 since both strains express either *psiH* or *pcCPR*, or both use high-copy number plasmids.

Hence, to ensure functional heterologous expression, the balance of CYP and CPR has to be considered. To compromise the expression level of CYP and CPR, one option is to fuse the CPR C-terminal part with CYP in yeast (Zhao et al., 2016), which led to 4.5-times higher yield of terpenoid protopanaxadiol. Alternatively, one-copy genomic integration of *CPR* either controlled by the weaker promoter *GAL3p* or a constitutive promoter has been documented to enhance the heterologous production of artemisinin or tropane alkaloids in the yeast *S. cerevisiae*, respectively (Paddon et al., 2013; Srinivasan & Smolke, 2019). Interestingly, in the latter example, the desired products had higher titer when the CPR was expressed from the genome compared with a low-copy-number plasmid. Last but not least, to express several CPR candidates individually with the target CYP is a considerable approach to pair a suitable redox partner with CYP (Trenchard & Smolke, 2015; Zhao et

al., 2016).

To assess different CPRs for one CYP is a considerable approach for yeast metabolic engineering. In most cases, the yeast *S. cerevisiae* endogenous CPR (scCPR) was not sufficient and required a comparison study to screen for the most suitable CPR from the list. In collaboration with CYPs identified from three different plants for the biosynthesis of sanguinarine, the native scCPR performed inefficiently compared with other exotic CPRs, in which CPR (ATR1) from *Arabidopsis thaliana* had the best performance (Trenchard & Smolke, 2015). In another case, the best product conversion rate has been achieved by coupling the *Fusarium oxysporum* CYP with its homologous CPR rather than with scCPR or CPR from *C. albicans* for the benzoate hydroxylation (Durairaj et al., 2015). Therefore, the compatibility between a selected CPR and CYP, which influences the coupling efficiency in electron transfer (Ebrecht et al., 2019), needs to be explored.

Besides harnessing the CPR/CYP pair in known bioactive compound production, their coupling application might also assist the discovery of unknown SMs, because a large number of CYPs are involved in SM biosynthetic pathways. Usually, only a single gene encoding CPR can be found in the majority of species, in contrast to numerous CYPs in a single organism. Typically, in the reported genetic annotation results, basidiomycetes *Phanerochaete chrysosporium* and *Sporobolomyces roseus*, present only one oxidoreductase-coding gene that belongs to the CPR family (Lah et al., 2008; Warrilow et al., 2002). This phenomenon is shown as well in filamentous fungi, including a large number of *Aspergillus* spp. (Lah et al., 2008). Therefore, over-expression of the orphan CPR might enhance the enzymatic activity of a wide range of CYPs and result in an increased formation of SMs, which could simplify metabolomic screening.

3.2.3 Other possible modifications to optimize psilocybin production

In this work, psilocybin production in yeast was increased by minimizing Trp dissimilation. To deliver an even better result, additional engineering strategies can be taken into account.

To enhance the stability and catalytic function of the essential enzyme, we could optimize codon usage of the corresponding gene or replace it with a more efficient one. Codon usage bias ubiquitously exists in the eukaryotic and prokaryotic genome, which highly relates to the gene transcriptional level, translational elongation speed, as well as the co-translational protein folding (Trotta, 2013; Zhou et al., 2016). However, the preferred codon could be non-optimal and optimal, and the same is true for the uncommon codon (Presnyak et al., 2015). The same study in yeast suggested that the optimal codon

significantly enhances mRNA stability, mRNA half-life, efficiency of ribosome translocation, and protein output without changing the ribosome occupancy. Codon optimization can be applied for heterologous genes involved in the pathway. For example, the codon-optimized gene *TyrH* encoding a Tyr hydroxylase facilitated the Tyr flux towards L-3,4-dihydroxyphenylalanine (L-DOPA) formation and increased the production of the alkaloid drug noscapine 2.5-fold (Li et al., 2018). Furthermore, in the biosynthetic pathway reconstruction, the key enzyme can be substituted to a synonymous one with a higher catalytic efficiency in the engineered host. Protein library construction screening or comparison has been performed for the Tyr hydroxylase (DeLoache et al., 2015), the CYP76AD1$^{W13L\ F309L}$ mutant given the L-DOPA titer 2.8-fold of the wild type enzyme. Besides, Milne et al. (2020) also substituted the PsiD with the more efficient tryptophan decarboxylase CrTdc from *Catharanthus roseus* for psilocybin production in yeast.

Besides making the changes to the enzyme itself, a mixed idea of "push-and-block" can guide the core-node substrate towards the target product more comprehensively in the cell factory. The idea includes overexpression of genes in the biosynthetic pathway, optimizing the catalytic-limiting enzyme, increasing precursor supply, and decreasing degradation of pathway intermediates. For instance, it has been applied to promote the production of the pharmaceutical compounds phenylethanediol, stilbenoids, and strictosidine in engineered yeasts (Brown et al., 2015; Li et al., 2016; Yuan et al., 2019). In our yeast platform strain, besides to "block" the Trp degradation pathway to enrich the intracellular pool of Trp, we can additionally enhance the PsiK production in future studies, as this enzyme not only helps to enrich the intermediate norbaeocystin but also 'repairs' psilocin back to psilocybin (Fricke et al., 2020).

Apart from these common ideas that intensify each step to get the high production, tuning metabolic fluxes in the biosynthetic pathway by controlling expression levels of genes has the potential to maximize the target product. In all of our strains, the *psi* gene cluster has been assembled in a pV2A-T-managed "polycistron" with a fixed gene order. In this condition, although the expression level of each gene cannot be adjusted individually, we can still rearrange the gene's position in a 2A-based co-translation to figure out which permutation has the best balance of gene expression levels in our future work. Moreover, when the gene expression depends on the shuttle plasmid, the plasmid stability and copy number are the other factors that influence the final product in the timeline. As observed, the strain that conveys a large size plasmid or high-copy number plasmid has the burden, which decreased cell growth rate and desired metabolites (Da Silva & Srikrishnan, 2012). In our developed pV2A-T backbone, origins of replication, selection markers, and

promoters can be switched according to different hosts and genes that are supposed to be expressed. Karim *et al.* deeply investigated the influences of these elements in growth rate and plasmid copy number (Karim et al., 2013). Although the *ori* is subject to the plasmid copy number, both the selective marker and promoter strength determined the plasmid load in the cell. Thus, further investigation can locate these elements, as they all affect the gene expression level through 'plasmid load' in the *S. cerevisiae* haploid strain BY4741.

Except taking a vector for heterologous expression, each biosynthetic gene can be introduced into the genomic DNA and regulated individually under distinct promoters for an even finer adjustment. The *TEF1p* promoter has been employed in all the yeast-based expression systems in our work, since it is a strong and constitutive promoter. Yet, to control each target gene precisely for the optimization of metabolic flux in a eukaryotic host, the optimal expression level could be found by screening suitable promoters with various strengths from the library (Choi et al., 2019). For example, Lu and Jeffries selected 6-phosphogluconate dehydrogenase promoter (*GND2p*) and hexokinase isoenzyme 2 promoter (*HXK2p*) that represented relatively weaker and stronger strength and tested them for three different gene expressions (Lu & Jeffries, 2007). By this they defined the best combination for the highest ethanol production in the xylose-metabolizing yeast strain. Noteworthy, the strength of the promoter is varies depending on carbon sources usage and metabolic modes shift between oxidative and fermentative growth. The study performed by Sun *et al.* suggested a consistent strength order of group promoters despite glucose and oxygen supplementation: *TEF1p* > *PYK1p* ~ *TDH3p* > *CYC1p* ~ *ADH1p* (Sun et al., 2012). Hence, according to this collected data, we can optimize the expression of *psi* genes by testing these promoters.

Last, the inducible promoter can be equipped for *psiD* expression, since PsiD is the first enzyme 'switch' to turn on psilocybin biosynthesis. The frequently used *GALp* family (Lv et al., 2016; Peng et al., 2017), including *GAL1*/*10p*, *GAL2p*, and *GAL7p*, provides wide options. In the wild-type strain, expression levels are regulated by the galactose concentration; in the Δ*gal80* background strain, the expression levels are controlled by the glucose concentration (Peng et al., 2018). Besides, a newly reported cyanamide hydratase promoter (*DDI2p*) that is induced by cyanamide can be considered, as it has higher strength compared to *GALp* (Wang et al., 2019). Nevertheless, the strength of an inducible promoter is more challenging to determine, because the inducer concentration, induction time, and growth conditions would impact the outcomes. Thus, all of these factors have to be considered before starting.

3.3 Concluding remarks

First of all, to fulfill the need for reconstructing the pathway of a SM in a fast and straightforward manner, a user-friendly tool has been developed in this work for multigene heterologous expression. The time-saving screening of positive transformants that employs the split-YFP, guaranteed the complete expression of multigene irrespective of assembled in the vector or integration in the genomic DNA. The practicability of this method was indicated by heterologous expression of the *aus* gene cluster from one polycistron and the rewiring of austinoids biosynthesis in *A. nidulans*.

Secondly, this developed system was harnessed for heterologous production of the psychotropic compound psilocybin in filamentous fungi, which was the first-time biosynthesizing this valuable prodrug in fermentation condition and had a considerable yield. Beyond the application in the biosynthesis of known and treasured SMs, this vector technology has the compatibility for the elucidation of unknown synthetic pathways in the future.

Finally, a reduced expenditure of Trp in the primary metabolism promised the yield of psilocybin in a high titer from the engineered yeast. Such yeast strains can serve as the platform to benefit other Trp derivatives that are of interest. Furthermore, blocking the Trp biosynthesis allowed the atom-economic production of stable isotope-labeled psilocybin. This acquired knowledge from the model yeast can be transferred to the industrially favored fungal strains, in which the genes encoding the enzymes in Trp catabolism remain speculative.

Chapter 4

Methods and Materials

4.1 Strains used in this work

4.1.1 Bacterial and *S. cerevisiae* strains

Table 2. Wild type and mutant strains of *E. coli* and *S. cerevisiae* used in this study.

Strain	Genotype	References
E. coli DH5α	*deoR endA*1 *recA*1 *relA*1 *gyrA*96 *hsd*R17($r_k^-m_k^+$) *supE*44 *thi*-1 Δ(*lacZYA argFV*169) Φ80*lacZ*ΔM15 F^- γ^-	Bioline
BY4741	*MATa*; Δ*his3*; Δ*leu2*; Δ*met15*; Δ*ura3*	Euroscarf
S. cerevisiae STH00331	Wild type	Jena Microbial Resource Collection
S. cerevisiae tSH00	BY4741; *URA3*	(Hoefgen et al., 2018)
S. cerevisiae tSH16	BY4741; *TEF1p-VenusN/VenusC*; *URA3*	(Hoefgen et al., 2018)
S. cerevisiae tSH17	BY4741; *TEF1p-VenusN/mRuby/VenusC*; *URA3*	(Hoefgen et al., 2018)
S. cerevisiae tSH18	BY4741; *TEF1p-VenusN/TEV/mRuby/VenusC*; *URA3*	(Hoefgen et al., 2018)
S. cerevisiae Y01965	BY4741; *MATa*; Δ*his3*; Δ*leu2*; Δmet*15*; Δ*ura3*; Δ*aro9*::*kanMX4*	Euroscarf
S. cerevisiae Y04569	BY4741, *MATa*; Δ*his3*; Δ*leu2*; Δmet*15*; Δ*ura3*; Δ*aro8*::*kanMX4*	Euroscarf
S. cerevisiae Y02556	BY4741, *MATa*; Δ*his3*; Δ*leu2*; Δmet*15*; Δ*ura3*; Δ*bna2*::*kanMX4*	Euroscarf
S. cerevisiae YtSJ01	Y01965, Δ*aro8*::*LEU2*	This study
S. cerevisiae YtSJ02	YtSJ01, Δ*bna2*::*HIS3*	This study
S. cerevisiae YtSJ03	Y04569*; TEF1p-VenusN/tev/psiH/psiD/psiK/psiM/VenusC; URA3*	This study
S. cerevisiae YtSJ04	Y01965; *TEF1p-VenusN/tev/psiH/psiD/psiK/psiM/VenusC; URA3*	This study
S. cerevisiae YtSJ05	Y02556; *TEF1p-VenusN/tev/psiH/psiD/psiK/psiM/VenusC; URA3*	This study
S. cerevisiae YtSJ06	YtSJ01; *TEF1p-VenusN/tev/psiH/psiD/psiK/psiM/VenusC; URA3*	This study
S. cerevisiae YtSJ07	YtSJ02*; TEF1p-VenusN/tev/psiH/psiD/psiK/psiM/VenusC; URA3*	This study
S. cerevisiae YtSJ08	BY4741; *TEF1p-VenusN/tev/psiH/psiD/psiK/psiM/VenusC; URA3*	This study
S. cerevisiae YtJL02	YtSJ02*; Δmet15*::*pcCPR*:*2A*:*MET15*	This study
S. cerevisiae YtJL04	YtJL02; *TEF1p-VenusN/tev/psiH/psiD/psiK/psiM/VenusC; URA3*	This study

S. cerevisiae YtJL06	YtSJ02; *TEF1p-VenusN/tev/psiH/psiD/psiK/psiM/PcCPR/VenusC; URA3*	This study
S. cerevisiae YtJL07	YtSJ02; Δ*trp4*::*MET15*	This study
S. cerevisiae Y04191	BY4741; *MATa*; Δ*his3*; Δ*leu2*; Δmet*15*; Δ*ura3*; Δ*trp4*::*kanMX4*	Euroscarf
S. cerevisiae YtJL08	YtJL07*; TEF1p-VenusN/tev/psiH/psiD/psiK/psiM/VenusC; URA3*	This study
S. cerevisiae YtJL10	Y04191*; TEF1p-VenusN/tev/psiH/psiD/psiK/psiM/VenusC; URA3*	This study

4.1.2 *Aspergillus* spp. strains

Table 3. Wild type and mutant strains of *Aspergillus* spp. were generated in this study.

Strain	Genotype	References
A. calidoustus SF006504	Wild type	(Horn et al., 2016)
A. nidulans RMS011	*pabaA1, yA2; argB*::*trpCAB; veA1, trpC801*	(Stringer et al., 1991)
A. nidulans NidtJL01	RMS011; *Tet*^{on}-*VenusN/tev/VenusC*; *argB*	This study
A. nidulans NidtJL02	RMS011; *xylP-VenusN/tev/ausP/ausO/ausT/ausV/VenusC*; *argB*	This study
A. nidulans NidtJF03	RMS011; *Tet*^{on}-*VenusN/tev/psiH/psiD/psiK/psiM/VenusC*; *argB*	This study

4.2. Molecular biology and genetics methods

4.2.1 Construction of expression vectors

All plasmids that were constructed during this study are listed in **Table 4**.

Table 4. Plasmids used in this study.

Plasmid name	Relevant features	References
pUC19	*ori*, *amp*^{R}	(Yanisch-Perron et al., 1985)
pACYC177	*kan*^{R}	(Schottel et al., 1981)
pRK793	*TEV*	(Kapust et al., 2001)
pYes2	*amp*^{R}*, URA3, 2μ*	Life Technologies
pYesTef2	pYes2, *TEF1p*, *eGfp*	(Hoefgen et al., 2018)
pV2A	Split-YFP, 2A peptides, *kan*^{R}	(Hoefgen et al., 2018)
pV2A-T	pV2A, *tev* cleavage site	(Hoefgen et al., 2018)
pSH001	pV2A-T, *TEV*	(Hoefgen et al., 2018)
mRuby-N1	*mRuby*	Addgene #54581
pSH012	pYes2, *xylP*, *lacZ*, *argB*	(Hoefgen et al., 2018)
pSH013	pYes2, *Tet*^{on}, *lacZ*, *argB*	(Hoefgen et al., 2018)

pSH014	pV2A-T, *mRuby*	(Hoefgen et al., 2018)
pSH015	pSH001, *mRuby*	(Hoefgen et al., 2018)
pSH016	pV2A-T, *TEF1p*, *URA3*	(Hoefgen et al., 2018)
pSH017	pSH014, *TEF1p*, *URA3*	(Hoefgen et al., 2018)
pSH018	pSH015, *TEF1p*, *URA3*	(Hoefgen et al., 2018)
pJL001	pV2A-T, *ausP*	(Hoefgen et al., 2018)
pJL002	pV2A-T, *ausO*	(Hoefgen et al., 2018)
pJL003	pV2A-T, *ausT*	(Hoefgen et al., 2018)
pJL004	pV2A-T, *ausV*	(Hoefgen et al., 2018)
pJL005	pV2A-T, *TEV*, *ausP*	(Hoefgen et al., 2018)
pJL006	pV2A-T, *ausO*, *ausT*	(Hoefgen et al., 2018)
pJL007	pV2A-T, *TEV*, *ausP*, *ausO*, *ausT*	(Hoefgen et al., 2018)
pJL008	pV2A-T, *TEV*, *ausP*, *ausO*, *ausT, ausV*	(Hoefgen et al., 2018)
pJL009	pJL008*, xylP*, *argB, URA3*	(Hoefgen et al., 2018)
pJL010	pSH001*, Tet*^{on}, *argB*, *URA3*	(Hoefgen et al., 2018)
pFB13	pET28a(+), *psiM*	(Fricke et al., 2017)
pJF23	pET28a(+), *psiD*	(Fricke et al., 2017)
pJF24	pET28a(+), *psiK*	(Fricke et al., 2017)
pJF25	pSM-Xpress, *psiH*	(Fricke et al., 2017)
pJF26	pV2A-T, *psiH*	(Hoefgen et al., 2018)
pJF27	pV2A-T, *psiD*	(Hoefgen et al., 2018)
pJF28	pV2A-T, *psiK*	(Hoefgen et al., 2018)
pJF29	pV2A-T, *psiM*	(Hoefgen et al., 2018)
pJF30	pV2A-T, *psiH, psiD*	(Hoefgen et al., 2018)
pJF31	pV2A-T, *psiK, psiM*	(Hoefgen et al., 2018)
pJF32	pV2A-T*, psiH*, *psiD*, *psiK*, *psiM*	(Hoefgen et al., 2018)
pJF33	pV2A-T, *TEV, psiH*, *psiD*, *psiK*, *psiM*	(Hoefgen et al., 2018)
pJF34	pJF33, *TEF1p, URA3*	This study
pJF36	pJF33, *Tet*^{on}, *argB*, *URA3*	(Hoefgen et al., 2018)
pV2A-T_pcCPR	pV2A-T, *pcCPR*	This study
pJF77	pJF34, *pcCPR*	This study
pΔbna2	pYes2, *HIS3*	This study

Seamless cloning methods were used for plasmid construction, including circular polymerase extension cloning (CPEC) (Quan & Tian, 2009), Gibson (Gibson et al., 2009), In-Fusion (Takara, Germany), and GeneArt (Life technologies, Germany). For plasmid amplification, *E. coli* DH5α strain (Bioline, Germany) was used according to the manufacturer's instructions. For the pYes2-derived plasmids and all the final expression vectors used for the transformation of *S. cerevisiae* and *Aspergillus* spp., the assembly was

achieved with transformation-associated recombination (TAR) cloning in *S. cerevisiae* based on a protocol described before (Kouprina & Larionov, 2008). All the restriction endonucleases used in this work were purchased from the NEB (Germany). Purification of plasmids and DNA fragments was done using the GeneJet Plasmid Miniprep Kit and GeneJet Gel Extractions Kit (ThermoFisher Scientific, Germany).

4.2.1.1 List of oligonucleotides used for PCR

PCR amplification of targeted genes and DNA fragments as probes for hybridization in southern blot analysis was processed by employing the Phusion Flash High-Fidelity PCR Master Mix (Thermo Scientific, Germany). Colony PCR was carried out by using the MyTaq PCR Red Mix (Bioline, Germany). PCR pipetting and cycling instructions were set up according to the manufacturers' instructions. The annealing temperature and elongation time of each PCR were given according to the Tm of the used oligonucleotides and the size of the amplified fragment. Utilized oligonucleotide primer pairs are listed below in **Table 5**.

Table 5. Oligonucleotides used for PCR.

No.	Primer Name	Sequence 5'-3'
1	pACYC_SwaI2_R	ATGTTGGAATTTAAATGCGGCCTCGAGCAAGACG
2	pACYC_SwaI2_F	TTGCTCGAGGCCGCATTTAAATTCCAACATGGATGC
3	pACYC_PmeI2_R	TCAGCCAGTTTAAACGGACCATCTCATCTGTAACATC
4	pACYC_PmeI2_F	CAGATGAGATGGTCCGTTTAAACTGGCTGACGGAATTTATGC
5	pV2A_1F	TTAAGGGATTTTGGTCTTAATTAAATGGATAAAGC
6	pV2A_2R	ACGCAGACCGTTCCGAGCTATCAGAGTAAAGAAGAG
7	pV2A_3F	TTTACTCTGATAGCTCGGAACGGTCTGCGTTGTCG
8	pV2A_4R	GATACCGCTCGCCGCGTCAAGTCAGCGTAATGCTC
9	pV2A_5F	TTACGCTGACTTGACGCGGCGAGCGGTATCAGCTC
10	pV2A_6R	ATCCATTTAATTAAGACCAAAATCCCTTAACGTGAG
11	pV2A-T_F	CGCGATATCGAAAATCTTTATTTTCAAGGTGCGATGGGAGGCTCTGGCGCC ACCAACTTC
12	pV2A-T_R	CCGGGATATCAGGGCCAGGGTTTTC
13	pV2AT_tev_F	GGCGACGTTGAAGAAAACCCTGGCCCTGATGGAGAAAGCTTGTTTAAGGG
14	pV2AT_tev_R	CATCGCACCTTGAAAATAAAGATTTTCGATGCGACGGCGACGACGATTC
15	pV2A_mRuby_F	GGCGACGTTGAAGAAAACCCTGGCCCTGATATGAACAGCCTGATCAAAGA AAAC
16	pV2A_mRuby_R	CATCGCACCTTGAAAATAAAGATTTTCGATCCCTCCGCCCAGGCCGGCG
17	ura3T_p2A_F	GAAAACTCACGTTAAGGGATTTTGGTCTTACTCTTCCTTTTTCAATGGG
18	Tef_pV2A_R	CTCGGGAATTAATTCCGCTTTATCCATTTATTTGTAATTAAAACTTAGATTA G
19	pV2AT_ausP_fw	GCGACGTTGAAGAAAACCCTGGCCCTGATATGGAGGTCGTCCGTTATTTC
20	pV2AT_ausP_rv	CATCGCACCTTGAAAATAAAGATTTTCGATCTAACGGGTTTGATTGATGG

21	pV2AT_ausO_fw	GGCGACGTTGAAGAAAACCCTGGCCCTGATATGAAAATTCCAGACAATCC
22	pV2AT_ausO_rv	CATCGCACCTTGAAAATAAAGATTTTCGATTCCAGCCATGGTTTGATTAC
23	pV2AT_ausT_fw	GCGACGTTGAAGAAAACCCTGGCCCTGATATGGTCGACAAGTCAAACAAG
24	pV2AT_ausT_rv	CATCGCACCTTGAAAATAAAGATTTTCGATGCACTGATGCAAAACATCCC
25	pV2AT_ausV_fw	GGCGACGTTGAAGAAAACCCTGGCCCTGATATGGCAGGAACTGACAGCTC
26	pV2AT_ausV_rv	CATCGCACCTTGAAAATAAAGATTTTCGATCGTAGCTACGTGGCTTGATC
27	Pv2A_ArgB_FW	GAAAACTCACGTTAAGGGATTTTGGTCTTATGTCGACGGCGACGGAGCGC
28	targB_ura3_RV	GGCCAGCAAAACTAATCTAGACTGATGATGCAGTG
29	targB_ura3_FW	CATCATCAGTCTAGATTAGTTTTGCTGGCCGCATC
30	XylP_Pv2A_RV	CTCGGGAATTAATTCCGCTTTATCCATTTAGGTTGGTTCTTCGAGTCGAT
31	TetOn_VenusN_RV	CTCGGGAATTAATTCCGCTTTATCCATTTATGTGATGTGATGGAGTTGAG
32	oJF65	GAAAACCCTGGCCCTATGATCGCTGTACTATTCTC
33	oJF66	AAAATAAAGATTTTCGGGTCCGGATACCG
34	oJF67	GAAAACCCTGGCCCTATGCAGGTGATACCCGCGTG
35	oJF68	AAAATAAAGATTTTCAGCCTTTAGAGCAGCGACGA
36	oJF69	GAAAACCCTGGCCCTATGGCGTTCGATCTCAAGAC
37	oJF70	AAAATAAAGATTTTCCGCAGTGGATGATTCCTTC
38	oJF71	GAAAACCCTGGCCCTATGCATATCAGAAATCCTTAC
39	oJF72	AAAATAAAGATTTTCGAAAAGAGAGCTGAGCTC
40	probe_Pxyl_F	ACGACTTTGGTGATCTGATAGG
41	probe_Pxyl_R	CGGGAATTAATTCCGCTTTATC
42	probe_TEV_F	AGGCCCTGAAGAAGGAGCTC
43	probe_TEV_R	GTTGAGTCGCTTCCTTAACTGG
44	AC-SB-53-fwd	AACTTTGTGGAAGGCAGTGG
45	AC-SB-53-rev	GGTTTGATTACTCCTCAGCC
46	probe_AusV_F	CTCAATACGACAATGTACTCC
47	probe_AusV_R	GAGTAGTGTTGGAATTCAAAG
48	aro8-Leu2-1	GTCAGGGGTTCGAGCCCCC
49	aro8-Leu2-2	ATCTTCTTAGGGGCAGACATGATAGTAACGATCGGTTGTC
50	aro8-Leu2-3	GACAACCGATCGTTACTATCATGTCTGCCCCTAAGAAGATC
51	aro8-Leu2-4	TCTTCCAACGTATTTACCTCTTTAAGCAAGGATTTTCTTAACTTC
52	aro8-Leu2-5	TTAAGAAAATCCTTGCTTAAAGAGGTAAATACGTTGGAAG
53	aro8-Leu2-6	GGAAAATGATTTGGGTTCG
54	bna2_5F	GTAATACGACTCACTATAGGGAATATTCCAAACCCGGTCAACAACGC
55	bna2_5R	AGAACAACAAGAAAAGCATTTCATATTATCGGCGTTGACTCTTTCTT
56	bna2_3F	AAGAAAATTGCGGGAAAGGACTGTGTTCATTATACATTTTATTAACG
57	bna2_3R	GACATAACTAATTACATGATGCGGCCCCTCCAGTCTGGAAATCAAATC
58	bna2_5diag	CCGAACTTGAAGGCACCTTGG
59	bna2_diag_R	CCCATGATGTGGCGAGATACAG
60	bna2_3diag	GTCCGTACTGAATTTGACCGGG

61	his3_Prom_F	AACACAGTCCTTTCCCGCAA
62	his3_Term_R	AATATGAAATGCTTTTCTTG
63	Met15_2A_F	TGGCGACGTTGAAGAAAACCCTGGCCCTATGCCATCTCATTTCGATACTG
64	Met15_CPR_R	GACGAAAACGTCTGAGGAAGAGGAGGCCATTGTATGGATGGGGGTAATAG
65	Met15_Fl_F	CTCCTCGAGGATTTAGGAATC
66	Met15_Fl_R	CCCATACTTTCAACGATGAGC
67	PcCPR_F	ATGGCCTCCTCTTCCTCAGAC
68	2AP_R	AGGGCCAGGGTTTTCTTCAAC
69	PcCPR_pV_F	GCGACGTTGAAGAAAACCCTGGCCCTGATATGGCCTCCTCTTCCTCAGAC
70	PcCPR_pV_R	ATCGCACCTTGAAAATAAAGATTTTCGATACTCCAGACATCCAACATGAG
71	met15_F	ATGCCATCTCATTTCGATACTG
72	met15_R	TCATGGTTTTTGGCCAGCG
73	trp4-972_F	CATTGGTGGTGGTGACTCTG
74	trp4+843_R	GCGTCCAGCTCTTTTTCCAG
75	trp4_met15_F	CTGTTTTCGCTGGCCAAAAACCATGAACATTATTTCATATGTTATACTTAAAC
76	trp4_met15_R	GTTGAACAGTATCGAAATGAGATGGCATGATAAGGGAATACTAAGTTTTCTTG
77	Tev_3_fw	CAGCCAGTTAAGGAAGCGACTC
78	VenusC_ana2_RV	CTCCACCTTGCGCTTCTTCTTG

4.2.1.2 pV2A-T vector and plasmids for co-expression of mRUBY with TEVp

The core plasmid pV2A-T (**Fig. 32B**) was designed to contain the following features: 1) the cutting sites of the rarely used restriction enzymes *Pme*I and *Swa*I; 2) two nearby short oligo sequences coding for 2A peptides that are spaced by a unique *Eco*RV cleavage site; 3) sequence-optimized split-YFP gene (*VenusN* and *VenusC*) flanks of the 2A peptide genes; 4) a single restriction site of *Pac*I located directly before the start codon of *VenusN*; 5) the *ori* site; and 6) a selective marker gene.

A parent plasmid pV2A was first constructed with three DNA fragments: an *ori*, a kanamycin-resistant gene *aph* (Kan^R), and a synthetic DNA fragment. Primers [1]/[2] and [3]/[4] were used to create the *Pme*I and *Swa*I restriction sites in the Kan^R of the pACYC177 plasmid (Schottel et al., 1981) by PCR-mutagenesis, and then the region including the modified Kan^R was amplified with primers [7]/[8]. The *ori* was directly amplified from pUC19 (Yanisch-Perron et al., 1985) using primer pair [9]/[10]. The DNA fragment harboring the sequences encoding split-YFP subunits, *2A* segments with *Pme*I and *Swa*I, and the *A. nidulans TrpC* terminator was synthesized (Biomatik, Canada) and amplified with primers [5]/[6]. Based on seamless cloning, these three fragments were assembled to form pV2A, which subsequently was re-amplified using [11]/[12] to

introduce a 30 bp specific *tev* site and a single *Eco*RV restriction site that can be used for a blunt-end cloning strategy in later applications. This PCR product was treated with *Eco*RV and ligated using the T4 DNA ligase (NEB, Germany) to achieve the backbone plasmid pV2A-T.

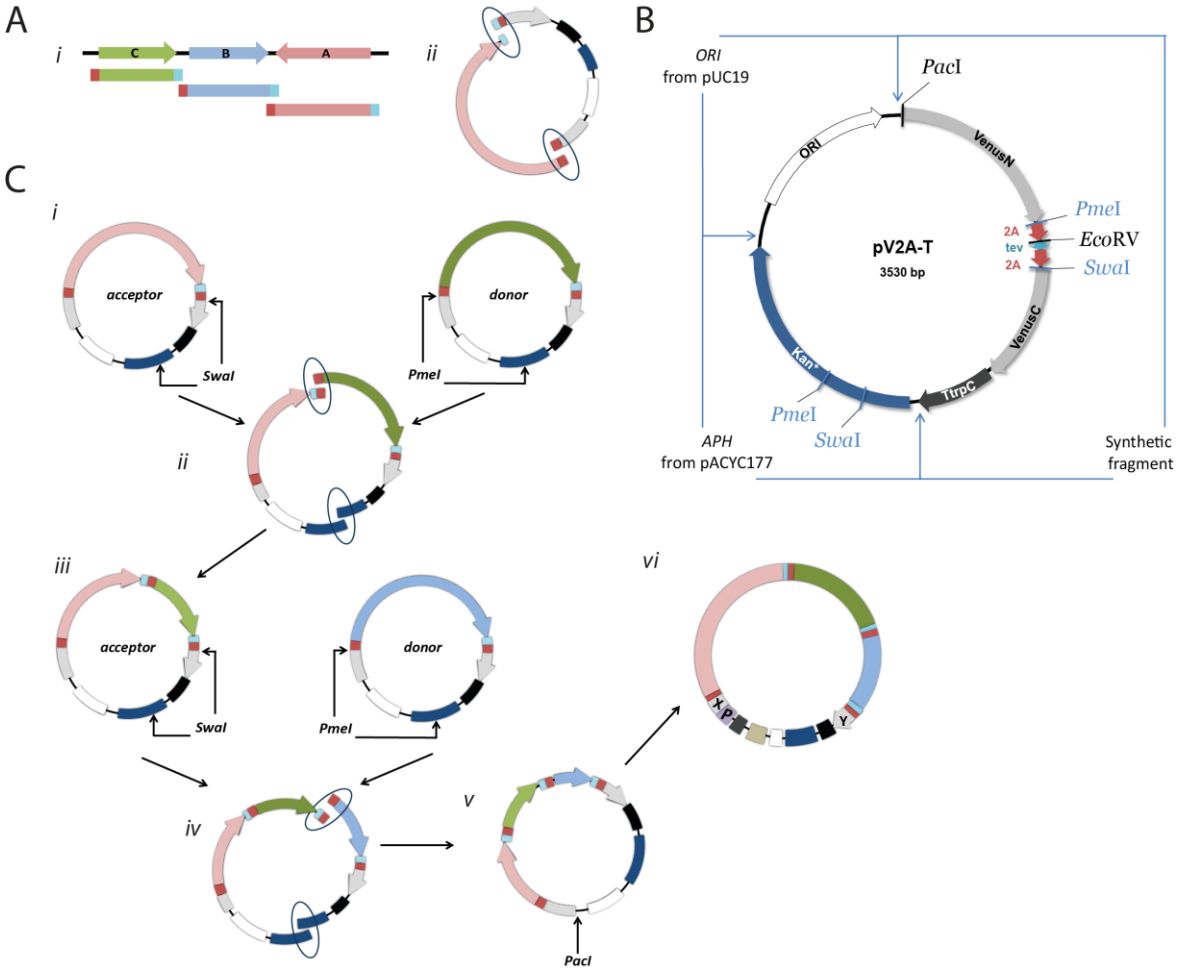

Fig. 32. Schematic structure of the pV2A-T design and cloning strategy. (A) Individual assembly of each gene of interest in the pV2A-T plasmid. (*i*) Isolation of the target genes by PCR using the primer pairs with 30 bp overhangs, which are homologous to both ends of the *Eco*RV-linearized pV2A-T (*ii*). Because of the homologous regions of the 2A peptide sequence (red) and the *tev* cleavage site (blue), every single gene can integrate into the pV2A-T backbone. (B) Overview of the pV2A-T backbone design and construction. (C) Artificial assembly line of a polycistronic operon in the pV2A-T system. (*i*) According to the designed order of genes in the polycistronic construct, each gene assembled in the pV2A-T plasmid is restriction digested with *Swa*I (as an acceptor) or *Pme*I (as a donor). (*ii*) Gene in the donor fragment is fused after the gene from acceptor fragment by seamless cloning. The homologous tails regions (marked with elliptical circles) generated automatically after *Swa*I or *Pme*I treatment. (*iii*) After the fusion of two genes, this built plasmid contains the restriction sites of *Swa*I and *Pme*I, as before. By repetition of the same step, a third gene is added to form that the vector has a tricistronic construct (*iv*). Step *iii* and step *iv* can be replicated several times for the multi-genes assembling purpose. (*v*) The essential DNA elements for gene expression in the host can be inserted at the *Pac*I restriction site located directly before the *VenusN* to generate the final expression plasmid (*vi*).

The pV2A-T backbone was linearized by *Eco*RV to introduce a target gene into the pV2A-T system. Meanwhile, using primers designed with a 30 bp homologous sequence specific

to the ends of the linearized backbone (**Fig. 32A**. *i*), the target gene was amplified from the template DNA and ligated with the pV2A-T backbone (**Fig. 32A**. *ii*) through seamless cloning. In this manner, the gene coding for TEVp was amplified from the template plasmid pRK793 (Kapust et al., 2001) with primers [13]/[14] and integrated into pV2A-T to build the plasmid pSH001. The pSH014 was built using same method: with primers [15]/[16], the *mRuby* gene sequence was amplified from the mRuby-N1 plasmid (Addgene #54581) and integrated into the pV2A-T. Based on the pV2A-T assembly pipeline (**Fig. 32C**), the plasmid pSH015 was generated from the *Swa*I-digested pV2A-T and the *Pme*I-cut pSH014.

4.2.1.3 Plasmid construction for TEVp function test *in vivo*

The DNA sequence containing *TEF1p*, *URA3*, and *2μ ori* features was amplified from the template plasmid pYes2Tef2 using primers [17] and [18]. In parallel, pSH001, pSH014, and pSH015 were linearized by *Pac*I. On account of the described manner of the final step assembly (**Fig. 32C**. *v* and *vi*), pSH016, pSH017, and pSH018 construction were carried out based on TAR cloning, respectively. The yeast strains that harbor pSH016, pSH017, and pSH018 are named as tSH16, tSH17, and tSH18, respectively.

4.2.1.4 Polycistronic construction of the *aus* and *psi* gene clusters

To evaluate the pV2A-T system for expression of multiple genes, *ausP*, *ausO*, *ausT*, and *ausV* from the *aus* biosynthetic cluster were selected to complete the austinoids production (Mattern et al., 2017) in *A. nidulans*. First of all, *ausP*, *ausO*, *ausT*, and *ausV* were isolated from *A. calidoustus* genomic DNA using primer pairs [19]/[20], [21]/[22], [23]/[24], and [25]/[26], respectively. Each gene was ligated separately into *Eco*RV-opened pV2A-T to build plasmids pJL001, pJL002, pJL003, and pJL004. The pJL05 that contains *ausP* and the gene *TEV* encoding TEVp was created by fusion of *Swa*I-digested pSH001 and *Pme*I-restricted pJL001. Similarly, pJL002 and pJL003 were fused to generate pJL006, containing *ausO* and *ausT*. Furthermore, plasmids pJL005 and pJL006 were combined to yield the pJL007, which was modified once again by adding the *ausV* from pJL004 to get the plasmid pJL008. The DNA fragments including the *xylP* promoter, *argB* and the *URA3* auxotrophic selection markers were amplified by PCR with primer pairs [27]/[28] and [29]/[30] from pSH012. Moreover, these two fragments were ligated into the *Pac*I-linearized pJL008 using TAR cloning, which resulted in the final expression vector pJL009 (**Fig. 33A**).

For psilocybin heterologous expression, primer pairs [36]/[37], [32]/[33], [34]/[35], and [38]/[39] were employed to amplify the cDNA of *psiH*, *psiD*, *psiK*, and *psiM* from

template plasmids pJF25, pJF23, pFJ24, and pFB13, respectively (Fricke et al., 2017). The amplified cDNA sequences of *psiH*, *psiD*, *psiK* and *psiM* were joined into opened pV2A-T, leading to plasmids pJF26, pJF27, pJF28, and pJF29. Using the pV2A-T assembling method, pJF26 and pJF27 were fused to get plasmid pJF30; similarly, pJF28 and pJF29 were combined for vector pJF31. Afterwards, pJF30 and pJF31 were ligated to produce the vector pJF32, which harbors the complete *psi* gene cluster. The pSH001 was also merged with pJF32 to give the *TEV* for plasmid pJF33.

Since the heterologous expression of the psilocybin gene cluster is controlled under the Tet^{on} promoter, the Tet^{on} sequence with *argB* and *URA3* were together amplified from the template plasmid pSH013 with oligo primers [27] and [31], and this PCR-yielded fragment was coalesced into *Pac*I-linearized pJF33 to fabricate the expression vector pJF36 (**Fig. 33C**). Additionally, pSH001 was fused with the same PCR-generated sequence, resulting in the plasmid pJL010 (**Fig. 33B**).

For heterologous production of psilocybin in yeast, the fragment containing *TEF1p*, *2µ ori*, and *URA3*, was isolated from the parent vector pYesTef2 by PCR using primer pair [17]/[18]. Secondly, the PCR product was inserted into pJF33, which was in advance linearized by *Pac*I, and yielded the yeast expression vector pJF34 (**Fig. 33D**).

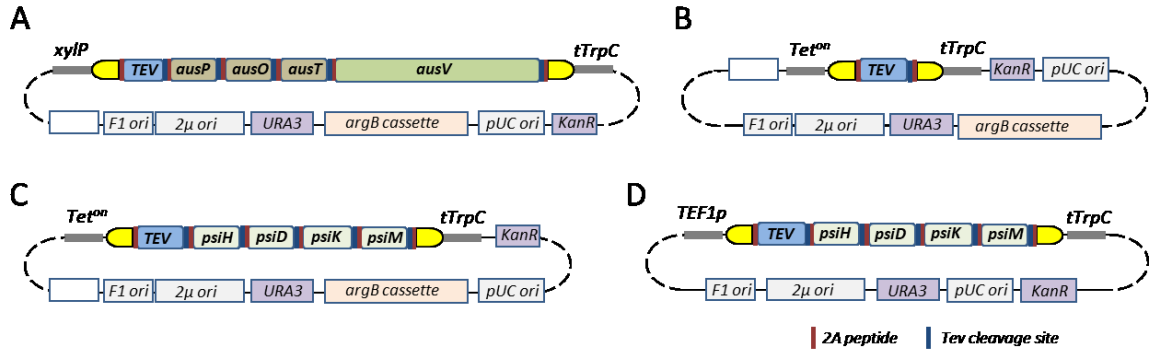

Fig. 33. Schematic structures of plasmids pJL009, pJL010, pJF36 and pJF34. (A) *Aus* gene cluster including one PKS gene and four genes encoding for tailoring enzymes controlled by an inducible *xylP* promoter, and the *argB* cassette, which is also part of pJL010 (B) and pJF36 (C), as selective marker gene for *A. nidulans* transformation. (B) Expression of *Venus N*, *Venus C*, and *TEV* genes is controlled by the Tet^{on} promoter that is induced with Dox. Psilocybin biosynthesis is fulfilled by expressing *psiH*, *psiD*, *psiK*, and *psiM*. For the heterologous expression of the *psi* gene cluster in *A. nidulans*, Tet^{on} promoter is employed (C); and for the heterologous production in *S. cerevisiae*, the yeast constitutive *TEF1p* promoter is utilized (D). The white frame indicates the *GAL1p* that belongs to the pYesTef2 backbone and was not used for the heterologous expression in *A. nidulans*. The gene drawn on the schematic diagram does not represent in the actual size scale.

4.2.1.5 pV2A-T-pcCPR and pJF77 plasmid construction

mRNA of *pcCPR* was extracted from *P. cubensis* using InviTrap Spin Plant RNA Mini Kit (Invitek Molecular GmbH, Germany) and reverse transcribed to cDNA using ProtoScript®

II First Strand cDNA Synthesis Kit (NEB, Germany). The obtained cDNA fragment was then PCR-amplified using primers [69] and [70], which created overhangs for ligation of this cDNA in the pV2A-T backbone, and then the fragment was inserted in the *Eco*RV-restricted pV2A-T to form pV2A-T-pcCPR. To further assemble the *pcCPR* in the pV2A-T based expression vector pJF34, pV2A-T-pcCPR was cut by *Pme*I and constructed after the *psi* gene cluster in the *Swa*I-digested pJF34 to achieve the final expression plasmid pJF77.

4.2.2 Generation of cassette fragments Δ*ARO8_LEU2*, Δ*BNA2_HIS3*, Δ*TRP4_MET15* and *pcCPR*_2A_*MET15*

For the deletion of *ARO8, BNA2*, and *TRP4*, as well as the insertion of *pcCPR* into the genome of yeast, the upstream and downstream flanking regions (>500 bp each) as well as the required homologous overhangs of every targeted gene, i.e., *ARO8*, *BNA2, TRP4*, and *MET15*, were amplified by standard PCR using gDNA of the prototrophic yeast strain STH00331.

The upstream flank and downstream flank of *ARO8* were obtained using primer pairs [48]/[49] and [52]/[53], respectively. The isolation of the upstream flank and the downstream flank of *BNA2* was achieved with [54]/[55] and [56]/[57]. The same was done for the amplification of the upstream and the downstream overlapping regions of *TRP4*, where primers [73]/[76] and [74]/[75] were applied. The auxotrophic selection makers for the gene deletions, which are *LEU2*, *HIS3* (including promoter and terminator) and *MET15*, were amplified with the primer pairs [50]/[51], [61]/[62], and [71]/[72], respectively.

The assembly of Δ*ARO8_LEU2* DNA fragment (**Fig. 34A**) was done by fusion PCR using obtained upstream/downstream flanks and marker gene *LEU2* as mixed templates with outer primers [48] and [53]. The processing of Δ*BNA2_HIS3* was achieved by TAR cloning. Yeast strain BY4741 was transformed with three gained PCR fragments including the flanking regions, *HIS3* and *Hind*III/*Xba*I-linearized pYes2 plasmid, resulting in vector pΔbna2. Later, Δ*BNA2_HIS3* (**Fig. 34B**) was amplified using [54]/[57] from plasmid pΔbna2, which was removed later from the PCR product by *Dpn*I restriction digestion. Δ*TRP4_MET15* (**Fig. 34C**) was built with two flanking sequences and *MET15* using outside primers [73] and [74].

To approach the *pcCPR_2A_MET15* DNA fragment, the upper flanking region before *MET15*, including necessary overhang sequences, was isolated with [65] and [64], and the *MET15* together with the downside flanking sequence was copied using primer pair [63]/[66]. The *pcCPR* with a 2A tag sequence was amplified using primers [67] and [68]

from the pV2A-T-pcCPR template vector, that was already mentioned in the previous section 4.2.1.5. These three PCR products were re-assembled into one complete cassette fragment *pcCPR_2A_MET15* (**Fig. 34D**), in which *pcCPR* and *MET15* were spaced by a 2A peptide sequence for a bicistronic transcript later during genes expression.

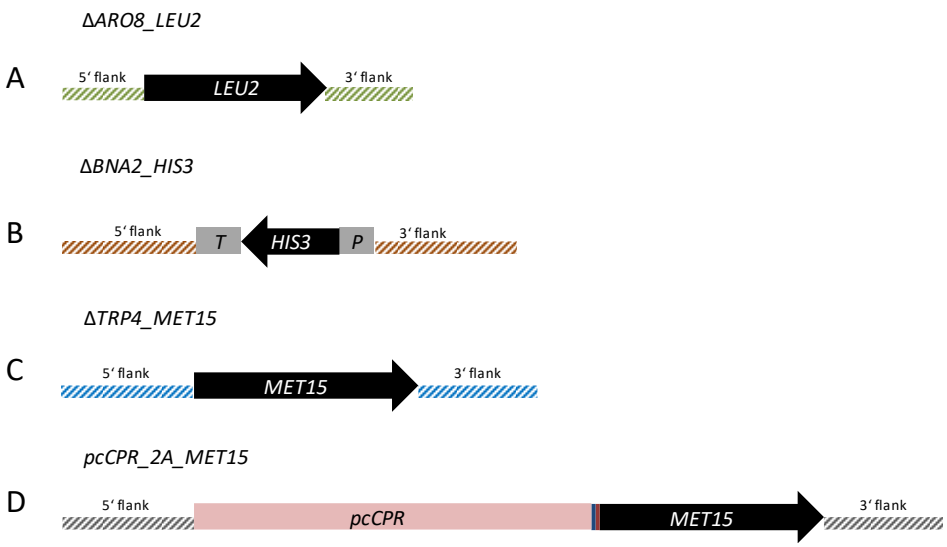

Fig. 34. Assembly of four DNA fragments for genetic deletion and insertion. Three auxotrophic selective makers *LEU2*, *HIS3* and *MET15* were chosen for the deletions of the *ARO8* (A), *BNA2* (B) and *TRP4* (C) genes. (D) *pcCPR* merged with the *2A* sequence and *MET15* for the insertion of *pcCPR* into the *MET15* locus in yeast gDNA.

4.2.3 Genetic engineering of *S. cerevisiae*

One of the yeast strains BY4741, according to its auxotrophic features for four markers (Δ*his3*/Δ*leu2*/Δ*met15*/Δ*ura3*), was engineered for several manipulations that are explained in the following sections. All the yeast transformations followed the TAR cloning protocol as mentioned in Methods and Materials Section 4.2.1. The first selection of positive transformants and further plate cultivations were done using synthetic defined (SD) agar, which was prepared according to the published recipe (Da et al., 2000) with specific amino acid(s) dropped out and 1% glucose as a carbon source, and if necessary, supplemented with geneticin (G418) (Invivogen, Germany). The Yeast Nitrogen Base without amino acids was purchased from Sigma-Aldrich (Germany) and all the required amino acids were obtained from SERVA (Germany). Different selective plates related for various strains were listed in **Table 6**.

Table 6. The selective SD plates for the constructed yeast strains.

strains	SD agar plate
S. cerevisiae tSH00	SD-Ura
S. cerevisiae tSH16	SD-Ura
S. cerevisiae tSH17	SD-Ura
S. cerevisiae tSH18	SD-Ura
S. cerevisiae YtSJ01	SD-Leu
S. cerevisiae YtSJ02	SD- Leu-His
S. cerevisiae YtSJ03	SD-Ura+G418
S. cerevisiae YtSJ04	SD-Ura+G418
S. cerevisiae YtSJ05	SD-Ura+G418
S. cerevisiae YtSJ06	SD-Leu-Ura+G418
S. cerevisiae YtSJ07	SD--Leu-His-Ura+G418
S. cerevisiae YtJL02	SD-Leu-His-Met+G418
S. cerevisiae YtJL04	SD-Leu-His-Met-Ura+G418
S. cerevisiae YtJL06	SD-Leu-His-Ura+G418
S. cerevisiae YtJL07	SD-His-Leu-Met+G418
S. cerevisiae YtJL08	SD-His-Leu-Met-Ura+G418
S. cerevisiae YtJL10	SD-Ura+G418

4.2.3.1 Double deletion, triple deletion and quadruple deletion in yeast

Strains Y04569, Y01965, and Y02556 were ordered from Euroscarf (Germany). All gene deletions/insertions into the genome of the yeast strains were processed by homologous recombination during yeast transformation. *ARO8* was exchanged with *LEU2* in the strain Y01965, using DNA fragment Δ*ARO8_LEU2*, to construct the *ARO8*/*ARO9* double deletion strain YtSJ01. Afterwards, in the strain YtSJ01, *BNA2* was replaced with *HIS3* using DNA fragment Δ*BNA2_HIS3* to form the triple deletion strain YtSJ02. *TRP4* in the YtSJ02 was exchanged with *MET15*, which led to the strain YtJL07.

After each step of deletion, two colonies of each strain were picked from the related selective plate, and the single colonies were purified through plate streaking twice. Importantly, each correct deletion *via* homologous recombination was proven by PCR diagnosis before manipulating the next deletion event (shown in Result Section 2.4.1 and Section 2.4.5.1). To check the strains YtSJ01 and YtSJ02, the parent strain BY4741 acted as a negative control for PCR; for the quadruple deletion strain YtJL07, the triple deletion strain YtSJ02 was used as a negative control. The complete deletion of *ARO8* was

confirmed using the outer primers [48]/[53]. Since the length of *BNA2* and *HIS3* are similar, a different strategy was applied to check the deletion of *BNA2*. A pair of diagnostic primers [58] and [61] was used to amplify the 5' upstream plus *HIS3*, including promoter. Another primer pair [60]/[62] was utilized to amplify the downstream sequence with *HIS3* at the 3' side. In parallel, a reverse primer [59] was designed in the *BNA2* gene, together with a forward primer [58] to check if *BNA2* is entirely removed from the deletion strain. To check the *TRP4* deletion event, the *Xba*I restriction enzyme was applied to digest the DNA fragments that were amplified from the quadruple deletion colony and triple deletion strain using the same outer primer pair [73] and [74]. Colonies carrying the correct Δ*trp4* deletion feature showed two bands (~1.1 kb and ~2 kb) in the electrophoresis gel.

4.2.3.2 Genomic integration of *pcCPR* into the triple deletion strain YtSJ02

The triple deletion strain YtSJ02 featuring Δ*aro8*/Δ*aro9*/Δ*bna2* was transformed with the DNA fragment *pcCPR_2A_MET15*, so that the *pcCPR* was specifically inserted in the *MET15* locus. The expression of *pcCPR* and *MET15* was driven by the endogenous promoter of *MET15*. The newly built strain was named YtJL02.

4.2.3.3 *S. cerevisiae* strains transformed with expression plasmids containing the *psi* gene cluster

The transformation of shuttle vector pJF34/pJF77 was processed based on the same TAR cloning protocol, as described above. Strain Y04191 with a single deletion of *TRP4* was purchased from Euroscarf (Germany). Y04569, Y01965, Y02556, and Y04191 commercial strains were transformed with the pJF34 plasmid to generate YtSJ03, YtSJ04, YtSJ05, and YtJL10, respectively. Strains YtSJ01, YtSJ02, and YtJL07 were transformed with pJF34 to construct the strains YtSJ06, YtSJ07, and YtJL08. Strains YtJL02 and YtSJ02 were transformed with pJF34 and pJF77, separately, to build strains YtJL04 and YtJL06.

The transformants grown on the selective plates were screened further by fluorescence microscopy and diagnostic PCR, to check for the complete *psi* gene cluster in pJF34 and the same cluster plus *pcCPR* in pJF77. Details for the fluorescence screening can be found in Methods and Materials Section 4.6. The diagnostic PCR was performed with primers [77]/[78].

4.2.4 Genetic transformation of filamentous fungi

For *A. nidulans* cultivation, the *Aspergillus* minimal medium (AMM) was prepared according to a recipe previously documented (Brakhage & Van den Brulle, 1995; Pontecorvo et al., 1953), except that the Hutner's trace element stock solution (1000×, pH 6.5) was prepared different: $ZnSO_4 \times 7\ H_2O$, 22 g/L; H_3BO_4, 11 g/L, $MnCl_2 \times 4\ H_2O$, 5

g/L; $FeSO_4 \times 7\ H_2O$, 5 g/L; $CoCl_2 \times 6\ H_2O$, 1.6 g/L; CuSO4 × 5 H2O, 1.6 g/L; $(NH_4)Mo_7O_{24} \times 4\ H_2O$, 1.1 g/L; EDTA, 5 g.

A pre-culture of the *A. nidulans* RMS011 strain was prepared by inoculation of spores in the AMM supplied with 1% (w/v) glucose as the carbon source, 5 mM Arg, and 3 mg/L p-aminobenzoic acid (PABA) to reach a final 1×10^6 conidia mL^{-1} concentration. This pre-culture was incubated under 180 rpm shaking conditions for 15~17 h at 37°C. Afterwards, the protoplast formation and a PEG/$CaCl_2$-mediated protoplast transformation were handled according to the protocol as reported in John & Peberdy (1984), except a few modifications. The lytic digestion was carried out using Vinotaste (100 mg/mL) (Novozymes, Copenhagen) and lysing enzymes (5 mg/mL) (Sigma-Aldrich, Germany), and incubated under shaking conditions (80 rpm) at 37°C for 3 h. *A. nidulans* RMS011 was transformed with 10 µg of the final expression vectors pJL010, pJL009, and pJF36 to achieve strains NidtJL01, NidtJL02, and NidtJF03, respectively. Within 5~7 days, transformants of each strain were grown on the prepared agar plates (AMM + 3 mg/L PABA + 1 M Sorbitol + 2% agar). Obtained transformants were streaked out for purification on the fresh selective plates (AMM + 3 mg/L PABA + 2% agar) twice to get single colonies.

Conidia of each strain were harvested in sterilized double-distilled water, filtered through a cell strainer (Greiner Bio-One, Germany) and counted using a cell counter (Beckman Coulter, Germany). Harvested spores were stored in sterilized glycerol solution with a 30% (v/v) final concentration at -80°C. Transformants of NidtJL01, NidtJL02, and NidtJF03 were checked by fluorescence screening (Methods and Materials Section 4.6). Southern hybridization analysis (Methods and Materials Section 4.2.5) was applied to verify the correct integration of the *aus* gene cluster in the strain NidtJL02.

4.2.5 Southern hybridization analysis of ectopic integration of *aus* gene cluster in *A. nidulans*

A. nidulans strain RMS011 was pre-cultured as described in Methods and Materials Section 4.2.4, as were the four mutants NidtJL02_V2, V3, V4, and V15 but without Arg supplementation, to obtain mycelium for total chromosomal DNA extraction. The genomic DNA extraction followed the manual of MasterPure™ Yeast DNA Purification Kit (LGC Biosearch Technologies, Germany). Isolated gDNA was treated with the restriction enzyme *Dra*I. Digested DNA fragments were separated by size during gel electrophoresis (Smith, 1996), in which the ethidium bromide was replaced by the HDGreen DNA dye (Intas Science Imaging, Germany). Primers (from [40] to [47]), the MyTaq PCR Red Mix

(Bioline, Germany), and the DIG-11-dUTP (Jena Bioscience, Germany) were used to prepare probes P1 to P4. Manipulation of agarose gel capillary blotting was detailed in the protocol (Smith & Murphy, 1996) using a Hybond N^+ membrane (Carl Roth, Germany). The hybridization, stringency washes, and detection of DNA probes were performed based on Kelsell's protocol (Kelsell, 1996) and the CDA-*Star* ready-to-use (Roche, Germany) manufacturer's protocol. The chemiluminescence imaging was carried out by Fusion Fx (Vilber, Germany).

4.3 Protein extraction and immunoblot

Yeast transformants (tSH00, tSH16, tSH17 and tSH18) were set up as described in Methods and Materials Section 4.5.2 for proteins extraction. A lysis solution (pH 6) containing 150 mM NaCl and 20 mM sodium phosphate buffer (0.5 M of Na_2HPO_4 and NaH_2PO_4) was prepared in advance. The following day, the cell pellets were collected from each culture and suspended in the lysis solution, to which 10 mg of lysing enzymes (Sigma-Aldrich, Germany) were added. After 3 h incubation at 30°C, the ultrasonic homogenizer (BANDELIN, Germany) was utilized to disrupt the cells, which were placed on ice. A 90 s of sonication was run two times for each sample. Afterwards, each sample was transferred to 2 mL tube and centrifuged at 4°C at maximum speed for 15 min, to pellet the cell debris. The supernatant was then transferred to a fresh tube. The concentration of total extracted proteins was determined *via* the Bradford protein assay (Pierce Coomassie Plus Assay Kit, ThermoFisher Scientific, Germany). 5 µg of protein from each sample were loaded onto a Bolt Bis-Tris Plus Gel with 4-12% gradient polyacrylamide (ThermoFisher Scientific, Germany) for electrophoretic separation (180 V, 30 min), and was transferred onto a nitrocellulose membrane using the iBlot2 Blotting System (ThermoFisher Scientific). The blocking solution was prepared using 5% (w/v) skimmed milk powder in the Tris Buffered Saline with Tween-20 (TBST) (Tris, 6.1 g/L; NaCl, 8.68 g/L; Tween-20, 0.05% (v/v); pH 8) and applied to prevent non-specific binding. A goat anti-rabbit IgG-HRP secondary antibody (sc-2004, Santa Cruz Biotechnology, US) was bound to the commercial anti-2A antibody (ABS31, Merck, Germany), that was used to detect the 2A peptides in the membrane. For the detection of horseradish peroxidase, the membrane was incubated with WesternSure PREMIUM Chemiluminescent Substrate (LI-COR Biosciences, Germany) and Fusion Fx (Vilber, Germany) was employed for imaging. The manipulation of each commercial product followed the manufacturer's instruction.

4.4 Trp sensitivity assay

For phenotype analysis of the *ARO8*, *ARO9* and *BNA2* deletion strains, a Trp sensitivity assay was performed. Each strain was pre-cultured in 15 mL of SD medium at 30°C for 24 h, and afterwards, pre-culture was ten-fold serial diluted from OD_{600} of 0.1 to OD_{600} of 10^{-4}. 10 µl of each dilution was dropped on the solid SD medium containing 0 mM, 1 mM, 5 mM and 10 mM of Trp, individually. The plates were incubated at 30°C for 3 days.

4.5 Cultivation and analytical methods

4.5.1 Cultivation conditions of *A. nidulans*

The fungal strains were grown in a complex medium or AMM with an initial spore concentration of 5×10^6 conidia mL^{-1}.

For austinoids production, the negative control strain NidtJL01 and the constructed mutants NidtJL02 were inoculated and statically grown in the complex medium the same as described in Mattern et al. (2017). For the inducing condition, 2% (w/v) D-xylose was supplemented.

The cultivation of NidtJF03 and NidtJL01 for psilocybin production was performed in AMM with supplementation of 3 mg/L PABA and the growth lasted for 4 days at 37°C under rotary shaking conditions (180 rpm). For the inducing condition, 50 µg/mL of Dox was appended 48 h after spores' inoculation to induce the expression of the *psi* gene cluster; oppositely, the non-inducing condition was carried out without Dox supplementation.

4.5.2 Growth conditions of budding yeast strains

For protein extraction, tSH00, tSH16, tSH17 and tSH18 were cultured over-night in the uracil/uridine omitted SD medium (SD-Ura) with 1% glucose at 30°C at 180 rpm.

All the strains for psilocybin production were streaked out freshly on new plates, and the cells streaked within a week were taken for inoculation. A 24 h pre-culture of SD-Ura medium (15 mL) was required for the growth of psilocybin-producing yeast strains in 100 mL Erlenmeyer flasks with four baffles. The following day, the main-culture was set up from pre-culture and inoculated with the initial OD_{600} of 0.5 in 20 mL of SD-Ura medium supplied with 1 mM Trp. Each strain was set up with three biological replicates of the main culture growing in the 100 mL Erlenmeyer flasks with three baffles at 180 rpm at 30°C for 48 h. And the OD_{600} was measured at the initial time point (0 h), after 6 h, and after 48 h to check the yeast growth.

Feeding experiments of *Trp4*-disintegrated strains were achieved in the same manner but

Trp was replaced with L-[$^{13}C_{11}$]Trp (Eurisotop, Germany) in both the media of pre-culture and main culture.

4.5.3 Chemical extraction and analysis methods

4.5.3.1 Extraction and detection of austinoids from the *A. nidulans* strains

Crude extracts were prepared from *A. nidulans* strains NidtJL01, NidtJL02_V2 and NidtJL02_V15 with equal volumes of ethyl acetate (v/v) twice from fungal culture that was homogenized using an Ultra-turrax T25 (IKA-Werke, Germany). Sample preparation, injection and analyses of HRMS were performed as previously records (Mattern et al., 2017; Valiante et al., 2017).

4.5.3.2 Extraction and quantification of indole alkaloids from *A. nidulans* strains and *S. cerevisiae* strains

The handling of psilocybin and its analogs is authorized according to the Narcotics Act of the Federal Republic of Germany. For *A. nidulans* strains NidtJL01 and NidtJF03, that were cultured with and without Dox addition, mycelia of each sample were filtered with Miracloth (Merck, Germany), and mycelia were lyophilized overnight. Mortar and pestle were applied to homogenize the dried mycelium, which was subsequently mixed thoroughly with 50 mL of methanol (MeOH). The extracted solvent was evaporated using a rotary evaporator (Rotavapor R-100, BÜCHI, Germany) and was dissolved in 5 mL of Milli-Q water. This aqueous sample was then washed with an equal volume of cyclohexane and was freeze-dried. Thereupon, the sample of each strain was dissolved in 1 mL of water:acetonitrile (ACN) (99:1, v/v). For extraction from *S. cerevisiae* strains YtSJ03-07, YtJL04, YtJL06, YtJL08, and YtJL10, each culture of yeast was harvested in a 50 mL reaction tube whose net weight was measured beforehand. After centrifugation, the liquid phase was transferred to a new tube, and both samples were lyophilized for two days. Cell pellets were weighed to calculate the biomass. Both freeze-dried cell pellets and liquid phase of the culture were mixed thoroughly with a total volume of 50 mL MeOH. The organic solvent was removed by reduced-pressure evaporation; the extracted sample was then dissolved in 2 mL of water with 0.1% formic acid (FA) and filtered before analysis. 1 µL of each sample was needed for further chromatographic analyses.

To detect the heterologously produced [$^{13}C_{10}$] psilocybin and its isotope-labeled analogs, HRMS analysis was performed on a liquid chromatography (Accela; ThermoFisher Scientific, Germany) with a C18-phase column (Grom-Sil ODS-0 AB, 100 Å, 3 µm, 250 × 4.6 µm; GROM, Germany). They were connected to the Exactive Orbitrap spectrometer coupled to an electrospray ionization (ESI) source, and mass spectra were registered in

both positive- and negative-ion modes. Mobile phases A (H_2O) and B (ACN) containing 0.1% (v/v) FA were applied on liquid chromatography with a flow rate of 1 mL/min, and the gradient was started with 5% B and followed by a linear rise to 100% B within 15 min.

The quantification of psilocybin, baeocystin, norpsilocin, KYN, and KA were achieved using ultra-high-performance liquid chromatography (UHPLC) (Agilent 1290 Infinity II LC System; Agilent, Germany) concatenated to an Omega Polar C18 column (Luna, 100 Å, 1.6 µm, 100 × 2.1 µm; Phenomenex, Germany) for separation. A diode-array detector (DAD) was used for absorbance data from 200 nm to 400 nm, and an Agilent 6130 mass spectrometer with ESI was handled in positive- and negative-ion modes. Mobile phases A (H_2O) and B (ACN) containing 0.1% (v/v) FA were applied on the liquid chromatography with a flow rate of 0.5 mL/min. The gradient was set up as follows: initiate with 1% B, and increase to 10% B in 3 min, further change to 100% B for 1 min. The chromatograms of psilocybin and its analogs were detected at a wavelength of 280 nm. The titers of psilocybin, baeocystin, norpsilocin, KYN, and KA were quantified by the AUC in the chromatography. They were calculated relative to the amount of biomass (mg/g) and culture volume (mg/L) using the standard curves of authentic compounds as references.

4.6 Fluorescence microscopy screening method

To detect the fluorescence signals in the cells, the Axiostar plus microscope equipped with different filter sets and a 506 mono Axiocam (Carl Zeiss, Germany) was used. For the imaging of yeast strains tSH17 and tSH18, the cultures were carried out in 15 mL of SD-Ura medium overnight. The nucleic staining of cells with Hoechst 33342 (Invitrogen, US) followed the manufacturer's instructions, and then the cells were fixed in a 1.5 mL centrifuge tube with 4% (v/v) formaldehyde before being applied on object slides. 5 µL cell solution of each strain was dropped for fluorescence detection using a 63 x oil objective and covered with a cover glass. The Hoechst staining, mRuby signal and YFP signal were detected at emission wavelengths of λ = 461 nm, 605 nm, and 527 nm, respectively.

Yeast cells and filamentous fungi were prepared in different ways for the YFP fluorescence screening. Every single transformant of budding yeast was pre-cultured in SD-Ura medium overnight. This culture was then diluted 1:10 with fresh SD-Ura medium in a 2 mL centrifuge tube punctured with a sterile needle. The cells were incubated under shaking conditions (500 rpm) for another 4 h to reach the log phase. 3 µL of this main culture was applied on an object slide for YFP signal detection with a 63 x oil objective. For transformants of *A. nidulans*, plates containing a thin layer (~6 mL) of solid AMM

agar were prepared. The AMM agar was supplied either with 20 µg/mL Dox and 3 mg/L PABA, or with 2% D-xylose plus 3 mg/L PABA, depending on the strain. Spore solution with 10^3 conidia/mL concentration was drawn on a fresh plate using an inoculation loop. The agar plates were then incubated for 15~17 h at 37°C for germination. The following day, the 0.8 cm diameter agar piece containing germinated spores was removed from the petri dish, placed on the object slide, covered with a cover glass, and the YFP signal was detected. To observe the fluorescence signal from the mycelium grown in AMM broth (**Fig. 8B**), the spores were inoculated in AMM (10^6 conidia/mL) in a 2 mL tube with supplementation of 3 mg/L PABA, and additional 2% D-xylose or 20 µg/mL Dox was added, according to the strain. The tube was incubated for 15~17 h at 37°C. The following day, 10 µL of the cell culture were dropped on an object slide, covered with a cover glass, and observed in a same manner.

4.7 Software and databases

The nucleic acid sequences of target genes from gDNA of budding yeast were downloaded from the Saccharomyces Genome Database (https://www.yeastgenome.org/). VectorNTI advanced software (version 11.5, Life Technologies, Germany) was employed for the design of plasmids for expression and DNA fragments for deletion. NCBI CD-search database (Marchler-Bauer et al., 2016) (www.ncbi.nlm.nih.gov/Structure/cdd/wrpsb.cgi) was used to check the conserved domain (CD) of putative PKS. The fluorescence imaging and post-processing of the obtained images was done by ZEN lite (Zeiss, Germany). HPLC chromatograms and MS data analyses were carried out using LabSolutions (Shimadzu, Germany) and Xcalibur (ThermoFisher Scientific, Germany).

Chapter 5

List of References

Adams, AM*, et al.* (2019). In vivo production of psilocybin in *E. coli*. *Metab Eng, 56*, 111-119.

Anyaogu, DC, & Mortensen, UH. (2015). Heterologous production of fungal secondary metabolites in Aspergilli. *Front Microbiol, 6*, 77.

Baghban, R*, et al.* (2018). New developments in *Pichia pastoris* expression system, review and update. *Curr Pharm Biotechnol, 19*(6), 451-467.

Bartolucci, S*, et al.* (2016). Observations concerning the synthesis of tryptamine homologues and branched tryptamine derivatives via the borrowing hydrogen process: synthesis of psilocin, bufotenin, and serotonin. *Tetrahedron, 72*(18), 2233-2238.

Bassard, JE*, et al.* (2012). A novel method for monitoring the localization of cytochromes P450 and other endoplasmic reticulum membrane associated proteins: a tool for investigating the formation of metabolons. *FEBS J, 279*(9), 1576-1583.

Becherer, KA*, et al.* (1996). Novel syntaxin homologue, Pep12p, required for the sorting of lumenal hydrolases to the lysosome-like vacuole in yeast. *Mol Biol Cell, 7*(4), 579-594.

Binder, A*, et al.* (2014). A modular plasmid assembly kit for multigene expression, gene silencing and silencing rescue in plants. *PLoS One, 9*(2), e88218.

Blei, F*, et al.* (2018). Biocatalytic production of psilocybin and derivatives in tryptophan synthase-enhanced reactions. *Chem Eur J, 24*(40), 10028-10031.

Blin, K*, et al.* (2019). antiSMASH 5.0: updates to the secondary metabolite genome mining pipeline. *Nucleic Acids Res, 47*(W1), W81-W87.

Bok, JW*, et al.* (2015). Fungal artificial chromosomes for mining of the fungal secondary metabolome. *BMC Genomics, 16*(1), 343.

Brakhage, AA. (2013). Regulation of fungal secondary metabolism. *Nat Rev Microbiol, 11*(1), 21-32.

Brakhage, AA, & Van den Brulle, J. (1995). Use of reporter genes to identify recessive trans-acting mutations specifically involved in the regulation of *Aspergillus nidulans* penicillin biosynthesis genes. *J Bacteriol, 177*(10), 2781-2788.

Brown, S*, et al.* (2015). *De novo* production of the plant-derived alkaloid strictosidine in yeast. *PNAS, 112*(11), 3205-3210.

Bulfer, SL*, et al.* (2013). Crystal structure of *Saccharomyces cerevisiae* Aro8, a putative alpha-aminoadipate aminotransferase. *Protein Sci, 22*(10), 1417-1424.

Burmeister, HR*, et al.* (1974). Antibiotic produced by *Fusarium Equiseti* NRRL 5537. *Antimicrob Agents Chemother, 5*(6), 634-639.

Cederbaum, AI. (2015). Molecular mechanisms of the microsomal mixed function oxidases and biological and pathological implications. *Redox Biol, 4*, 60-73.

Cesaratto, F*, et al.* (2016). *Tobacco etch virus* protease: a shortcut across biotechnologies. *J Biotechnol, 231*, 239-249.

Chen, X*, et al.* (2010). TEV protease-facilitated stoichiometric delivery of multiple genes using a single expression vector. *Protein Sci, 19*(12), 2379-2388.

Cherest, H*, et al.* (1969). Genetic and regulatory aspects of methionine biosynthesis in *Saccharomyces cerevisiae*. *J Bacteriol, 97*(1), 328-336.

Chiang, YM*, et al.* (2013). An efficient system for heterologous expression of secondary metabolite genes in *Aspergillus nidulans*. *J Am Chem Soc, 135*(20), 7720-7731.

Choi, KR*, et al.* (2019). Systems metabolic engineering strategies: integrating systems and synthetic biology with metabolic engineering. *Trends Biotechnol, 37*(8), 817-837.

Clevenger, KD*, et al.* (2017). A scalable platform to identify fungal secondary metabolites and their gene clusters. *Nat Chem Biol, 13*(8), 895-901.

Da, B*, et al.* (2000). Methods in yeast genetics. In Dan, B (Ed.), *a Cold Spring Harbor Laboratory Course Manual.* New York: Cold Spring Harbor Laboratory Press.

Da Silva, NA, & Srikrishnan, S. (2012). Introduction and expression of genes for metabolic engineering applications in *Saccharomyces cerevisiae*. *FEMS Yeast Res, 12*(2), 197-214.
Daicho, K*, et al.* (2009). Sorting defects of the tryptophan permease Tat2 in an *erg2* yeast mutant. *FEMS Microbiol Lett, 298*(2), 218-227.
Daniels, RW*, et al.* (2014). Expression of multiple transgenes from a single construct using viral 2A peptides in *Drosophila*. *PLoS One, 9*(6), e100637.
Davy, AM*, et al.* (2017). Cell factory engineering. *Cell Syst, 4*(3), 262-275.
de Felipe, P, & Ryan, MD. (2004). Targeting of proteins derived from self-processing polyproteins containing multiple signal sequences. *Traffic, 5*(8), 616-626.
Deed, RC*, et al.* (2019). The role of yeast *ARO8*, *ARO9* and *ARO10* genes in the biosynthesis of 3-(methylthio)-1-propanol from L-methionine during fermentation in synthetic grape medium. *FEMS Yeast Res, 19*(2), foy109.
DeLoache, WC*, et al.* (2015). An enzyme-coupled biosensor enables (*S*)-reticuline production in yeast from glucose. *Nat Chem Biol, 11*(7), 465-471.
Deng, H*, et al.* (2017). CRISPR system in filamentous fungi: current achievements and future directions. *Gene, 627*, 212-221.
Dickinson, JR*, et al.* (2003). The catabolism of amino acids to long chain and complex alcohols in *Saccharomyces cerevisiae*. *J Biol Chem, 278*(10), 8028-8034.
Dohn, J*, et al.* (2018). New multi-marker strains and complementing genes for *Aspergillus nidulans* molecular biology. *Fungal Genet Biol, 111*, 1-6.
Durairaj, P*, et al.* (2015). Comparative functional characterization of a novel benzoate hydroxylase cytochrome P450 of *Fusarium oxysporum*. *Enzyme Microb Technol, 70*, 58-65.
Ebrecht, AC*, et al.* (2019). Biochemical and structural insights into the cytochrome P450 reductase from *Candida tropicalis*. *Sci Rep, 9*(1), 20088.
Ehrlich, F. (1907). Über die Bedingungen der Fuselölbildung und über ihren Zusammenhang mit dem Eiweißaufbau der Hefe. *Berichte der deutschen chemischen Gesellschaft, 40*(1), 1027-1047.
Engler, C*, et al.* (2014). A golden gate modular cloning toolbox for plants. *ACS Synth Biol, 3*(11), 839-843.
Fernandes, JD*, et al.* (2015). The role of amino acid permeases and tryptophan biosynthesis in *Cryptococcus neoformans* survival. *PLoS One, 10*(7), e0132369.
Forsberg, H, & Ljungdahl, PO. (2001). Genetic and biochemical analysis of the yeast plasma membrane Ssy1p-Ptr3p-Ssy5p sensor of extracellular amino acids. *Mol Cell Biol, 21*(3), 814-826.
Fricke, J*, et al.* (2017). Enzymatic synthesis of psilocybin. *Angew Chem Int Ed, 56*(40), 12352-12355.
Fricke, J*, et al.* (2020). Scalable hybrid synthetic/biocatalytic route to psilocybin. *Chemistry*. (Just accepted)
Fricke, J*, et al.* (2019). Production options for psilocybin: making of the magic. *Chemistry, 25*(4), 897-903.
Fujita, K*, et al.* (2006). The genome-wide screening of yeast deletion mutants to identify the genes required for tolerance to ethanol and other alcohols. *FEMS Yeast Res, 6*(5), 744-750.
Galanie, S*, et al.* (2015). Complete biosynthesis of opioids in yeast. *Science, 349*(6252), 1095-1100.
Gmes, D*, et al.* (1991). An autonomously replicating plasmid transforms *Aspergillus nidulans* at high frequency. *Genes*, *98*(1), 61-67.
Ghiaci, P*, et al.* (2014). 2-Butanol and butanone production in *Saccharomyces cerevisiae* through combination of a B_{12} dependent dehydratase and a secondary alcohol dehydrogenase using a TEV-based expression system. *PLoS One, 9*(7), e102774.
Gibson, DG*, et al.* (2009). Enzymatic assembly of DNA molecules up to several hundred kilobases. *Nature Methods, 6*(5), 343-345.
Grinkova, YV*, et al.* (2010). Functional reconstitution of monomeric CYP3A4 with multiple cytochrome P450 reductase molecules in Nanodiscs. *Biochem Biophys Res Commun, 398*(2), 194-198.
Hamid, HA*, et al.* (2017). Indole alkaloids from plants as potential leads for antidepressant drugs: a mini review. *Front Pharmacol*, *8*, 96.
Harvey, CJB*, et al.* (2018). HEx: a heterologous expression platform for the discovery of fungal natural products. *Sci Adv, 4*(4), eaar5459.

Hazelwood, LA, *et al.* (2008). The Ehrlich pathway for fusel alcohol production: a century of research on *Saccharomyces cerevisiae* metabolism. *Appl Environ Microbiol*, *74*(8), 2259-2266.
He, B, *et al.* (2019). Functional genomics of *Aspergillus oryzae*: strategies and progress. *Microorganisms*, *7*(4), 103.
He, Y, *et al.* (2018). Recent advances in reconstructing microbial secondary metabolites biosynthesis in *Aspergillus* spp. *Biotechnol Adv, 36*(3), 739-783.
Hendrickson, L, *et al.,* (1999). Lovastatin biosynthesis in *Aspergillus terreus*: characterization of blocked mutants, enzyme activities and a multifunctional polyketide synthase gene. *Chem Biol*, *6*(7), 429-439.
Hertweck, C. (2009). The biosynthetic logic of polyketide diversity. *Angew Chem Int Ed, 48*(26), 4688-4716.
Hirasawa, T, *et al.* (2007). Identification of target genes conferring ethanol stress tolerance to *Saccharomyces cerevisiae* based on DNA microarray data analysis. *J Biotechnol, 131*(1), 34-44.
Hoefgen, S, *et al.* (2018). Facile assembly and fluorescence-based screening method for heterologous expression of biosynthetic pathways in fungi. *Metab Eng, 48*, 44-51.
Homer, JA, & Sperry, J. (2017). Mushroom-derived indole alkaloids. *J Nat Prod, 80*(7), 2178-2187.
Hommes, FA. (1966). Mechanism of the Crabtree effect in yeast grown with different glucose concentrations. *Arch Biochem Biophys, 113*(2), 324-330.
Horn, F, *et al.* (2016). Draft genome sequences of fungus *Aspergillus calidoustus*. *Genome Announc, 4*(2), e00102- e00116.
Hrycay, E, & Bandiera, S. (2015). Monooxygenase, peroxidase and peroxygenase properties and reaction mechanisms of cytochrome P450 enzymes. in Hrycay, EG (Ed.) *Advances in Experimental Medicine and Biology* (*851*, pp. 1-61). Heidelberg: Springer Nature.
Hu, J, *et al.* (2014). Characterization of two acetyltransferase genes in the pyripyropene biosynthetic gene cluster from *Penicillium coprobium*. *Biotechnol Biotechnol Equip, 28*(5), 818-826.
Hu, XH, *et al.* (2007). Genetic dissection of ethanol tolerance in the budding yeast *Saccharomyces cerevisiae*. *Genetics, 175*(3), 1479-1487.
Ignea, C, *et al.* (2016). Carnosic acid biosynthesis elucidated by a synthetic biology platform. *PNAS 113*(13), 3681-3686.
Iraqui, I, *et al.* (1998). Characterisation of *Saccharomyces cerevisiae ARO8* and *ARO9* genes encoding aromatic aminotransferases I and II reveals a new aminotransferase subfamily. *Mol Gen Genet, 257*(2), 238-248.
Jensen, PR. (2016). Natural products and the gene cluster revolution. *Trends Microbiol, 24*(12), 968-977.
John, MA, & Peberdy, JF. (1984). Transformation of *Aspergillus nidulans* using the *argB* gene. *Enzyme Microb Technol, 6*(9), 386-389.
Kalderon, D, *et al*. (1984) A short amino acid sequence able to specify nuclear location. *Cell*, *39*, 499-509.
Kapust, RB, *et al.* (2001). *Tobacco etch virus* protease: mechanism of autolysis and rational design of stable mutants with wild-type catalytic proficiency. *Protein Eng Des Sel, 14*(12), 993-1000.
Karim, AS, *et al.* (2013). Characterization of plasmid burden and copy number in *Saccharomyces cerevisiae* for optimization of metabolic engineering applications. *FEMS Yeast Res, 13*(1), 107-116.
Karim, K. (2019). Polymerase Chain Reaction (PCR): Principle and Applications. In Nagpal, ML (Ed.), *Synthetic Biology: New Interdisciplinary Science*. London: IntechOpen.
Kataoka, S, *et al.* (2011). Three austin family compounds from *Penicillium brasilianum* exhibit selective blocking action on cockroach nicotinic acetylcholine receptors. *Neurotoxicology, 32*(1), 123-129.
Kautsar, SA, *et al.* (2019). MIBiG 2.0: a repository for biosynthetic gene clusters of known function. *Nucleic Acids Res, 48*(D1), D454-D458.
Keasling, JD. (2008). Synthetic biology for synthetic chemistry. *ACS Chemical Biology, 3*(1), 64-76.

Keller, NP. (2019). Fungal secondary metabolism: regulation, function and drug discovery. *Nat Rev Microbiol, 17*(3), 167-180.
Keller, NP*, et al.* (2005). Fungal secondary metabolism - from biochemistry to genomics. *Nat Rev Microbiol, 3*(12), 937-947.
Kelsell, RE. (1996). Hybridization and competition hybridization of Southern blots. In A. J. Harwood (Ed.), *Basic DNA and RNA Protocols* (pp. 31-39). Totowa, NJ: Humana Press.
Kim, JH*, et al.* (2011). High cleavage efficiency of a 2A peptide derived from porcine teschovirus-1 in human cell lines, zebrafish and mice. *PLoS One, 6*(4), e18556.
Kistler, HC, & Broz, K. (2015). Cellular compartmentalization of secondary metabolism. *Front Microbiol, 6*, 68.
Knight, T. (2003). Idempotent vector design for standard assembly of BioBricks. *MIT Synthetic Biology Working Group Technical Reports*.
Koh, EYC*, et al.* (2013). An internal ribosome entry site (IRES) mutant library for tuning expression level of multiple genes in mammalian cells. *PloS One, 8*(12), e82100-e82100.
Kotopka, BJ*, et al.* (2018). Synthetic biology strategies toward heterologous phytochemical production. *Nat Prod Rep, 35*(9), 902-920.
Kouprina, N, & Larionov, V. (2008). Selective isolation of genomic loci from complex genomes by transformation-associated recombination cloning in the yeast *Saccharomyces cerevisiae*. *Nat Protoc, 3*(3), 371-377.
Kriz, A*, et al.* (2010). A plasmid-based multigene expression system for mammalian cells. *Nat Commun, 1*, 120.
Kubota, S*, et al.* (2004). Effect of ethanol on cell growth of budding yeast: genes that are important for cell growth in the presence of ethanol. *Biosci Biotechnol Biochem, 68*(4), 968-972.
Kudla, J, & Bock, R. (2016). Lighting the Way to Protein-Protein Interactions: Recommendations on Best Practices for Bimolecular Fluorescence Complementation Analyses. *Plant Cell, 28*(5), 1002-1008.
Kurnasov, O*, et al.* (2003). NAD biosynthesis: identification of the tryptophan to quinolinate pathway in bacteria. *Chem Biol, 10*(12), 1195-1204.
Lah, L*, et al.* (2008). High diversity and complex evolution of fungal cytochrome P450 reductase: cytochrome P450 systems. *Fungal Genet Biol, 45*(4), 446-458.
Lenz, C*, et al.* (2020). Injury-triggered blueing reactions of psilocybe "magic" mushrooms. *Angew Chem Int Ed, 59*(4), 1450-1454.
Leonard, E*, et al.* (2005). Investigation of two distinct flavone synthases for plant-specific flavone biosynthesis in *Saccharomyces cerevisiae*. *Appl Environ Microbiol, 71*(12), 8241-8248.
Li, M*, et al.* (2016). Engineering yeast for high-level production of stilbenoid antioxidants. *Sci Rep, 6*, 36827.
Li, S*, et al.* (2012). Biochemical characterization of NotB as an FAD-dependent oxidase in the biosynthesis of notoamide indole alkaloids. *J Am Chem Soc, 134*(2), 788-791.
Li, S*, et al.* (2018). Strategies for microbial synthesis of high-value phytochemicals. *Nat Chem, 10*(4), 395-404.
Li, Y, & Smolke, CD. (2016). Engineering biosynthesis of the anticancer alkaloid noscapine in yeast. *Nat Commun, 7*, 12137.
Lian, J*, et al.* (2014). Design and construction of acetyl-CoA overproducing *Saccharomyces cerevisiae* strains. *Metab Eng, 24*, 139-149.
Lin, L*, et al.* (2003). Efficient linking and transfer of multiple genes by a multigene assembly and transformation vector system. *PNAS, 100*(10), 5962-5967.
Lin, TS*, et al.* (2016). Biosynthetic pathway of the reduced polyketide product citreoviridin in *Aspergillus terreus var. aureus* revealed by heterologous expression in *Aspergillus nidulans*. *Org Lett, 18*(6), 1366-1369.
Liu, J*, et al.* (2014). Unusual acetylation-dependent reaction cascade in the biosynthesis of the pyrroloindole drug physostigmine. *Angew Chem Int Ed, 53*(1), 136-139.
Liu, X*, et al.* (2017a). Engineering microbial cell factories for the production of plant natural products: from design principles to industrial-scale production. *Microb Cell Fact, 16*(1), 125-133.
Liu, Z*, et al.* (2017b). Systematic comparison of 2A peptides for cloning multi-genes in a polycistronic vector. *Sci Rep, 7*(1), 2193.

Lo, HC, *et al.* (2012). Two separate gene clusters encode the biosynthetic pathway for the meroterpenoids austinol and dehydroaustinol in *Aspergillus nidulans*. *J Am Chem Soc, 134*(10), 4709-4720.
Lu, C, & Jeffries, T. (2007). Shuffling of promoters for multiple genes to optimize xylose fermentation in an engineered *Saccharomyces cerevisiae* strain. *Appl Environ Microbiol, 73*(19), 6072-6077.
Lundemo, MT, & Woodley, JM. (2015). Guidelines for development and implementation of biocatalytic P450 processes. *Appl Microbiol Biotechnol, 99*(6), 2465-2483.
Lv, X, *et al.* (2016). Dual regulation of cytoplasmic and mitochondrial acetyl-CoA utilization for improved isoprene production in *Saccharomyces cerevisiae*. *Nat Commun, 7*, 12851.
Magliery, TJ, *et al.* (2005). Detecting protein−protein interactions with a green fluorescent protein fragment reassembly trap: scope and mechanism. *J Am Chem Soc, 127*(1), 146-157.
Mahmood, ZA. (2013). Bioactive alkaloids from fungi: psilocybin. In Ramawat, KG (Ed.), *Natural Products: Phytochemistry, Botany and Metabolism of Alkaloids, Phenolics and Terpenes* (pp. 523-552). Berlin, Heidelberg: Springer Berlin Heidelberg.
Mansouri, M, & Berger, P. (2014). Strategies for multigene expression in eukaryotic cells. *Plasmid, 75*, 12-17.
Mao, X-M, *et al.* (2015). Efficient biosynthesis of fungal polyketides containing the dioxabicyclo-octane ring system. *J Am Chem Soc, 137*(37), 11904-11907.
Marchler-Bauer, A, *et al.* (2016). CDD/SPARCLE: functional classification of proteins via subfamily domain architectures. *Nucleic Acids Res, 45*(D1), D200-D203.
Matsuda, Y, & Abe, I. (2016). Biosynthesis of fungal meroterpenoids. *Nat Prod Rep, 33*(1), 26-53.
Matsuda, Y, *et al.* (2013). Spiro-ring formation is catalyzed by a multifunctional dioxygenase in austinol biosynthesis. *J Am Chem Soc, 135*(30), 10962-10965.
Matsuda, Y, *et al.* (2016). Discovery of key dioxygenases that diverged the paraherquonin and acetoxydehydroaustin pathways in *Penicillium brasilianum*. *J Am Chem Soc, 138*(38), 12671-12677.
Mattern, DJ, *et al.* (2017). Rewiring of the austinoid biosynthetic pathway in filamentous fungi. *ACS Chem Biol, 12*(12), 2927-2933.
Mattern, DJ, *et al.* (2015). Synthetic biology of fungal natural products. *Front Microbiol, 6*, 775.
Meijer, WH, *et al.* (2010). Peroxisomes are required for efficient penicillin biosynthesis in *Penicillium chrysogenum*. *Appl Environ Microbiol, 76*(17), 5702-5709.
Metzger, U, *et al.* (2009). The structure of dimethylallyl tryptophan synthase reveals a common architecture of aromatic prenyltransferases in fungi and bacteria. *Proc Natl Acad Sci U S A, 106*(34), 14309-14314.
Meyer, V, *et al.* (2011). Fungal gene expression on demand: an inducible, tunable, and metabolism-independent expression system for *Aspergillus niger*. *Appl Environ Microbiol, 77*(9), 2975-2983.
Mignon, C, *et al.* (2015). Antibiotic-free selection in biotherapeutics: now and forever. *Pathogens, 4*(2), 157-181.
Milne, N, *et al.* (2020). Metabolic engineering of *Saccharomyces cerevisiae* for the *de novo* production of psilocybin and related tryptamine derivatives. *Metab Eng, 60*, 25-36.
Miozzari, G, *et al.* (1978). Tryptophan biosynthesis in *Saccharomyces cerevisiae*: control of the flux through the pathway. *J Bacteriol, 134*(1), 48-59.
Mumberg, D, *et al.* (1994). Regulatable promoters of *Saccharomyces cerevisiae*: comparison of transcriptional activity and their use for heterologous expression. *Nucleic Acids Res, 22*(25), 5767-5768.
Nayak, T, *et al.* (2006). A versatile and efficient gene-targeting system for *Aspergillus nidulans. Genetics, 172*(3), 1557-1566.
Nielsen, J. (2015). Yeast cell factories on the horizon. *Science, 349*(6252), 1050-1051.
Ohashi, K, *et al.* (2017). Kynurenine aminotransferase activity of Aro8/Aro9 engage tryptophan degradation by producing kynurenic acid in *Saccharomyces cerevisiae. Sci Rep, 7*(1), 12180.
Paddon, CJ, *et al.* (2013). High-level semi-synthetic production of the potent antimalarial artemisinin. *Nature, 496*(7446), 528-532.
Panozzo, C, *et al.* (2002). Aerobic and anaerobic NAD^+ metabolism in *Saccharomyces cerevisiae*. *FEBS Lett, 517*(1), 97-102.

Peng, B*, et al.* (2017). Coupling gene regulatory patterns to bioprocess conditions to optimize synthetic metabolic modules for improved sesquiterpene production in yeast. *Biotechnol Biofuels, 10*, 43.
Peng, B*, et al.* (2018). An expanded heterologous *GAL* promoter collection for diauxie-inducible expression in *Saccharomyces cerevisiae. ACS Synth Biol, 7*(2), 748-751.
Petersen, LM*, et al.* (2014). Dereplication guided discovery of secondary metabolites of mixed biosynthetic origin from *Aspergillus aculeatus*. *Molecules, 19*(8), 10898-10921.
Pontecorvo, G*, et al.* (1953). The Genetics of *Aspergillus nidulans*. In M. Demerec (Ed.), *Advances in Genetics* (*5*, pp. 141-238), New York: Academic Press.
Presnyak, V*, et al.* (2015). Codon optimality is a major determinant of mRNA stability. *Cell, 160*(6), 1111-1124.
Puig, S*, et al.* (1998). Optimized method to obtain stable food-safe recombinant wine zeast strains. *J Agric Food Chem, 46*(4), 1689-1693.
Quan, J, & Tian, J. (2009). Circular polymerase extension cloning of complex gene libraries and pathways. *PLoS One, 4*(7), e6441.
Quinn, R. (2013). Rethinking antibiotic research and development: World War II and the penicillin collaborative. *Am J Public Health, 103*(3), 426-434.
Richter, L*, et al.* (2014). Engineering of *Aspergillus niger* for the production of secondary metabolites. *Fungal Biol Biotechnol, 1*, 1-13.
Riquelme, M, & Sánchez-León, E. (2014). The Spitzenkörper: a choreographer of fungal growth and morphogenesis. *Curr Opin Microbiol, 20*, 27-33.
Rokas, A*, et al.* (2018). The birth, evolution and death of metabolic gene clusters in fungi. *Nat Rev Microbiol, 16*(12), 731-744.
Romagnoli, G*, et al.* (2015). Deletion of the *Saccharomyces cerevisiae ARO8* gene, encoding an aromatic amino acid transaminase, enhances phenylethanol production from glucose. *Yeast, 32*(1), 29-45.
Romei, MG, & Boxer, SG. (2019). Split green fluorescent proteins: scope, limitations, and outlook. *Annu Rev Biophys, 48*, 19-44.
Rząd, K*, et al.* (2017). Versatility of putative aromatic aminotransferases from *Candida albicans*. *Fungal Genet Biol, 110*, 26-37
Sanchez, MI, & Ting, AY. (2020). Directed evolution improves the catalytic efficiency of TEV protease. *Nat Methods, 17*(2), 167-174.
Schmidt, A*, et al.* (1994). Two FK506 resistance-conferring genes in *Saccharomyces cerevisiae*, *TAT1* and *TAT2*, encode amino acid permeases mediating tyrosine and tryptophan uptake. *Mol Cell Biol, 14*(10), 6597-6606.
Schneider, P*, et al.* (2008). The *Aspergillus nidulans* enzyme TdiB catalyzes prenyltransfer to the precursor of bioactive asterriquinones. *Fungal Genet Biol, 45*(3), 302-309.
Schottel, JL*, et al.* (1981). Cloning and expression in *Streptomyces lividans* of antibiotic resistance genes derived from *Escherichia coli*. *J Bacteriol, 146*(1), 360-368.
Schuetze, T, & Meyer, V. (2017). Polycistronic gene expression in *Aspergillus niger*. *Microb Cell Fact, 16*(1), 162.
Sharma, P*, et al.* (2012). 2A peptides provide distinct solutions to driving stop-carry on translational recoding. *Nucleic Acids Res, 40*(7), 3143-3151.
Sherwood, AM*, et al.* (2020). Synthesis and biological evaluation of tryptamines found in hallucinogenic mushrooms: norbaeocystin, baeocystin, norpsilocin, and aeruginascin. *J Nat Prod, 83*(2), 461-467.
Shetty, RP*, et al.* (2008). Engineering BioBrick vectors from BioBrick parts. *J Biol Eng, 2*, 5.
Shih, YP*, et al.* (2005). Self-cleavage of fusion protein *in vivo* using TEV protease to yield native protein. *Protein Sci, 14*(4), 936-941.
Shirota, O*, et al.* (2003). Concise large-scale synthesis of psilocin and psilocybin, principal hallucinogenic constituents of "magic mushroom". *J Nat Prod, 66*(6), 885-887.
Silberstein, SD, & Hargreaves, RJ. (2000). The history and pharmacology of ergotamine and dihydroergotamine. In: Diener HC (Ed.), *Drug treatment of migraine and other headaches* (pp. 52–65). Basel: Karger.
Smith, D. (1996). Agarose gel electrophoresis. In Harwood, AJ (Ed.), *Basic DNA and RNA Protocols* (pp. 17-21). Totowa, NJ: Humana Press.
Smith, D, & Murphy, D. (1996). Capillary blotting of agarose gels. *Methods Mol Biol, 58*, 23-25.

Souza-Moreira, TM, *et al.* (2018). Screening of 2A peptides for polycistronic gene expression in yeast. *FEMS Yeast Res, 18*(5), foy036.
Sporty, J, *et al.* (2009). Quantitation of NAD^+ biosynthesis from the salvage pathway in *Saccharomyces cerevisiae*. *Yeast, 26*(7), 363-369.
Srinivasan, P, & Smolke, CD. (2019). Engineering a microbial biosynthesis platform for *de novo* production of tropane alkaloids. *Nat Commun, 10*(1), 3634.
Stringer, MA, *et al.* (1991). Rodletless, a new *Aspergillus* developmental mutant induced by directed gene inactivation. *Genes Dev, 5*(7), 1161-1171.
Stroe, MC, *et al.* (2020). Targeted induction of a silent fungal gene cluster encoding the bacteria-specific germination inhibitor fumigermin. *Elife, 9*, e52541.
Subramanian, V, *et al.* (2017). A versatile 2A peptide-based bicistronic protein expressing platform for the industrial cellulase producing fungus, *Trichoderma reesei. Biotechnol Biofuels, 10*, 34.
Sun, J, *et al.* (2012). Cloning and characterization of a panel of constitutive promoters for applications in pathway engineering in *Saccharomyces cerevisiae*. *Biotechnol Bioeng, 109*(8), 2082-2092.
Szymczak, AL, & Vignali, DAA. (2005). Development of 2A peptide-based strategies in the design of multicistronic vectors. *Expert Opin Biol Ther, 5*(5), 627-638.
Taylor, GM, *et al.* (2019). Start-Stop Assembly: a functionally scarless DNA assembly system optimized for metabolic engineering. *Nucleic Acids Res, 47*(3), e17.
Toyn, J, *et al.* (2000). A counterselection for the tryptophan pathway in yeast: 5-Fluoroanthranilic acid resistance. *Yeast, 16*(6), 553-560.
Trenchard, IJ, & Smolke, CD. (2015). Engineering strategies for the fermentative production of plant alkaloids in yeast. *Metab Eng, 30*, 96-104.
Trotta, E. (2013). Selection on codon bias in yeast: a transcriptional hypothesis. *Nucleic Acids Res, 41*(20), 9382-9395.
Umebayashi, K, & Nakano, A. (2003). Ergosterol is required for targeting of tryptophan permease to the yeast plasma membrane. *J Cell Biol, 161*(6), 1117-1131.
Unkles, SE, *et al.* (2014). Synthetic biology tools for bioprospecting of natural products in eukaryotes. *Chem Biol, 21*(4), 502-508.
Upshall, A. (1986). Genetic and molecular characterization of *argB*$^+$ transformants of *Aspergillus nidulans*. *Curr Genet, 10*(8), 593-599.
Valiante, V, *et al.* (2017). Discovery of an extended austinoid biosynthetic pathway in *Aspergillus calidoustus. ACS Chem Biol, 12*(5), 1227-1234.
Varshavsky, A. (2011). The N-end rule pathway and regulation by proteolysis. *Protein Sci, 20*(8), 1298-1345.
Vecchione, S, & Fritz, G. (2019). CRIMoClo plasmids for modular assembly and orthogonal chromosomal integration of synthetic circuits in *Escherichia coli*. *J Biol Eng, 13*, 92.
Wach, A, *et al.* (1994). New heterologous modules for classical or PCR-based gene disruptions in *Saccharomyces cerevisiae*. *Yeast, 10*(13), 1793-1808.
Wang, Y, *et al.* (2015). 2A self-cleaving peptide-based multi-gene expression system in the silkworm *Bombyx mori. Sci Rep, 5*(1), 16273.
Wang, Y, *et al.* (2019). Fine-tuning the expression of target genes using a *DDI2* promoter gene switch in budding yeast. *Sci Rep, 9*(1), 12538.
Warrilow, AGS, *et al.* (2002). *Phanerochaete chrysosporium* NADPH-cytochrome P450 reductase kinetic mechanism. *Biochem Biophys Res Commun, 299*(2), 189-195.
Waugh, DS. (2011). An overview of enzymatic reagents for the removal of affinity tags. *Protein Expr Purif, 80*(2), 283-293.
Wong, YK, *et al.* (2017). Artemisinin as an anticancer drug: recent advances in target profiling and mechanisms of action. *Med Res Rev, 37*(6), 1492-1517.
Xia, C, *et al.* (2019). Structural and functional studies of the membrane-binding domain of NADPH-cytochrome P450 oxidoreductase. *Biochemistry, 58*(19), 2408-2418.
Xia, N, *et al.* (2017). Antioxidant effects of resveratrol in the cardiovascular system. *Br J Pharmacol, 174*(12), 1633-1646.
Xu, P, *et al.* (2012). ePathBrick: a synthetic biology platform for engineering metabolic pathways in *E. coli*. *ACS Synth Biol, 1*(7), 256-266.
Xu, W, *et al.* (2014). Biosynthesis of fungal indole alkaloids. *Nat Prod Rep, 31*(10), 1474-1487.

Xu, Z, & Tsurugi, K. (2006). A potential mechanism of energy-metabolism oscillation in an aerobic chemostat culture of the yeast *Saccharomyces cerevisiae. FEBS J, 273*(8), 1696-1709.

Yang, J*, et al.* (2018). Polyprotein strategy for stoichiometric assembly of nitrogen fixation components for synthetic biology. *PNAS, 115*(36), E8509-E8517.

Yanisch-Perron, C*, et al.* (1985). Improved M13 phage cloning vectors and host strains: nucleotide sequences of the M13mpl8 and pUC19 vectors. *Gene, 33*(1), 103-119.

Yuan, J*, et al.* (2019). *De Novo* biosynthesis of (*S*)- and (*R*)-phenylethanediol in zeast *via* artificial enzyme cascades. *ACS Synth Biol, 8*(8), 1801-1808.

Zadra, I. (2000). *xylP* promoter-based expression system and its use for antisense downregulation of the *Penicillium chrysogenum* nitrogen regulator NRE. *Appl Environ Microbiol, 66*(11), 4810-4816.

Zhang, S*, et al.* (2017). Self-excising Cre/mutant *lox* marker recycling system for multiple gene integrations and consecutive gene deletions in *Aspergillus oryzae*. *J Biosci Bioeng, 123*(4), 403-411.

Zhao, F*, et al.* (2016). Optimization of a cytochrome P450 oxidation system for enhancing protopanaxadiol production in *Saccharomyces cerevisiae*. *Biotechnol Bioeng, 113*(8), 1787-1795.

Zhou, Z*, et al.* (2016). Codon usage is an important determinant of gene expression levels largely through its effects on transcription. *PNAS, 113*(41), E6117-E6125.

Zhu, K*, et al.* (2017). Cleavage of fusion proteins on the affinity resins using the TEV protease variant. *Protein Expr Purif, 131*, 27-33.

Zhu, L*, et al.* (2013). Further enhanced production of heterologous proteins by double-gene disruption (Δ*AosedD* Δ*Aovps10*) in a hyper-producing mutant of *Aspergillus oryzae*. *Appl Microbiol Biotechnol, 97*(14), 6347-6357.

List of abbreviations

Abbreviation	Full description
°C	degree Celsius
%	the sign indicated the percentage or the ratio as a fraction of 100
A.	*Aspergillus*
AAT	aminotransferase
ACN	acetonitrile
ADH	alcohol dehydrogenase gene
AMM	*Aspergillus* minimal medium
amp^R	ampicillin resistant gene marker; *bla* gene
Arg	L-arginine
argB	gene coding for ornithine carbamoyltransferase in *A. nidulans*
ARO	aromatic amino acid gene
AUC	area under the curve
BGC	biosynthetic gene cluster
BNA	gene for biosynthesis of nicotinic acid
bp	base pairs
CD	conserved domain
cDNA	complementary DNA
CoA	coenzyme A
CPR	NADPH-dependent cytochrome P450 reductase
CRISPR-Cas 9	clustered regularly interspaced short palindromic repeats and CRISPR-associated protein 9
CYC	gene coding cytochrome C
CYP	cytochromes P450
DAD	diode-array detector
DMAPP	dimethylallyl pyrophosphate
Dox	doxycycline
4-DMAT	4-dimethylallyl tryptophan
DNA	deoxyribonucleic acid
EIC	extracted ion chromatogram
ER	endoplasmic reticulum
ESI	electrospray ionization
et al.	*et aliī* (“and others”)
FA	formic acid
g	gram
G418	geneticin
GALp	galactose-inducible promoter
GFP	green fluorescent protein
h	hour
HIS	gene for biosynthesis of histidine

His	L-histidine
HPLC	high-performance liquid chromatography
HRMS	high resolution mass spectrometry
IGP	indole-3-glycerol-phosphate
IPA	indole-3-pyruvate
KA	kynurenic acid or kynurenate
Kan^{R}	kanamycin-resistant gene marker; *aph* gene
kb	kilobase pairs
KYN	kynurenine
L	liter
LB	Lysogeny broth
L-DOPA	l-3,4-dihydroxyphenylalanine
LEU	gene for biosynthesis of leucine
Leu	L-leucine
Lys	L-lysine
LzA	leucine zipper helix A
LzB	leucine zipper helix B
LZD	leucine zipper domain
M	molar (mol/L)
m/z	mass-to-charge ratio
MAT	mating types
MeOH	methanol
MET	gene for biosynthesis of methionine
Met	methionine
MET15p	promoter of *MET15* gene
mg	milligram
min	minute(s)
mL	milliliter
mM	millimolar (mmol/L)
mRNA	messenger RNA
MS	mass spectrometry
NAD^{+}	oxidized form of nicotinamide adenine dinucleotide
NADH	reduced form of nicotinamide adenine dinucleotide
NADP	nicotinamide adenine dinucleotide phosphate
NADPH	reduced form of nicotinamide adenine dinucleotide phosphate
NC	negative control
NCBI	National Center for Biotechnology Information
ng	nanogram
NHEJ	non-homologous end joining
NLS	nuclear localization signal
nm	nanometer
NRP	non-ribosomal peptide

NRPS	non-ribosomal peptide synthetase
OD_{600}	the optical density of a sample measured at a wavelength of 600 nm
ORF	open reading frame
ori	origin of replication
PABA	*para*-aminobenzoic acid
PCR	polymerase chain reaction
Phe	L-phenylalanine
PK	polyketide
PKS	polyketide synthases
PLP	pyridoxal phosphate
PP	phosphate
PYK1p	promoter of gene coding pyruvate kinase
DMSO	dimethyl sulfoxide
RNA	ribonucleic acid
ROS	reactive oxygen species
rpm	revolutions per minute
S.	*Saccharomyces*
scCPR	yeast *S. cerevisiae* endogenous CPR
SD medium / agar	synthetic defined medium / agar
SM	secondary metabolite
spp.	*species pluralis* (spp.), Latin for multiple species
SV40	simian vacuolating virus 40
TAR	transformation-associated recombination
TDH3p	promoter of gene coding isozyme 3
TEF1p	promoter of gene coding elongation factor 1-alpha 1
Tet^{on}	tetracycline (Tet)-inducible promoter
TEV	*tobacco etch virus*
tev	TEVp cleavage site
TEV	gene coding TEV protease
TEVp	TEV protease
TRP	gene for biosynthesis of tryptophan
Trp	L-tryptophan
Tyr	L-tyrosine
UHPLC	ultra-high-performance liquid chromatography
URA	gene for biosynthesis of uridine / uracil
Ura	uracil / uridine
v/v	volume per volume
w/v	weight per volume
wt	wild type
xylP	xylose-inducible promoter
YFP	yellow fluorescent protein
Δ	deletion

λ	wavelength
μg	microgram
μL	microliter
μM	micromolar

List of schemes and figures

List of tables

Scientific publication and conference contributions

Publication

05/2018 Hoefgen S*, **Lin J***, Fricke J*, Stroe MC, Mattern DJ, Kufs JE, Hortschansky P, Brakhage AA, Hoffmeister D, Valiante V. *Metab Eng* 2018, 48, 44-51.

*Shared first authorship

Talk and poster presentations

Talks

03/2019 30th Fungal Genetics Conference + Asperfest 16, Asilomar, USA

Flexible assembling platform built up for heterologous expression of secondary metabolites in filamentous fungi

05/2018 ILRS Symposium 2018, Jena, Germany

Quick assembly and fluorescence-screening method scaled up biosynthesis of psilocybin by polycistronic gene expression in filamentous fungi

Posters

05/2019 ILRS Symposium 2019, Wittenberg, Germany

Biosynthetic pathway elucidation of a unique PKS gene cluster identified from the human-pathogenic fungus Aspergillus calidoustus

04/2019 Leibniz Wirkstofftage 2019, Dresden, Germany

Flexible assembling platform built up for heterologous expression of secondary metabolites in filamentous fungi

03/2019 30th Fungal Genetics Conference, Asilomar, USA

Flexible assembling platform built up for heterologous expression of secondary metabolites in filamentous fungi

09/2017 12th Symposium of the VAAM special group Molecular Biology of Fungi, Jena, Germany

Biosynthesis of austinoid derivatives based on an improved expression platform

03/2017 MiCom2017 – 6th International Conference on Microbial Communication for Young Scientists, Jena, Germany

Discovery of eukaryotic cryptic natural products by heterologous expression

09/2016 Next Generation of Biotechnological Processes – Biotechnology 2020+, Jena, Germany

Natural product trapping using updated tools for heterologous expression in fungi

Acknowledgements

First and foremost, I am grateful to my doctoral supervisor Prof. Axel A. Brakhage. He provided me with this excellent opportunity to work at the Hans-Knöll-Institut which is an interdisciplinary and international research environment. I appreciate his encouragement, all his effort in reviewing my thesis, and invaluable supports through this challenging journey of science. Plus, I wish to express my deepest gratitude to my co-supervisor, Dr. Vito Valiante, who selected me and paved the way for me to study and do research in his dynamic group. I thank Vito for all his trust, supports, guides, ideas, and help during these years. I learned a lot from his experience and knowledge.

Secondly, the physical and technical contribution of ILRS and the 'Leibniz Research Cluster' is truly appreciated. Without their support and funding, this project could not have reached its goal. Especially, the LRC Summer School organized each year was a great opportunity to explore other areas of research interactively.

Thirdly, I wish to thank all the people who worked in the completion of this work. I am indebted to Dr. Sandra Höfgen, as she contributed a lot to this work with her professional skills. She always supports me in life and research. I am grateful to Johann Kufs for his work in the manipulation of fluorescence microscope. I also thank my previous colleague Dr. Slavica Janevska for her efforts in the construction of yeast triple deletion strains and the tryptophan sensitivity assay. And I appreciate her support in my first international conference. Additionally, I would like to thank the generous assistance, contributions, and experience sharing from Dr. Maria Stroe and Dr. Derek Mattern in this work. Besides, I appreciate the close collaboration with Prof. Hoffmeister and his group. Janis Fricke helped in the plasmids' construction, psilocybin extraction, and quantification during this cooperation.

Next, I would like to thank Daniela Hildebrandt, my other lab mates, and the neighboring group. I wholeheartedly appreciate their aids and great advice for my study and experiments. I enjoy the lively and friendly atmosphere around. Moreover, I wish to acknowledge the support from Dr. Huijuan Guo and Dr. Daniel Braga de Lima through my study in the HKI. Beyond the scientific field, I am grateful to Dr. Christine Vogler, who assisted me in many aspects.

In the end, my sincere gratitude goes to my family and to all my friends, especially to my mom Weizhen, my dad Tongchun, and my boyfriend Jonatan for their unconditional support and great love. Furthermore, I especially want to thank one of my best friends, Lia, for proofreading this thesis. They kept me going on, and this work would not have been possible without their input.

Eigenständigkeitserklärung

Die geltende Promotionsordnung der Fakultät für Biowissenschaften der Friedrich-Schiller-Universität Jena ist mir bekannt. Die vorliegende Dissertation habe ich selbständig verfasst und dabei weder Textabschnitte aus einer eigenen Prüfungsarbeit oder von dritten ohne Kennzeichnung übernommen. Es wurden keine anderen als die von mir angegebenen Quellen, persönliche Mitteilungen und Hilfsmittel verwendet. Ich versichere, dass die aufgelisteten Publikationen und Manuskripte, ausschließlich auf Ergebnissen beruhen, die während meiner Promotion generiert wurden.

Bei der Auswahl und Auswertung des Materials, wie auch bei der Herstellung der Manuskripte haben mich die in der Danksagung meiner Dissertation genannten Personen unterstützt. Personen, die bei der Anfertigung der Publikationen und Manuskripte beteiligt waren, sowie deren Eigenanteil sind gekennzeichnet. Die Hilfe eines kommerziellen Promotionsberaters wurde nicht in Anspruch genommen. Auch haben Dritte weder unmittelbar noch mittelbar geldwerte Leistungen, die im Zusammenhang mit dem Inhalt der vorliegenden Dissertation stehen, erhalten.

Ich habe die Dissertation noch nicht als Prüfungsarbeit für eine staatliche oder andere wissenschaftliche Prüfung eingereicht. Ferner habe ich nicht versucht, diese Arbeit oder eine in wesentlichen Teilen ähnliche oder eine andere Abhandlung bei einer anderen Hochschule als Dissertation einzureichen.

Jena, den 24.06.2020

Jun Lin